COO-4261-11

SIMULATION OF HEAT AND MASS TRANSFER PROCESSES IN MOLTEN CORE DEBRIS-CONCRETE SYSTEMS

By

David Kent Felde

A Thesis Submitted in Partial Fulfillment

of the Requirements for the Degree of

MASTER OF SCIENCE

(Nuclear Engineering)

At The

UNIVERSITY OF WISCONSIN-MADISON

1979

DISCLAIMER

ACKNOWLEDGEMENT

I would like to express my appreciation to my advisor, Dr. S.I. Abdel-Khalik, for his guidance and support throughout the course of this work. I would like to thank Mr. H.S. Kim for his assistance in running the experiment and data reduction. I would also like to thank Mr. T. Anklam, Mr. Z. Musicki, and Mr. I.K. Paik for their assistance on this work.

Financial support by the Department of Energy through contract #EN-77-S-02-4261 is acknowledged.

TABLE OF CONTENTS

LIST OF TABLES

LIST OF FIGURES

NOMENCLATURE

c_p	specific heat capacity (J/kg°C)
D	pool diameter (cm)
Fr	Froude number $\equiv (\frac{V^2}{gL_g})$
g	gravitational constant (cm/s^2)
h_0	downward heat transfer coefficient (W/cm^2°C)
h_1	upward heat transfer coefficient (W/cm^2°C)
$h_{dry\ air}(T_{in})$	enthalpy of dry air at the air inlet temperature (J/kg)
$h_{sat\ air}(T_{out})$	enthalpy of saturated air at the air exit temperature (J/kg)
h_s	sideward heat transfer coefficient (W/cm^2°C)
k	thermal conductivity of the pool fluid (W/cm°C)
L	layer depth (cm)
L_g	characteristic dimension for the gas bubbles (cm)
L^*	characteristic length of the system (cm)
$\dot{m}_{air}$	mass flow rate of air (kg/s)
$\dot{m}_W$	mass flow rate of cooling water (kg/s)
M	inverse non-dimensional pool temperature rise $\equiv \frac{QL^2}{8k\Delta T}$
M^*	averaged inverse non-dimensional pool temperature rise $\equiv \frac{M(\text{Porous Lower Boundary}) + M(\text{Porous Side Boundary})}{2}$
Nu_0	downward Nusselt number $\equiv \frac{h_0 L}{k}$
Nu_1	upward Nusselt number $\equiv \frac{h_1 L}{k}$
Nu_s	sideward Nusselt number $\equiv \frac{h_s L}{k}$

Pr	Prandtl number $\equiv \frac{\nu}{\alpha} \equiv \frac{\mu c_p}{k}$
q	rate of heat transfer to the plate (W)
q''	heat flux (W/cm^2)
q_{air}	heat removed by air (W)
q_0	initial power density (W/cm^3)
q''_{wall}	heat flux at the wall (W/cm^2)
Q	heat generation rate per unit volume of the pool (W/cm^3)
Ra_c	critical Rayleigh number; minimum Rayleigh number necessary to initiate convection in the fluid
Ra_I	Internal Rayleigh number $\equiv \frac{g\beta QL^5}{\alpha\nu 64k}$
Re	Reynolds number $\equiv (\rho V L_g/\mu)$
T_{max}	maximum pool temperature (°C)
T_{wall}	wall temperature (°C)
ΔT	maximum temperature difference between the pool and the average of the measured plate temperatures (°C)
ΔT^*	characteristic destabilizing temperature difference $\equiv \frac{QL^2}{8k}$ (°C)
V	superficial gas velocity (cm/min)
V^*	non-dimensional gas velocity $\equiv \frac{V^3\rho}{\mu g} \equiv$ (ReFr)
W	pool width (cm)
(W/L)	aspect ratio
$(W/L)_{min}$	minimum aspect ratio

- -

α	thermal diffusivity $\equiv \frac{k}{\rho c_p}$
β	coefficient of volume expansion
ν	kinematic viscosity $\equiv \frac{\mu}{\rho}$

η_{up}	upward power fraction
μ	viscosity of pool fluid (poise)
ρ	density of pool fluid (kg/cm^3)
ρ_b	density of pool bed (kg/cm^3)
ρ_p	density of pool fluid (kg/cm^3)
τ_{min}	characteristic time at which pool reaches minimum aspect ratio (min)

SUMMARY

The heat and mass transport phenomena taking place in volumetrically-heated fluids have become of interest in recent years due to their significance in assessments of fast reactor safety and post-accident heat removal (PAHR). Following a hypothetical core disruptive accident (HCDA), the core and reactor internals may melt down. The core debris melting through the reactor vessel and guard vessel may eventually contact the concrete of the reactor cell floor. The interaction of the core debris with the concrete as well as the melting of the debris pool into the concrete will significantly affect efforts to prevent breaching of the containment and the resultant release of radioactive effluents to the environment.

To assess the integrity of the containment, it becomes necessary to determine the heat transfer paths from the debris pool heated by the radioactive decay of the dissolved fission products to the surrounding environment. Earlier work on volumetrically-heated pools has focused on natural convection phenomena. These, however, do not apply for molten core debris/concrete systems. Therefore, the main objectives of this study have been to experimentally simulate the evolution of gas at the concrete boundary and investigate the effects of gas release on the heat transfer rates along the boundaries of a heated pool.

The experimental apparatus consists of a rectangular geometry test cell bounded by porous brass plates on the sides and bottom

through which a noncondensable gas is injected. Joule heating of an electrolyte solution provides the volumetric heat source to the test cell. A wide range of internal Rayleigh number, gas injection rates, and pool aspect ratio are investigated.

The results obtained in this study show that gas injection at the boundaries of a volumetrically-heated pool have a significant effect onthe heat transfer rates at the pool boundaries. Pool maximum temperatures are reduced considerably with gas injection as compared to natural convection. The pools are well stirred by the gas and show nearly isothermal temperature distributions.

Natural convection effects are found to be negligible in the gas mixed pool; the sideward, downward, and upward Nusselt numbers are independent of the internal Rayleigh number.

The sideward and downward Nusselt numbers to porous plates with gas evolution are directly correlated to the product of Reynolds and Froude numbers; $(Re \cdot Fr) \equiv (\frac{v^3\rho}{\mu g})$ which is a measure of the buoyancy and viscous drag effects produced by the gas as it mixes the liquid.

The following Nusselt-type correlations have been obtained.

1. Downward Nusselt Number

For a porous lower boundary and a solid upper surface with the power to the test cell applied between the upper plate and lower porous plate the downward Nusselt number is

$$Nu_0 \cdot \frac{W}{L} = 204[ReFr]^{0.05} \quad (5 \times 10^{-10} \leq ReFr \leq 5 \times 10^{-3})$$

For the same case with the power applied between a wire grid electrode placed immediately below the top plate and the lower porous plate, the downward Nusselt number is given by:

$$Nu_0 \cdot \frac{W}{L} = 193[ReFr]^{0.048} \quad (5 \times 10^{-10} \leq ReFr \leq 5 \times 10^{-3})$$

The correlation of a downward Nusselt number for a porous lower boundary and a free upper surface is

$$Nu_0 \cdot \frac{W}{L} = 231[ReFr]^{0.074} \quad (5 \times 10^{-10} \leq ReFr \leq 5 \times 10^{-3})$$

2. Sideward Nusselt Number

The sideward Nusselt number for test cells with porous side boundaries is given by

$$Nu_s \cdot \frac{W}{L} = 194[ReFr]^{0.043} \quad (5 \times 10^{-10} \leq ReFr \leq 5 \times 10^{-3})$$

These correlations show that for volumetrically heated pools with gas injection at the boundaries, the downward and sideward Nusselt numbers for porous boundaries are comparable. This is in contrast to the natural convection case where sideward Nusselt numbers are significantly higher than the downward Nusselt numbers.

Chapter 1

INTRODUCTION

The heat and mass transport phenomena taking place in volumetrically heated fluids have become of interest in recent years due to their significance in assessments of fast reactor safety and post-accident heat removal (PAHR).

To ensure the safety of the public, extensive investigations have been conducted to determine possible accident scenarios for the Liquid Metal Fast Breeder Reactor (LMFBR). To this extent, two highly unlikely accident scenarios, the transient over power (TOP) and the loss of coolant flow (LOF) have been defined [G1]. Following a worst case LOF or TOP scenario a Hypothetical Core Disruptive Accident (HCDA) may lead to possible meltdown of the core and reactor internals. The core debris melting through the reactor vessel and guard vessel may eventually contact the concrete of the reactor cell floor.

The interaction of the core debris with the concrete as well as the melting of the debris pool into the concrete will significantly affect efforts to prevent breaching of the containment and the resultant release of radioactive effluents to the environment. Release of large amounts of water vapor and CO_2 gas from the melting concrete may cause eventual overpressurization of the containment building. In addition, hydrogen gas may be produced as a result of interaction of the water vapor with molten steel or sodium.

To assess the integrity of the containment, it becomes necessary to determine the heat transfer paths from the debris pool heated by the radioactive decay of the dissolved fission products to the surrounding environment. To date, most work on volumetrically heated pools has focused on natural convection phenomena. The intent of this study is to experimentally simulate the evolution of gas at the concrete boundary and investigate the effects of gas release at the boundary of a volumetrically heated pool on the heat transfer rates along the boundaries. In particular, the effect of gas release on the relative amounts of pool power convected in the downward and sideward directions will be examined. Such information is necessary for predicting the evolution of pool shape along the transient. A comparison of these results with those previously reported for natural convection will then be made.

Chapter II provides a background on the PAHR problem and summarizes previous investigations on heat and mass transfer in volumetrically heated pools. Chapter III describes the experimental apparatus and procedures used in this investigation. The results of this study are presented in Chapter IV and a summary of the conclusions made is given in Chapter V.

Chapter II

BACKGROUND

II.1 Problem Definition

In looking at the heat transfer problems associated with the molten core debris-concrete system, it is necessary to have an understanding of the basic physical phenomenon involved. The material reaching the concrete will consist primarily of fuel and structural steel, with the possiblity of some liquid sodium remaining. The magnitude of the decay heat associated with the debris will be strongly influenced by such factors as the original disposition and state of the fuel and other molten material, the effect of fuel-coolant interaction, the disposition of fission products, and the manner in which the hot fuel reaches the retention structure as well as the elapsed time [C1].

Layering of the steel above the volumetrically heated fuel is expected since steel is immiscible in UO_2; various combinations of solid, molten, and boiling layers in both the steel and fuel are possible. The steel layers will also be volumetrically heated, although to a lesser extent, as a result of induced radioactivity from gamma decay in the fuel and the diffusion of fission products from the fuel into the steel. Figure 1, taken from a summary of PAHR technology by Kazimi [K1], shows relative contributions to the decay heat of an LMFBR equilibrium core following shutdown. The decay heat from stainless steel activation can be seen to produce a greater percentage of

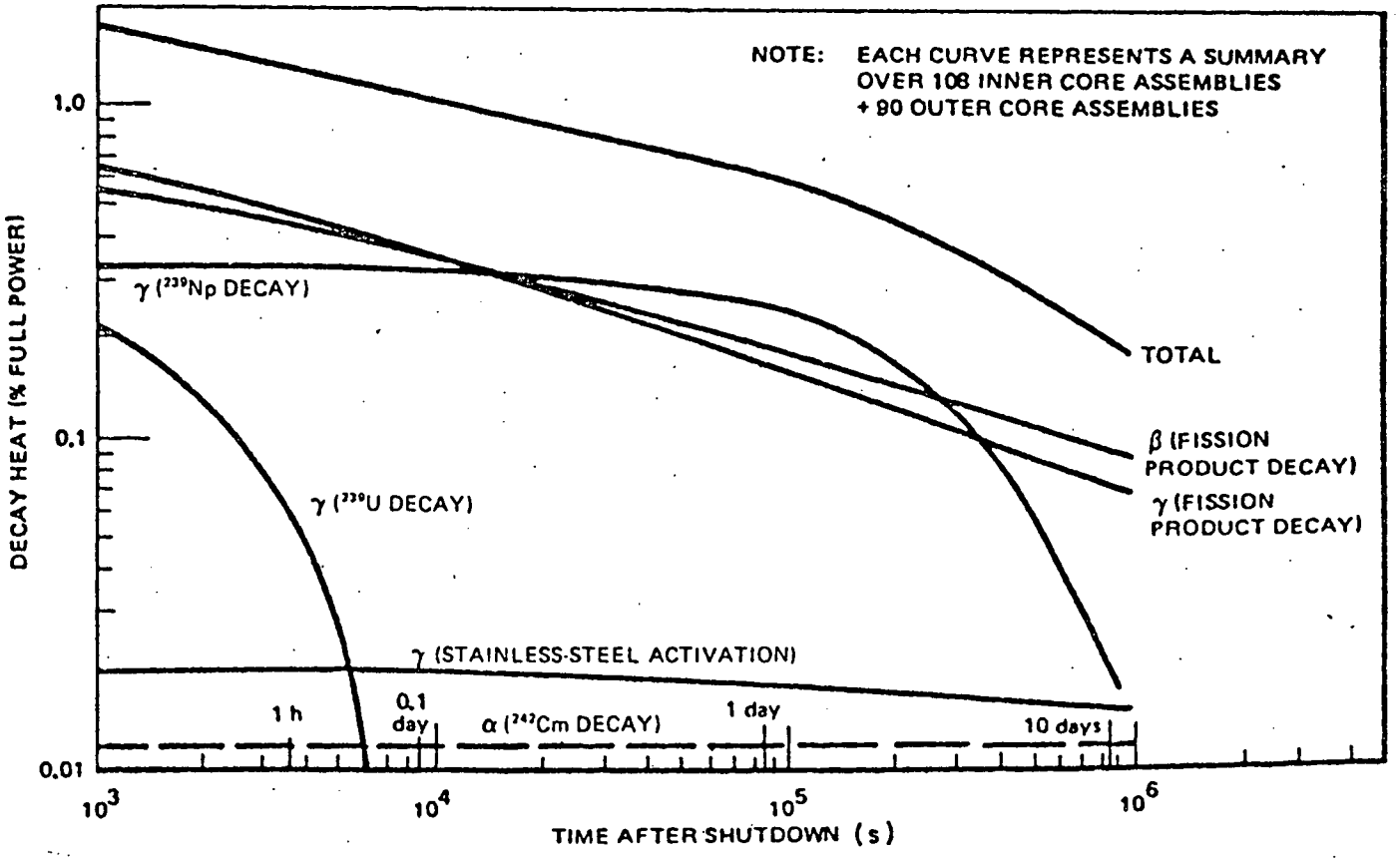

Figure 1. Fission Product Decay Heat of LMFBR Equilibrium Core (Taken from Kazimi and Chen [K1]).

the generated heat as time after shutdown increases. Figure 2, also from [K1], shows the approximate distribution of fission product decay heat among the fuel, steel, and gaseous phases. The fraction of fission product heat in the UO_2-PuO_2 fuel phase is seen to dominate at longer times following shutdown.

The concrete forming the boundary of the system is characterized by its high water and CO_2 content. Typical values are 9 wt % water (of which 55% is evaporable and 45% is combined as water of hydration) and 26 wt % CO_2 [B1]. Heating and melting of the concrete will result in large amounts of water vapor and CO_2 being released. Values in the range of 200 ft^3 at STP/ft^3 of concrete for both water vapor and CO_2 have been reported [M1].

As the debris melts into the concrete it is expected that the lower density oxides of concrete will rise into the melt and mix with the fuel oxides reducing the volumetric heat generation rate. Large scale tests with actual materials being conducted at Sandia and Argonne provide useful information on the gross effects of melt-concrete interactions. Experiments with molten UO_2 and concrete by Baker, et al. [B1] indicate that concrete oxides are mutually soluble with UO_2 and oxides derived from stainless steel. Powers, et al. [P1] report distinct stratification of the oxide and steel layers in molten steel-concrete experiments. The melt is vigorously agitiated by gas-induced forced convection with surface crust formation observed only for the oxides melt. The erosion rate is dependent on the heat flux or melt temperature. This is consistent with the large scale heat

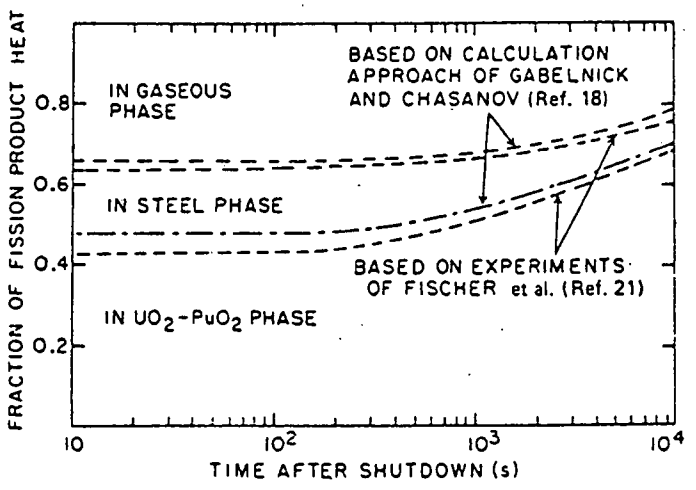

Figure 2. Distribution of Fission Product Decay among the Fuel, Steel, and Gaseous Phases. (Taken from Kazimi and Chen [K1]).

flux tests carried out by Muir, Powers, and Dahlgren [M2] who determined that the dominant erosion mechanism for concrete is the melting of the cementitious material accompanied by dehydration and decomposition of the concrete beneath the melt. Partitioning of heat in the different directions for the molten steel-concrete system was found to be dependent on the gas generation rate with estimates of 21% to 32% transported into the concrete. Spallation and reinforcing steel in the concrete were found to have insignificant effects on the interactions.

In order to determine the eventual disposition of the molten core debris following a HCDA it is necessary to investigate the heat and mass transfer processes involved. Modelling of the system is complicated by the uncertainties in core debris composition upon reaching the concrete interface. As mentioned earlier, layering of fuel, steel, and sodium may occur in several postulated configurations leading to variations in the thermal boundary conditions. It is desirable then to solve the single layer heat transfer problem and combine results to obtain a solution for the multilayered case. Fieg [F1] has shown experimentally that the heat transfer through stratified liquid layers may be expressed fairly well in terms of the known heat transfer characteristics of single fluid layers.

Although solutions for non-volumetrically heated layers are well defined, the same is not true for volumetrically heated layers. The intent of this study then is to investigate heat transfer from volumetrically heated pools in relation to PAHR studies. As Peckover indicated in Ref. [P2], by considering only the volumetrically heated

layer, the number of possible boundary conditions may be reduced. The upper surface may be modelled as an isothermal boundary at the melting temperature of the overlying solid crust of oxides or as a free surface. The lower boundary may be modelled as isothermal at the melting temperature of the concrete bed or possibly approximated as adiabatic for low heat conducting barriers.

II.2 Natural Convection in Volumetrically-Heated Pools

Early studies of volumetrically heated pools were concerned with natural convection effects. A nondimensional parameter may be defined, the internal Rayleigh number, that couples the volumetric energy generation rate to the natural convective motion in the fluid.

$$Ra_I = \frac{g\beta}{\alpha\nu} \Delta T^* L^{*3},$$

where ΔT^* is the characteristic destabilizing temperature difference and L^* is the characteristic length of the system. It may also be considered as the ratio of the buoyant forces to the viscous forces times the ratio of heat convected to the heat conducted. For the purposes of this study, ΔT^* will be defined as the temperature difference produced in a volumetrically heated fluid with isothermal upper and lower boundaries when only conduction is considered:

$$\Delta T^* = \frac{QL^2}{8k},$$

where Q is the heat generation rate per unit volume of the pool. The characteristic length L^* will be defined as L/2 where L is the layer depth. The internal Rayleigh number then becomes

$$Ra_l = \frac{g\beta}{\alpha\nu} \frac{QL^5}{64k}$$

To allow comparison, correlations by other authors presented in this report will be adjusted to the preceding definition.

Early qualitative work by Tritton and Zarraga [T1] and Schwab and Schwiderski [S1] showed the general convective motion for internally heated fluids with Ra/Ra_c less than 80 to be different than that of Bénard convection with downflow in the center of the cell rather than along the walls. For a given set of boundary conditions the critical Rayleigh number, Ra_c, is defined as the minimum Rayleigh number necessary to initiate convection in the fluid.

Quantitative investigations were carried out by Kulacki and Goldstein [K2] using interferometric techniques to measure temperature distributions in a volumetrically-heated fluid layer between two isothermal horizontal plates. They found that for Rayleigh numbers only slightly above critical values the maximum temperature occurs above the geometric center. Figure 3 shows a schematic of the temperature distribution of the layer. Buoyancy effects of the warm central region apparently cause the assymetrical temperature distribution and the resultant different rates of energy transport at the upper and lower boundaries. They summarized the observed motion fields in terms of the internal Rayleigh number as follows:

a) gentle laminar convection with conduction still important for $Ra_c \leq Ra_l \leq 5 \times 10^3$,

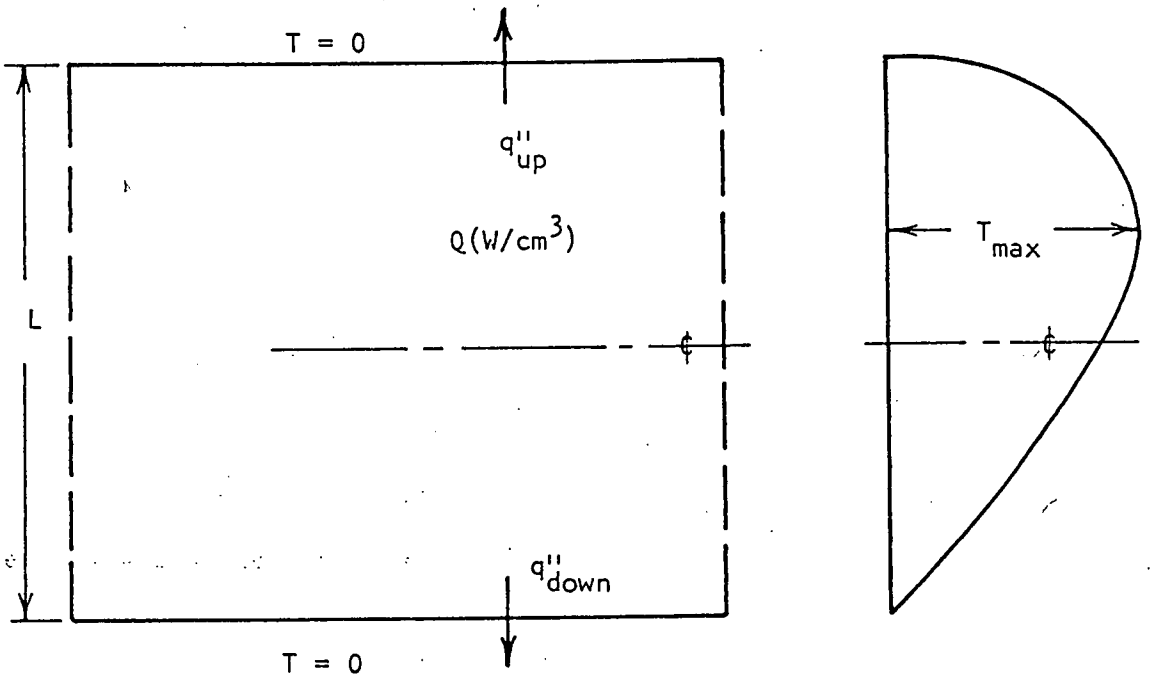

Figure 3. Schematic of Temperature Profile between Two Isothermal Plates in a Volumetrically Heated Fluid layer.

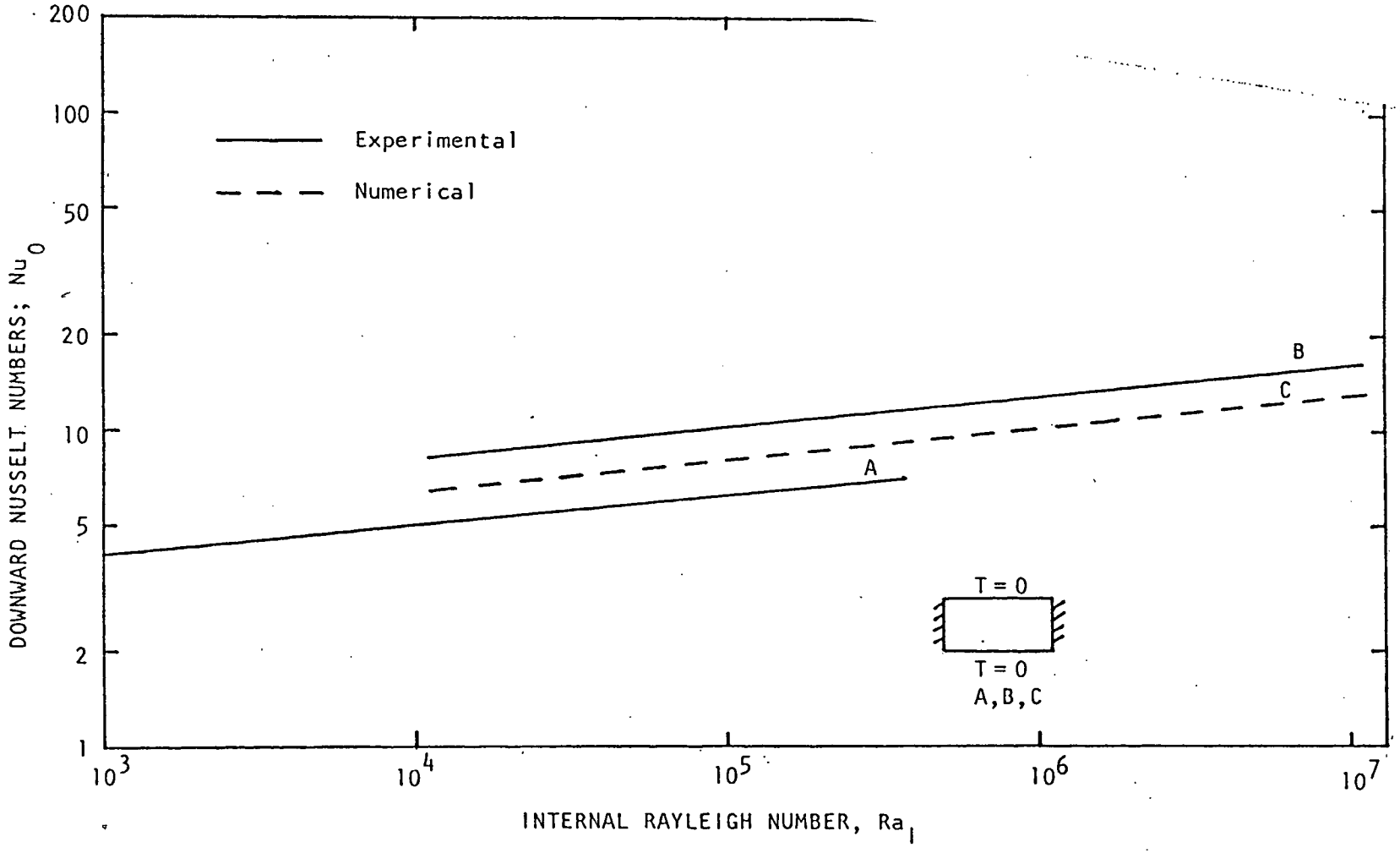

Figure 5. Downward Nusselt Number vs. Internal Rayleigh Number for Two-Dimensional Rectangular Cavities. (See References in Table I.)

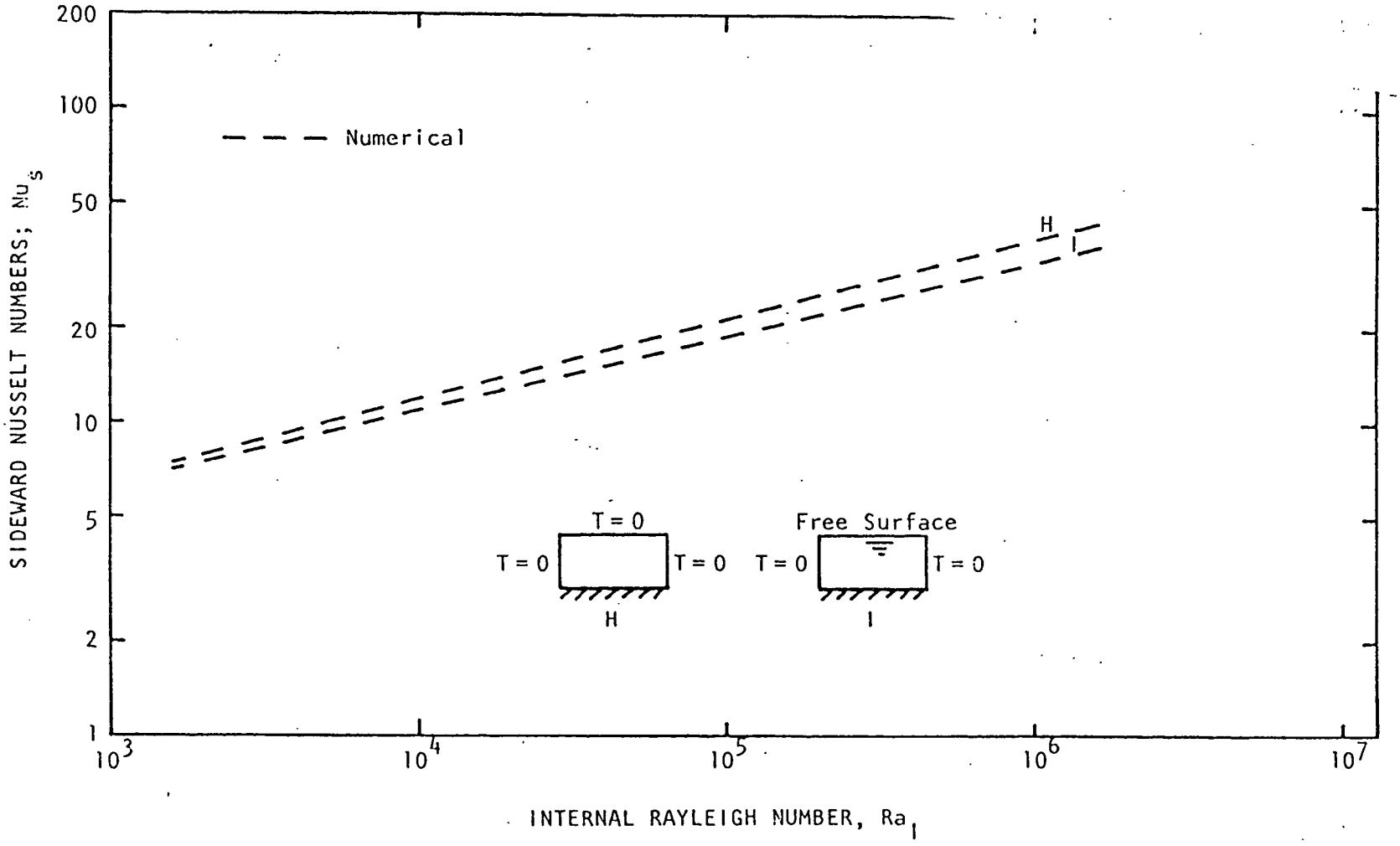

Figure 6. Sideward Nusselt Number vs. Internal Rayleigh Number for Two-Dimensional Rectangular Cavities. (See References in Table 1.)

This trend is shown in Figure 7 where the upward, sideward, and downward Nusselt numbers are plotted as a function of the internal Rayleigh number for three different boundary conditions. In terms of the PAHR problem it is instructive to look at the relative fractions of heat that would flow up to containment versus into the concrete for the models presented. The upward power fraction, η_{up}, may be defined in terms of upward, sideward, and downward Nusselt numbers as

$$\eta_{up} = \frac{Nu_1}{Nu_1 + 2(\frac{L}{W})Nu_s + Nu_0}$$

The upward power fraction, η_{up}, is shown in Figure 8 as a function of the internal Rayleigh number. For models with adiabatic sidewalls, the fraction of power removed from the upper surface is dominated by the upward Nusselt number variation with Ra_1 and increases with Ra_1. For models with isothermal sidewalls, the majority of heat is removed from the side and upper surfaces, and the fraction of power carried upward varies little with Ra_1.

Figures 9 through 12 present the same comparisons for the cylindrical cavity cases presented by Kulacki, et al. [K3]. The same effects of Nusselt number variation with Ra_1 are observed as were seen in the rectangular cavities. Figure 12 shows the upward power fraction, η_{up}, as a function of Ra_1. For the cylindrical cavity, η_{up} is defined as:

$$\eta_{up} = \frac{Nu_1}{Nu_1 + 4(\frac{L}{D})Nu_s + Nu_0}$$

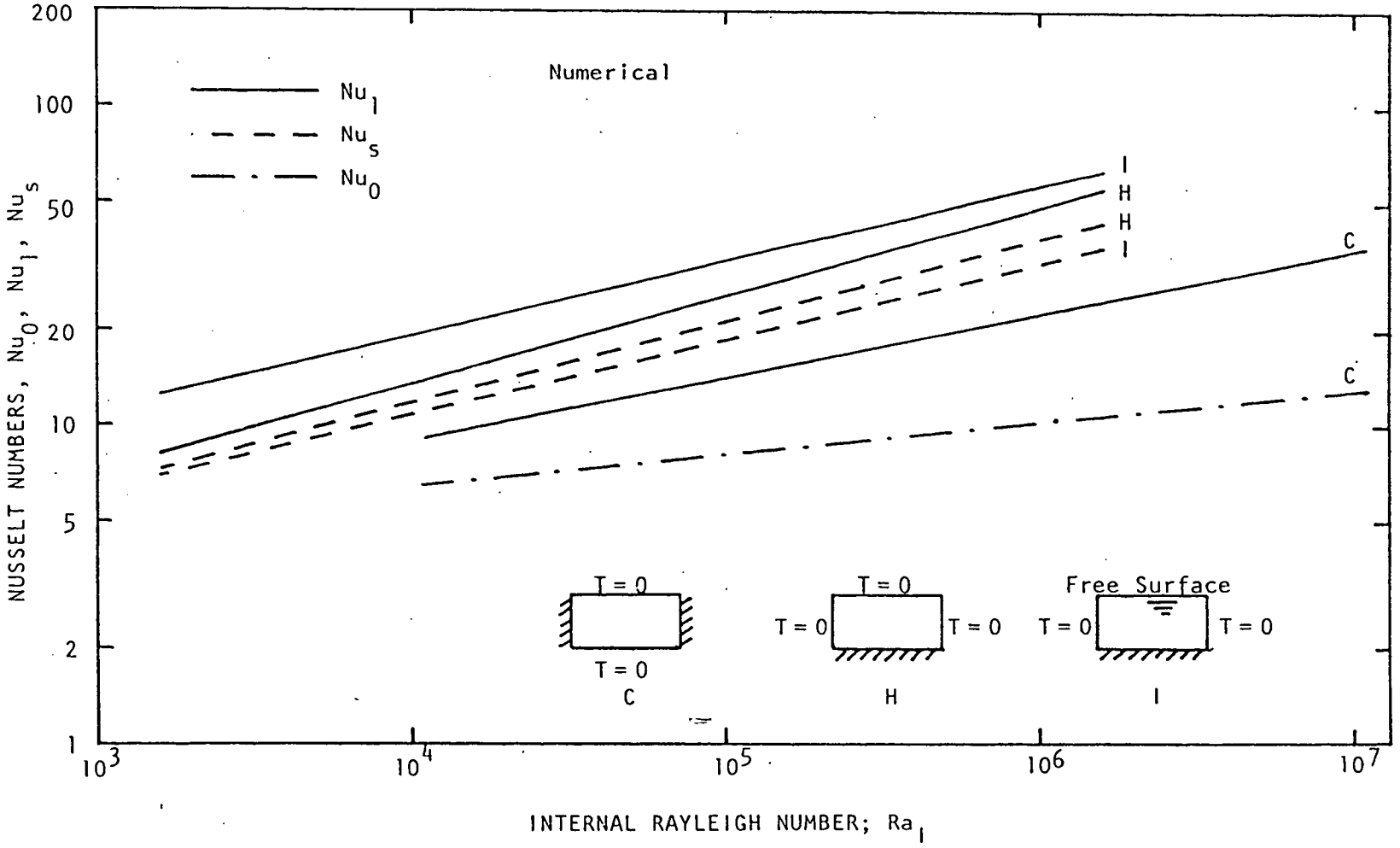

Figure 7. Comparison of Upward, Sideward, and Downward Nusselt Numbers vs. Internal Rayleigh Number for Two-Dimensional Rectangular Cavities. (See References in Table 1.)

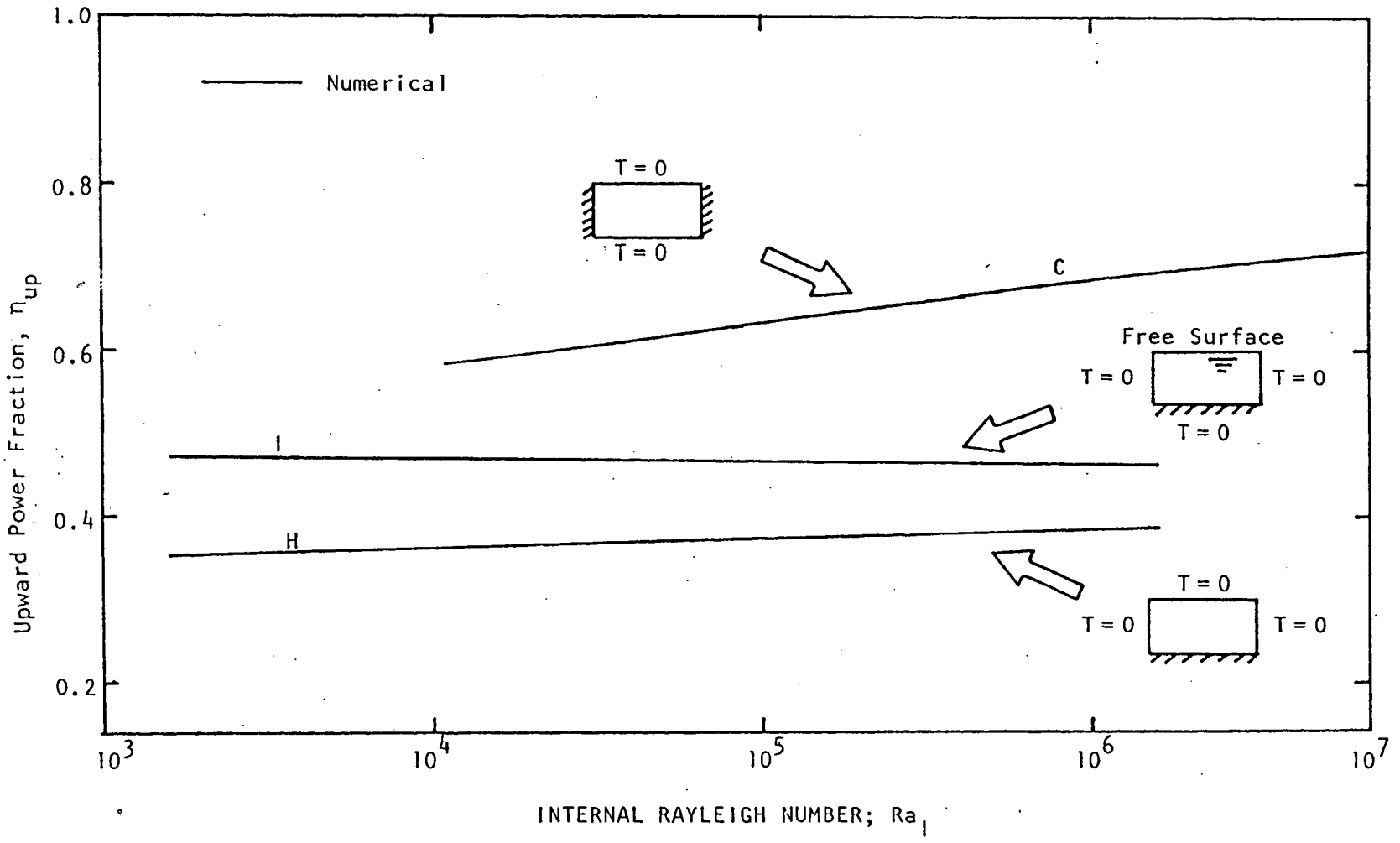

Figure 8. Fraction of Heat Transferred in the Upward Direction, η_{up}, vs. Internal Rayleigh Number For Two-Dimensional Rectangular Cavities. (See References in Table 1.)

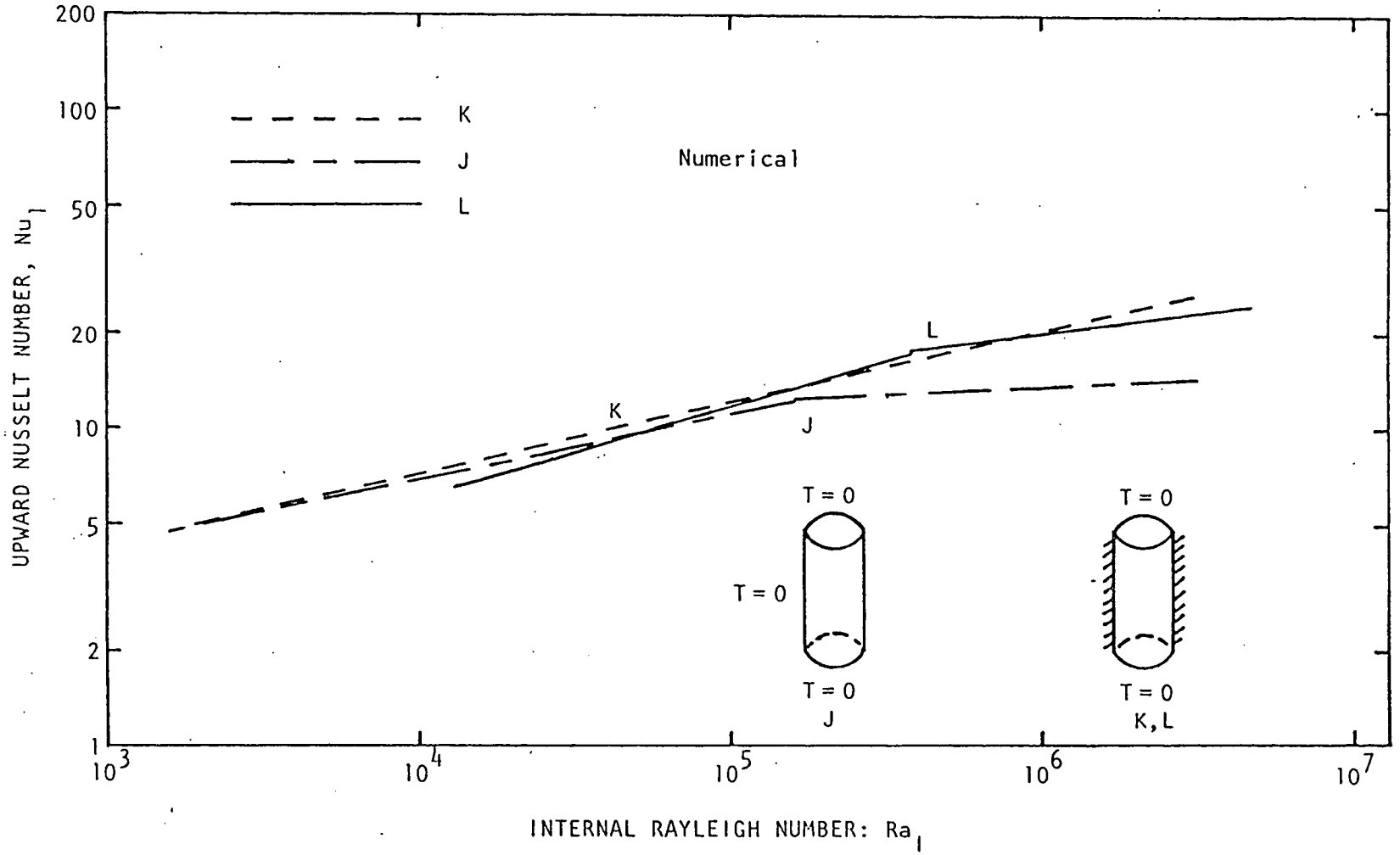

Figure 9. Upward Nusselt Number vs. Internal Rayleigh Number for Cylindrical Cavities. (See References in Table 3.)

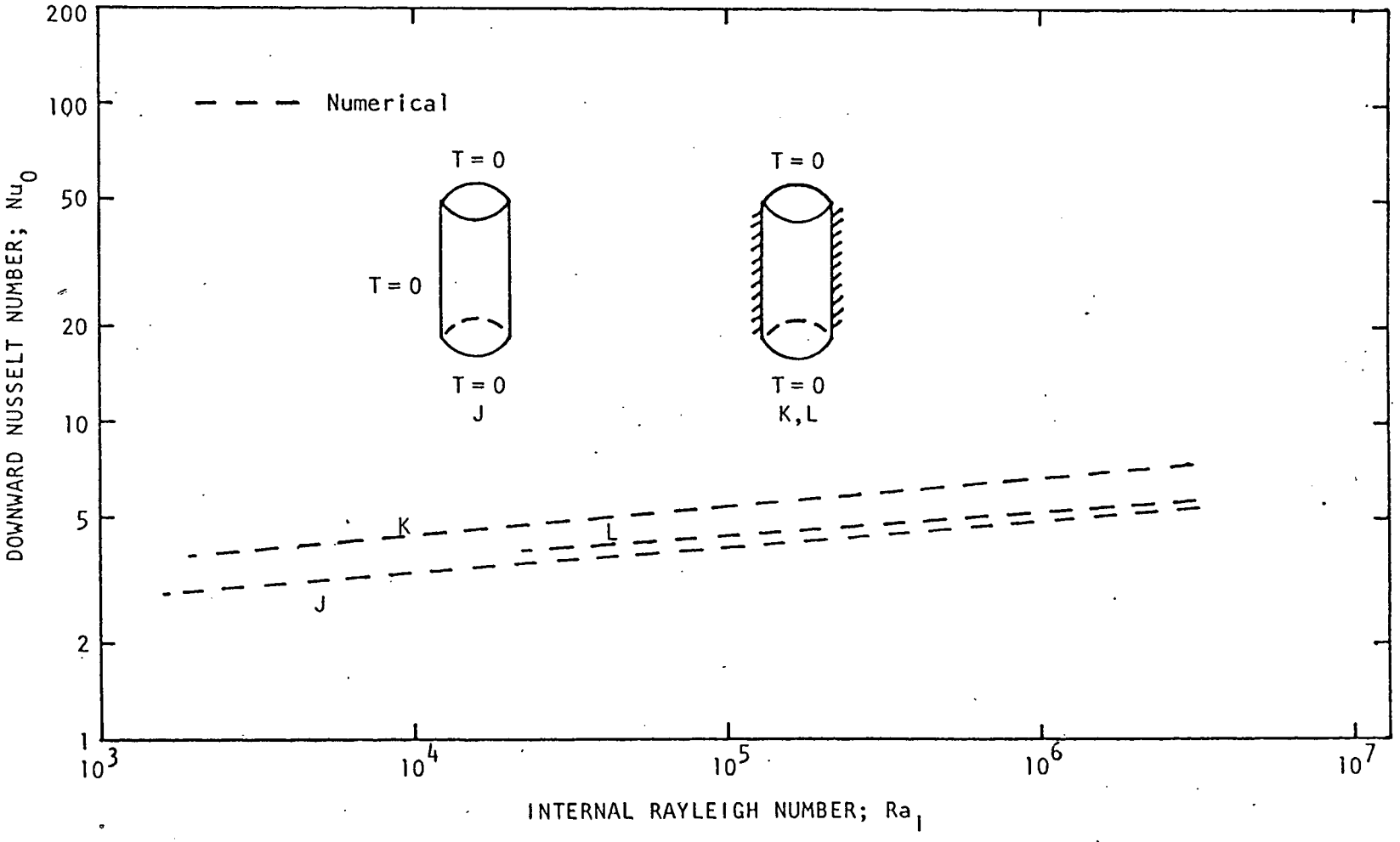

Figure 10. Downward Nusselt Number vs. Internal Rayleigh Number for Cylindrical Cavities. (See References in Table 3.)

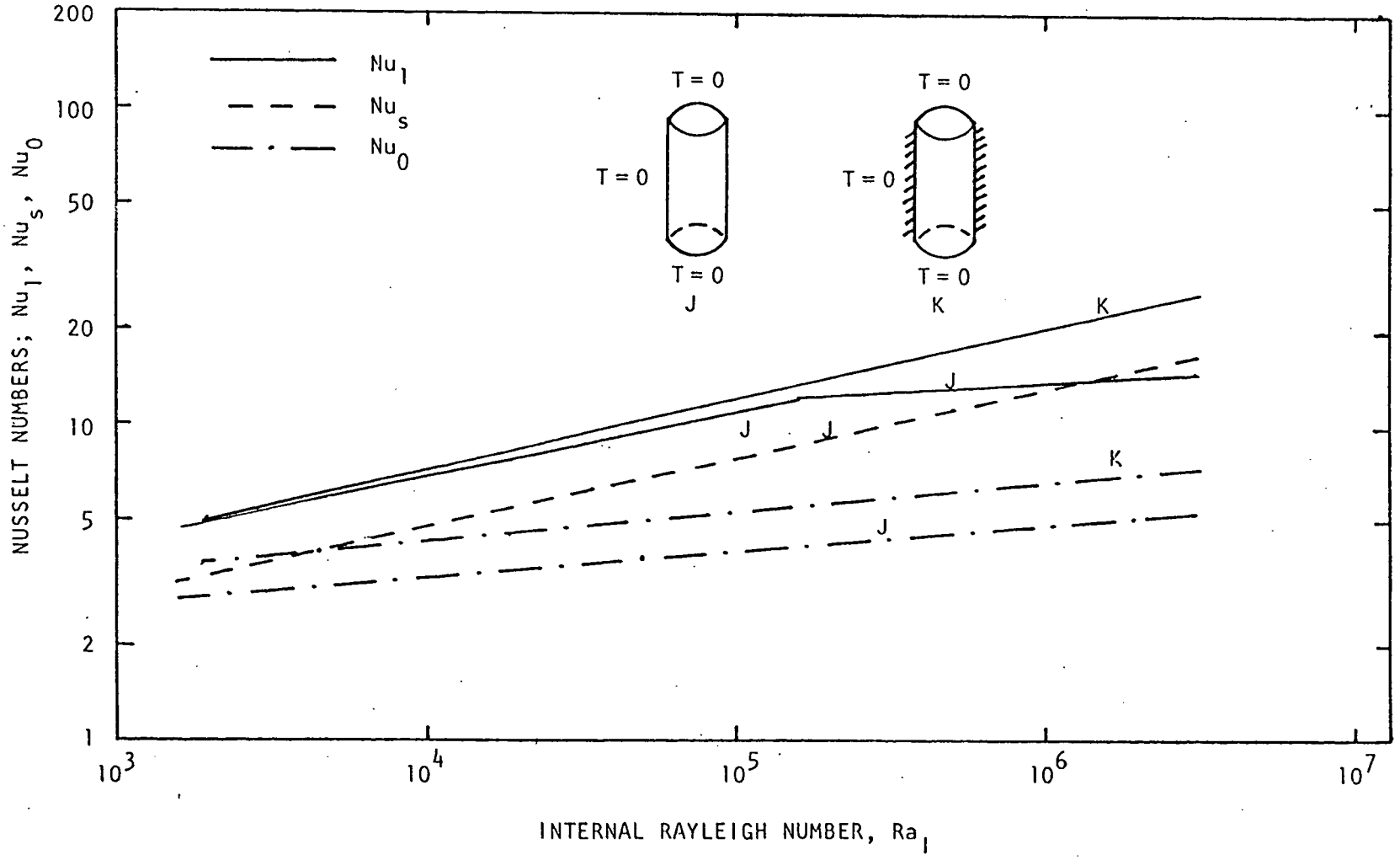

Figure 11. Comparison of Upward, Sideward, and Downward Nusselt Numbers vs. Internal Rayleigh Numbers for Cylindrical Cavities. (See References in Table 3.)

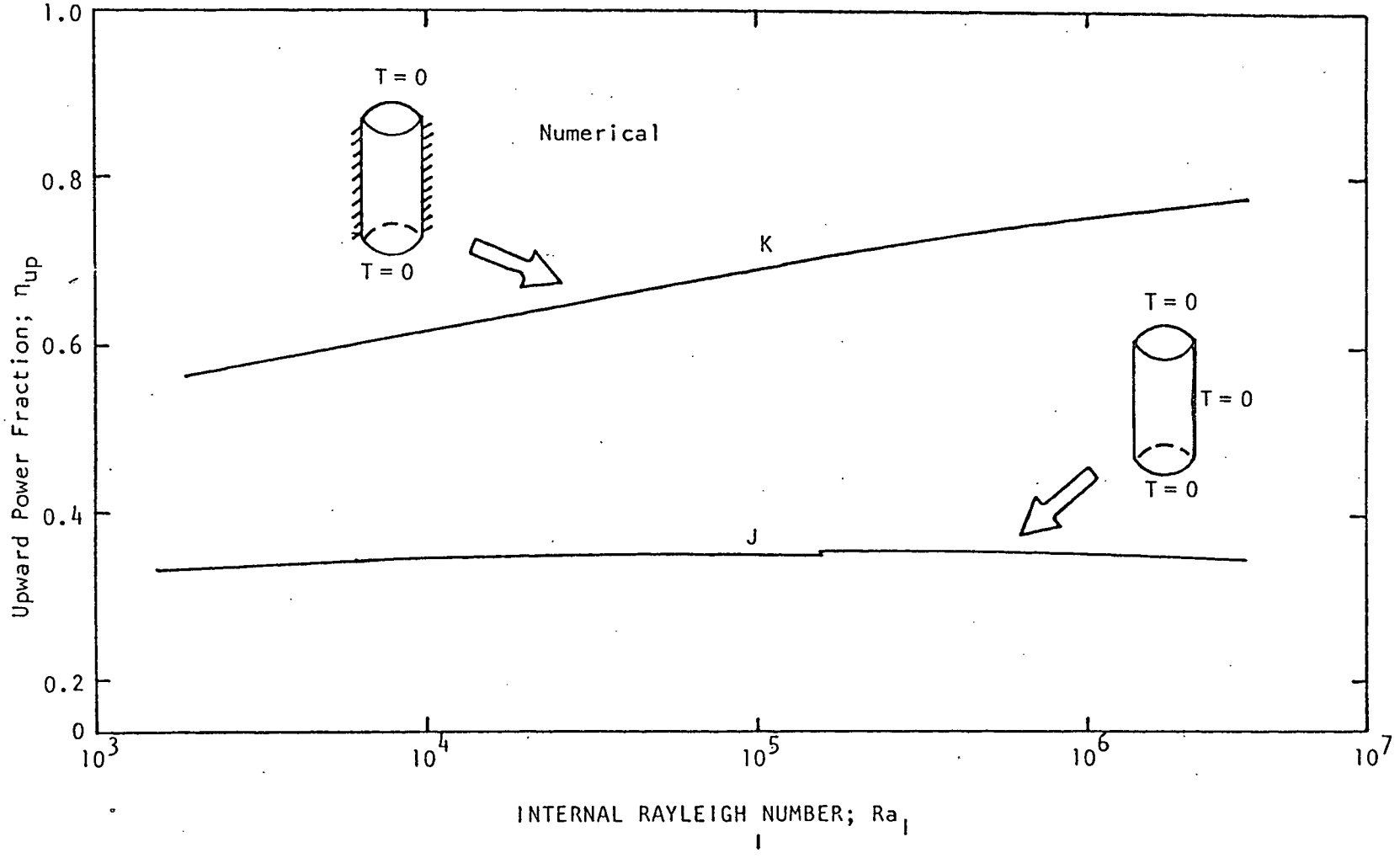

Figure 12. Fraction of Heat Transferred in the Upward Direction η_{up}, vs. Internal Rayleigh Number for Cylindrical Cavities. (See References in Table 3.)

Again, as in the rectangular case, η_{up} increases with Ra_I for the case with adiabatic sidewalls. For both the rectangular and cylindrical cavities, the upward power fraction does not appear to be strongly dependent on the lower boundary condition, but is dependent on the side and upper boundary conditions. Figure 13 shows a comparison of Nusselt numbers with Ra_I between some of the rectangular and cylindrical cavity cases. In general, the correlations show similar behavior and magnitude.

II.3 Effect of Gas Release on Pool Behavior

Large scale experimental results have indicated the importance of the gas-induced convection effects on the core debris-concrete system. Although exact theoretical results are not available, there are several qualitiative heat transfer processes that may be looked at in assessing the effects of gas injection at the boundaries of volumetrically heated pools. Kudirka [K5] presented several processes - microconvection, vapor-liquid exchange, and convective area reduction - as being important to heat transfer in air-water systems. The microconvection mechanism is the turbulence increase in the boundary layer caused by the evolving gas bubbles as they leave the surface. The vapor-liquid exchange mechanism is the displacement of colder fluid at the wall into the hotter fluid body with the hotter fluid moving into the wall following the disturbance. This displacement in volumetrically heated layers is the opposite of that for heated walls since the fluid near the wall is hotter than that of the

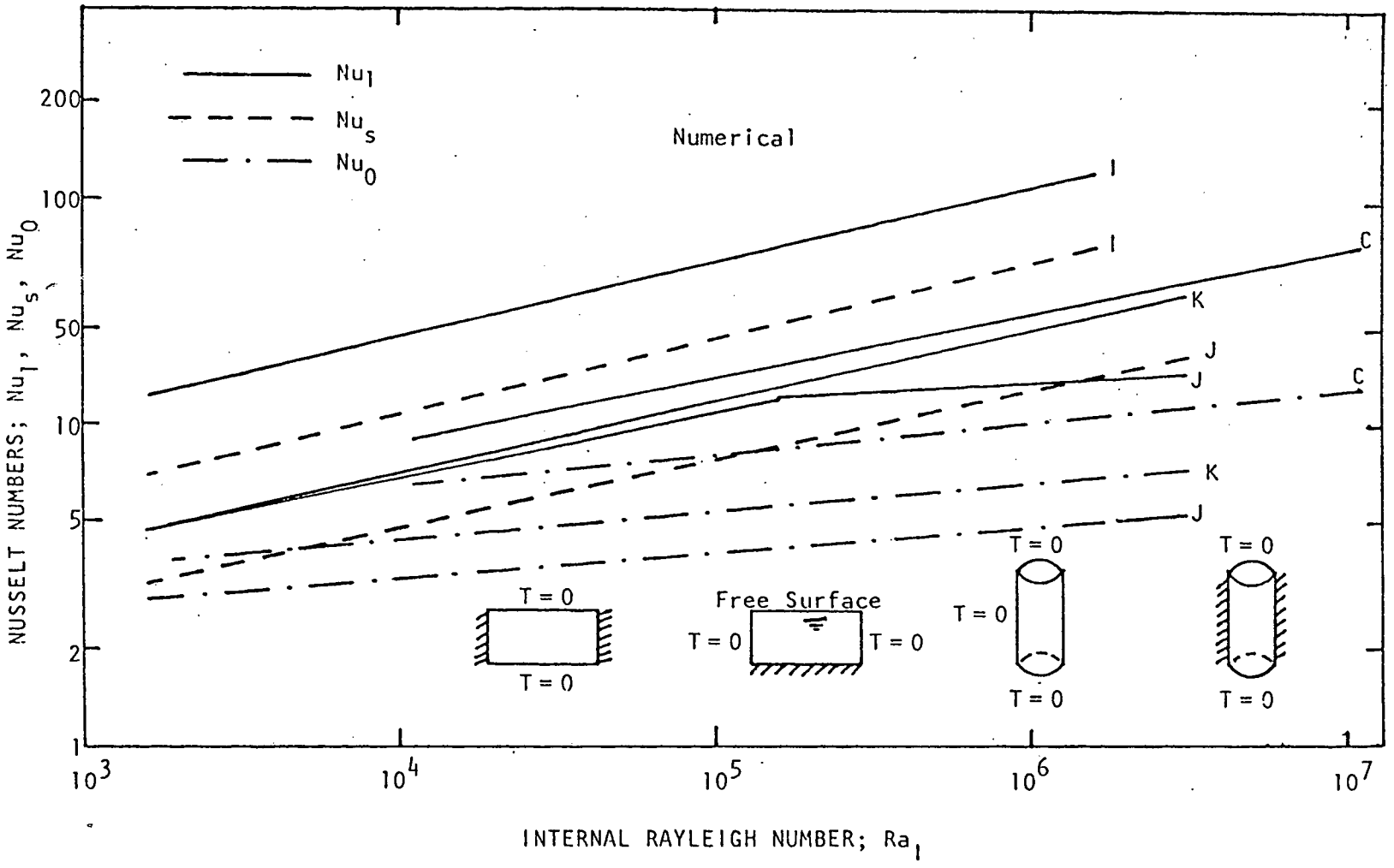

Figure 13. Comparison of Upward, Sideward and Downward Nusselt Numbers for Cylindrical and Rectangular Cavities. (See References in Tables 1 and 3.)

main body in the heated wall case. However, in either case, this mechanism will increase the rate of heat transfer between the wall and the fluid. Heat transfer to the boundaries may eventually be impeded by convective area reduction as the time-averaged area occupied by gas bubbles becomes large compared with the total surface area. As well as reducing the effective boundary layer, gases rising through the fluid produce an essentially isothermal pool. For the molten debris-concrete system under consideration, gas evolution and the resultant vigorous mixing may also break up possible solidifying material on the surface.

Experimental studies on gas injection from porous surfaces into volumetrically-heated pools have been carried out by Abdel-Khalik and Felde [A1] and Bergholz and Bjorge [B2]. The present study is a continuation of [A1] and will be discussed in later sections. Bergholz and Bjorge looked at a cylindrical geometry with an isothermal porous lower boundary through which air was injected, adiabatic side walls, and a bounded, uncooled upper boundary. The heat transfer coefficient at the lower boundary, h_0, was found to be essentially independent of the internal Rayleigh number but dependent on the superficial gas velocity, V.

$$h_0 = 0.4487\ V^{0.396}\ W/cm^2 \quad \text{for } 0.036 \leq V \leq 5\ cm/s$$

$$1.6 \times 10^6 \leq Ra_I \leq 1.6 \times 10^9$$

where

$$V = \frac{\text{Volume Flow of Gas}}{\text{Surface Area of the Lower Porous Boundary}}$$

The heat transfer coefficient was found to depend slightly upon the pool depth, L, for small superficial gas velocities.

Small scale melt simulation studies have been carried out by Farhadieh and Baker [F3] and Felde, Musicki, and Abdel-Khalik [F4] who examined the evolution of volumetrically-heated pools in miscible solid beds. Farhadieh and Baker reported that the horizontal to vertical penetration rate is dependent on such parameters as the pool-to-bed density ratio, ρ_p/ρ_b, and the power density. The vertical penetration increases faster as ρ_p/ρ_b is increased. Greater power densities produce greater horizontal expansion. All pools were observed to penetrate to some depth before horizontal expansion became dominant. These results support the previously discussed variation of Nusselt numbers with Ra_l. Higher Ra_l as a result of power density increases and layer depth increases will result in greater sideward and upward Nusselt numbers compared with the downward Nusselt number. Felde, Musicki, and Abdel-Khalik [F4] extended the work of Farhadieh and Baker [F3] to determine the effects of gas evolution at the boundary. The evolution of gas from concrete was simulated by introduction of ammonium bicarbonate into a bed of polyethylene glycol wax. Aqueous solutions of potassium iodide and zinc bromide were used to simulate the molten core debris pool. Carbon dioxide gas is released at the pool boundary as the electrolytically-heated pool moves into the solid bed. In agreement with [F3] the results show that the pool height, L, initially increases at a faster rate than its width, W; however, the rate of change of L with time gradually decreases until the trend is reversed. Figure 14 [F4] shows this effect for pools

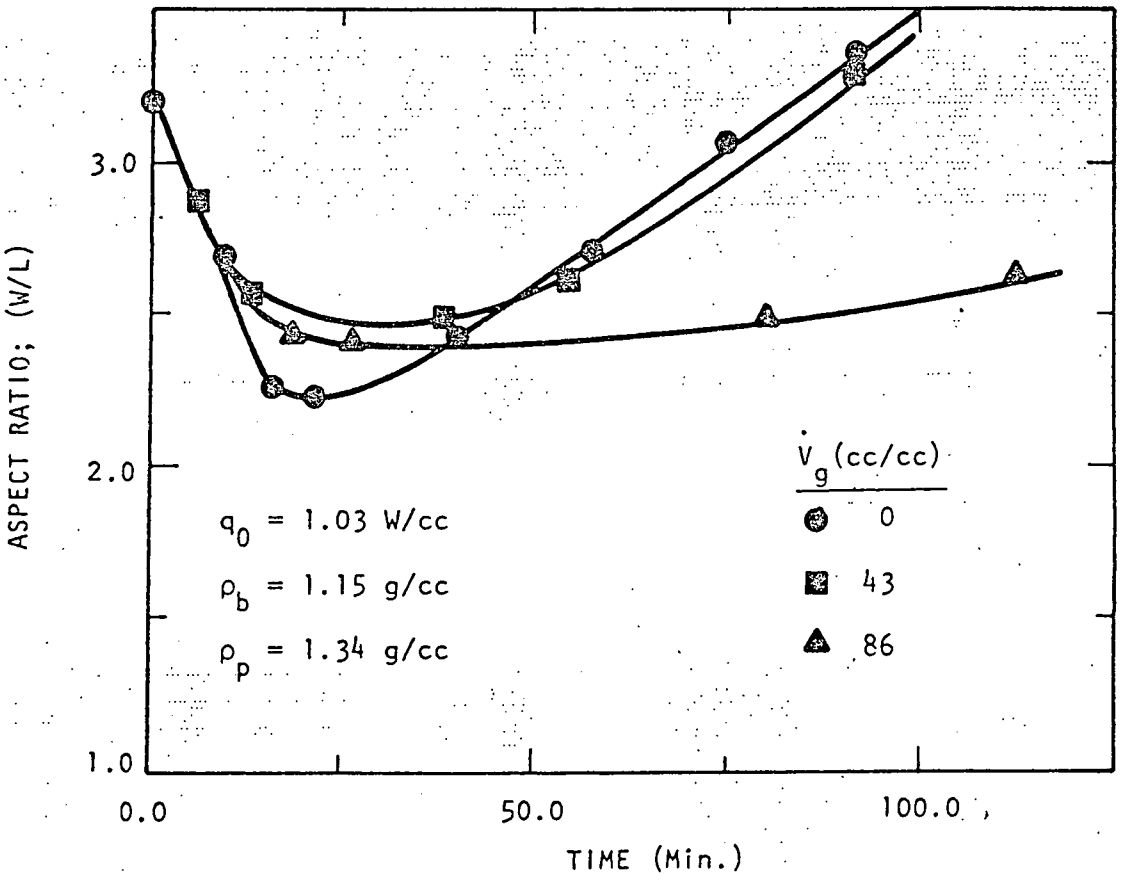

Figure 14. Effect of Gas Release at the Boundaries of a Volumetrically Heated Pool on Pool Growth Behavior.

with and without gas release at the boundaries. The highest gas velocity case shown is seen to produce a more even distribution of the volumetric energy produced in the pool at longer times. The characteristic time, τ_{min}, at which the pool reaches a configuration of minimum aspect ratio, $(W/L)_{min}$, is a function of the initial power density, q_0, and is slightly affected by both the initial density ratio and the gas release rate. Figures 15 and 16 from [F4] show the effect of the characteristic time, τ_{min}, for cases without and with gas release, respectively. As q_0 increases, τ_{min} is seen to decrease slightly. Again in agreement with [F3], the minimum aspect ratio, $(W/L)_{min}$, increases with the pool density ratio (ρ_p/ρ_b), i.e. pools of higher initial density tend to penetrate deeper into the solid bed. For higher pool densities the molten bed material rises more rapidly because of increased buoyancy forces. The enhanced convection along the lower boundaries apparently increases the Nusselt number and hence the downward penetration rate. The minimum aspect ratio slightly decreases with increasing gas evolution rate. However, for the same power level and initial density ratios, gas-releasing pools are always larger than those with no gas release, indicating that the fraction of heat transferred upward through the free surface decreases with the introduction of gas at the boundaries. Also, for times greater than τ_{min} the depth of a gas-releasing pool continues to grow at a rate nearly equal to that of the pool width whereas for pools with no gas release the pool depth increases at a much slower rate than its width.

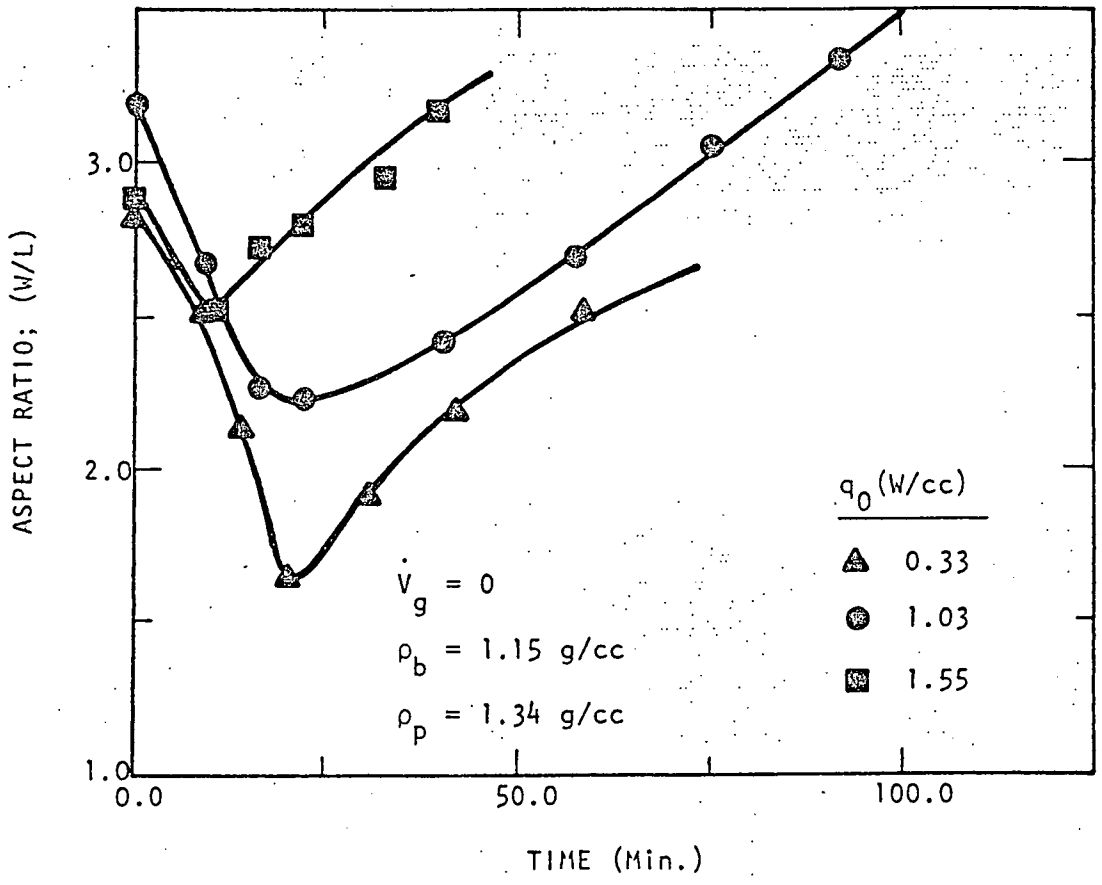

Figure 15. Effect of Power Density on the Growth of Volumetrically Heated Pools in Miscible Beds without Gas Release at the Boundaries.

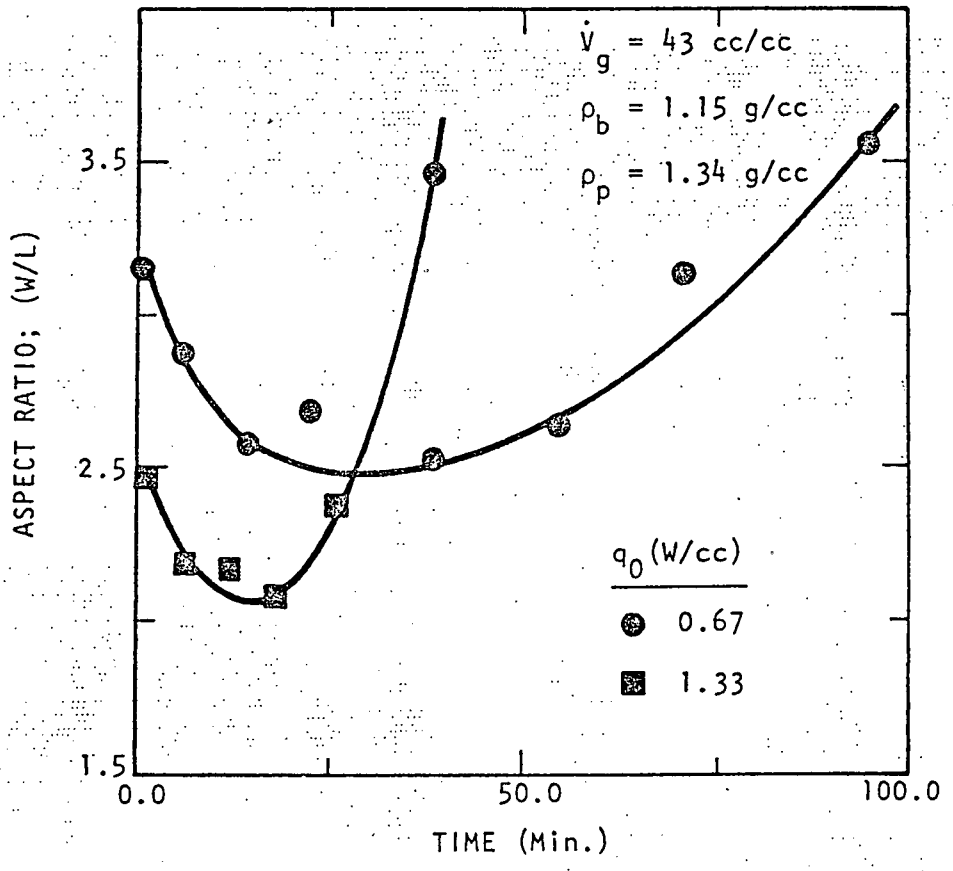

Figure 16. Effect of Power Density on the Growth of Volumetrically Heated Pools in Miscible Beds with Gas Release at the Boundaries.

The previous discussion clearly indicates that gas release from the concrete will significantly affect the evolution of the core debris pool. Hence, the objective of this study has been to quantify the effect of gas release at the boundaries of a volumetrically heated pool on the heat transfer rates in the different directions. Specifically, correlations for the sideward, downward, and upward Nusselt numbers in such systems will be obtained.

Chapter III

EXPERIMENTAL APPARATUS AND PROCEDURES

III.1 Experimental Apparatus

The design of the experimental apparatus is determined by two fundamental modelling requirements for the molten debris-concrete system, namely, the volumetric heat generation in the core debris and the gas evolution at the surface of the concrete. Simulation of volumetric heat generation is produced by Joule heating of an electrolyte solution. Simulation of gas evolution from the concrete is accomplished by forcing noncondensable gas, air, through porous plates which are used to construct the walls of the test cell.

A schematic diagram of the test cell used in this investigation is shown in Figure 17. The electrically-heated fluid (0.05 molar $CuSO_4$ solution) is bounded from the bottom and two sides by water-cooled porous brass plates mounted on 1.25 cm thick plexiglas frames. Air is injected into the test cell through these three porous plates. A limitation on using porous brass plates for the sides and lower boundaries simultaneously is incurred as a result of using the electrical heating method due to the current leakage that would result if plates adjacent to the electrodes are not insulated. An approximation to a porous surface is made by attaching a thin layer of Mylar insulation with a discrete number of holes onto the brass plates to allow for injection of gas into the pool. Power connections are available on all four plates so that either

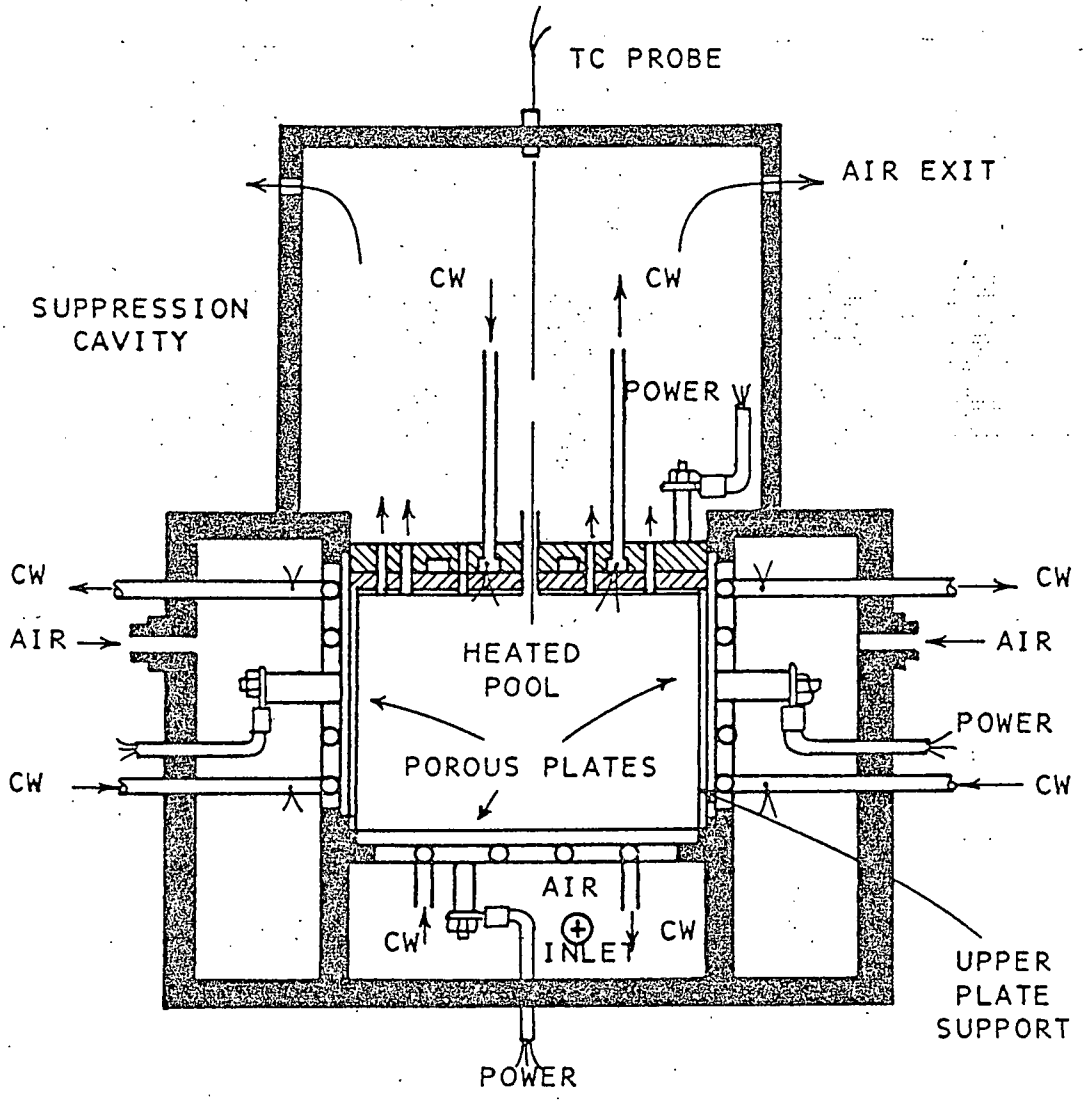

Figure 17: Schematic Diagram of the Test Cell Used in this Investigation.

the upper and lower plates or the two side plates may serve as electrodes for the passage of alternating current through the electrolyte solution. The other two plates not serving as electrodes during the experiment are covered with the Mylar film. Holes of 0.16 cm diameter are burned in the Mylar in a square grid of approximately 0.6 cm pitch. The front and back sides of the test cell are made of 1.25 cm thick plexiglas plates. The upper surface of the test cell is a water-cooled copper plate. The suppression cavity above the upper cooling plate (see Fig. 17) acts to prevent splashing of the solution as the injected gas escapes through holes drilled in the upper plate.

The fluid cell is 10.2 cm wide and 15.2 cm long with an adjustable height from 1.9 to 9.7 cm. Narrow plexiglas supports of selected heights for various aspect ratios are fastened into the front and back plates to allow setting of the aspect ratio at preset values in a repeatable manner.

A detailed diagram of the porous brass cooling plates is shown in Figure 18. The 14.6 x 9.5 cm porous brass plates are machined to produce a series of slots and fins (see Side View). The fins are soldered to the interlocking copper cooling plate to provide efficient heat removal capability. Air is supplied to the open channels between the fins and flows through the porous plate into the volumetrically-heated pool. Also shown in Figure 18 (Top View) is the cooling water flow channel machined into the 1.25 cm thick copper cooling plate. The double spiral water flow

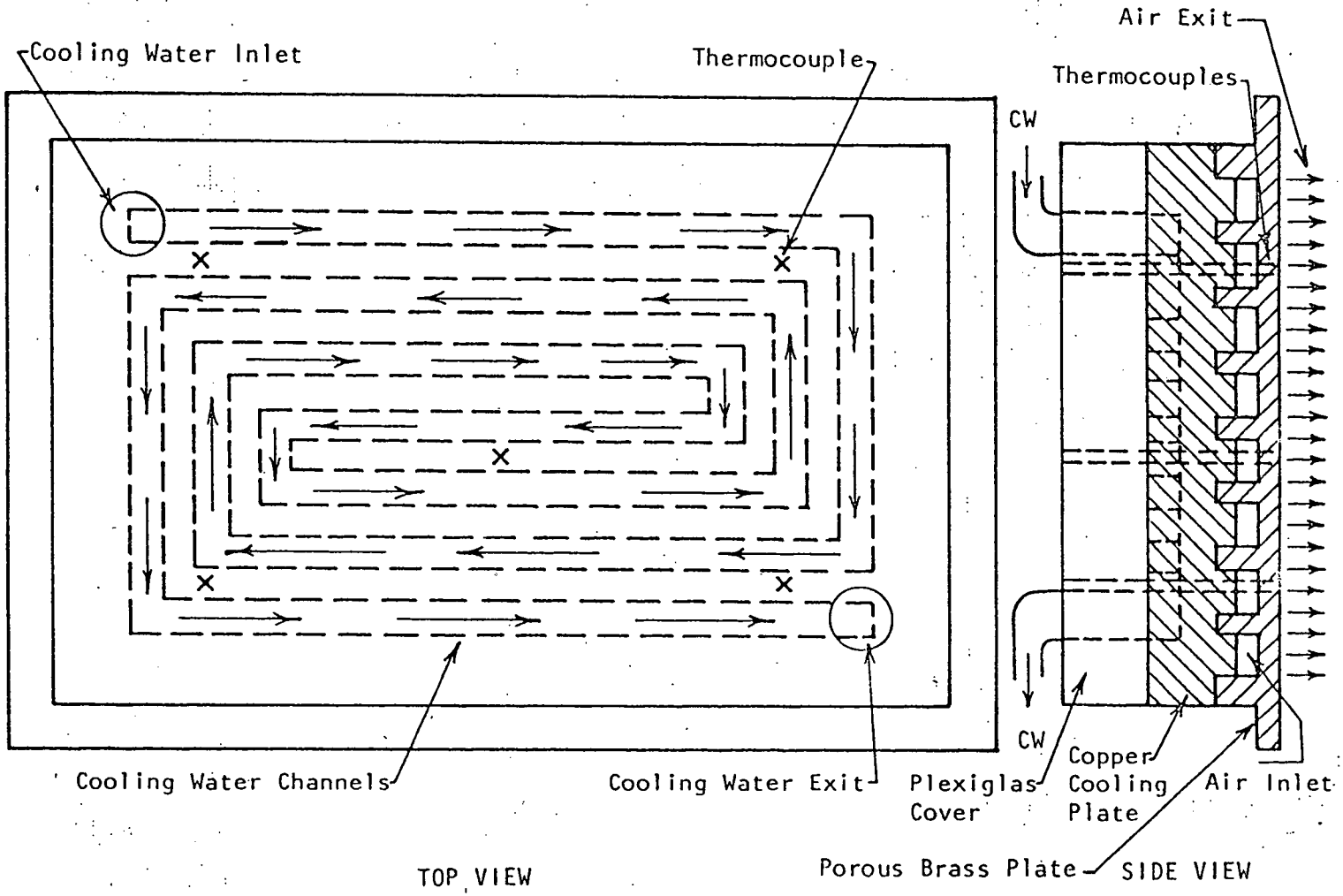

Figure 18. Porous Side and Bottom Plate Design .

pattern designed to alternate hot and cold legs of the flow path results in nearly-isothermal plates for all the conditions tested in the investigation. A plexiglas cover and rubber gasket seal the cooling channel of the cooling plate. The upper plate, shown in Figure 19, is constructed of copper and plexiglas and also utilizes the double spiral cooling water flow pattern. Holes of 0.40 cm diameter are drilled through the plates at the locations shown to allow for the escape of the injected gas from the pool.

Experimental measurements are made to provide information for making an energy balance over the system and determining the average Nusselt number for heat transfer to the boundaries of the system. The heat transfer rates to the different sides are determined by measuring their coolant flow rates and corresponding temperature rise of the coolant;

$$q = \dot{m}_w c_p \Delta T$$

where

q = heat flow to the plate (W)

$\dot{m}_w$ = mass flow rate of cooling water (kg/s)

c_p = specific heat capacity of water (J/kg°C)

ΔT = temperature rise of water across the plate (°C)

In addition, temperature measurement of the incoming air and the air leaving the test cell are made in order to estimate the amount of heat carried upward with the escaping air. The air is assumed to be dry when entering the cell and saturated with water vapor when leaving. The net heat removed by the air is then determined from the enthalpy

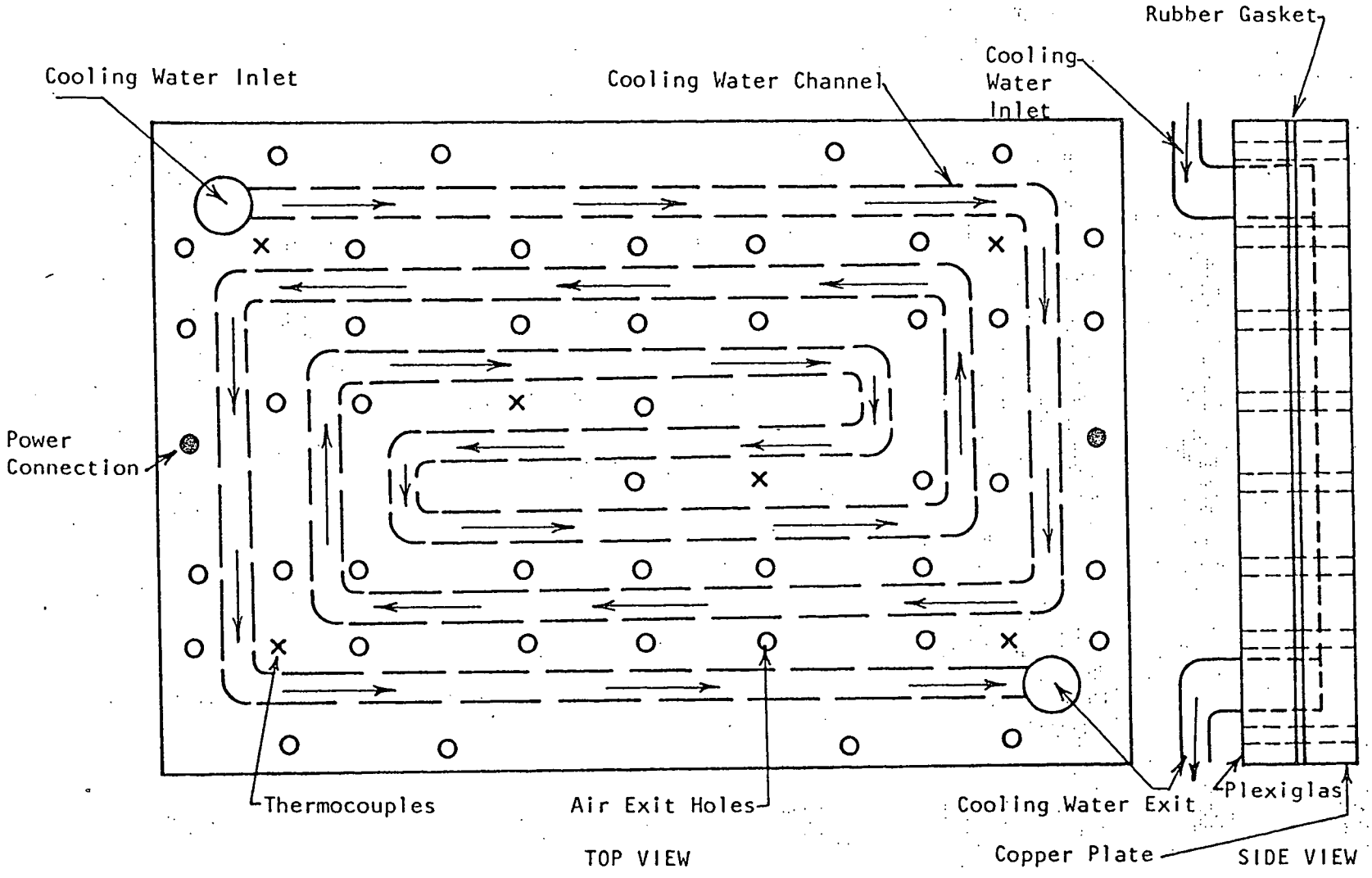

Figure 19. Schematic of Upper Plate Design

change and total mass flow rate of air using a psychrometric chart assuming standard pressure;

$$q_{air} = \dot{m}_{air}(h_{dry\ air}(T_{in}) - h_{sat\ air}(T_{out}))$$

where

q_{air} = heat removed by air

$\dot{m}_{air}$ = mass flow rate of air (kg/s)

$h_{dry\ air}(T_{in})$ = enthalpy of dry air at the air inlet temperature (J/kg)

$h_{sat\ air}(T_{out})$ = enthalpy of saturated air at the air exit temperature (J/kg)

The actual contribution of q_{air} to the energy balance was found to be very small, even for high gas velocities (less than 4% of total applied power).

Nusselt numbers are defined in terms of the rate of heat transfer to the plate, the measured maximum pool temperature and averaged plates temperatures, and the layer depth;

$$Nu = \frac{qL}{kA\Delta T}$$

where

q = rate of heat transfer to the plate (W)

L = layer depth (cm)

k = thermal conductivity of fluid (W/cm°C)

A = area of plate (cm^2)

ΔT = maximum temperature difference between the pool and the average of the measured plate temperatures.

Plate surface temperature of all four plates are measured using iron-constantan thermocouples distributed as shown in Figures 18 and 19. The thermocouples are made of 30 gage glass braid-insulated wire with a 0.08 cm welded junction. The thermocouples are soldered into the ends of bored-through tapered screws and wedged into the plates to a position nearly flush with the plate surface in contact with the pool.

Pool temperature is measured with a glass-encased iron-constantan thermocouple probe made of 30 gage teflon-insulated wire with a 0.08 cm diameter junction. The probe is inserted into the pool through the upper plate. A micrometer drive may also be attached to the probe to obtain vertical temperature distributions in the pool.

A schematic of the cooling water flow circuit is shown in Figure 20. Cooling water is supplied independently to each of the four cooling plates by a positive displacement Masterflex variable speed pump. A constant temperature source ($\pm$ 0.1°C) is maintained by two Haake KT 33 temperature baths. Flow integrators following the pumps act to reduce the cyclic output of the positive displacement pumps. Coolant flow rates are measured for each circuit using two calibrated Matheson Gas Products R7630 series rotameters (#604 and #605 tubes) in series in order to extend measurement range and accuracy.

Measurements of the inlet and outlet water temperatures are made using Yellow Springs Instruments 44202 linear thermistor net-

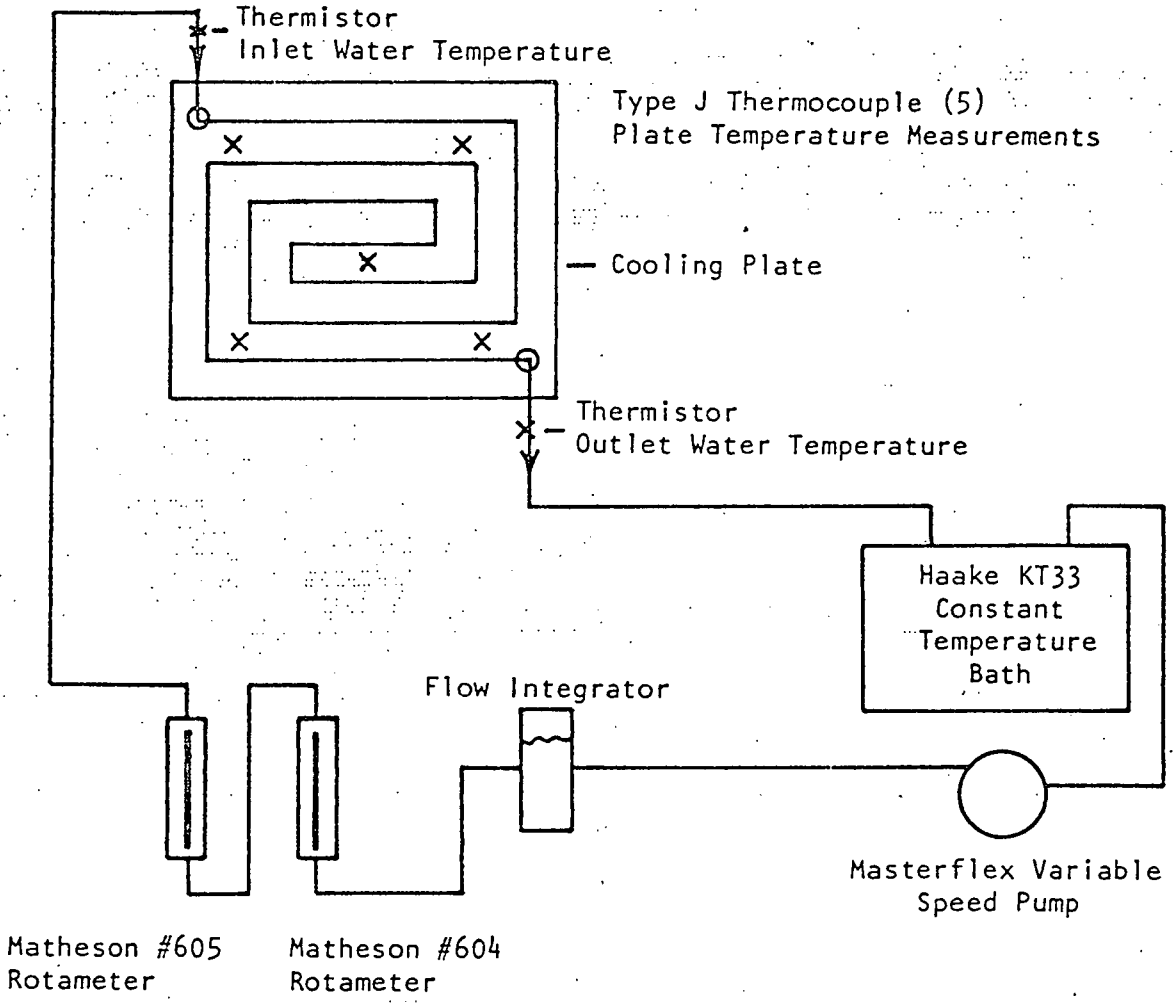

Figure 20. Cooling Water Flow Circuit

works sealed with epoxy in pyrex probes. The higher accuracy thermistors were chosen rather than thermocouples to allow greater flow rates and hence more uniform plate temperatures while maintaining reasonable accuracy for the temperature difference measurements (absolute accuracy of thermistors is $\pm$ 0.15°C).

The main frame box of the test cell is divided into three separate chambers so that gas may be injected into the fluid cell through the three porous plates at independently controlled rates. The air flow circuit is shown in Figure 21. Air is supplied from a house line through a filter and regulator. Air flow rates are measured with a Matheson Gas Products R7630 series (#603 tube) rotameters. Fine control is maintained with valves integral to the rotameter assembly. Temperature measurements of the incoming air and the air escaping through the upper plate are made using 0.08 cm diameter iron-constantan thermocouples. The inlet air temperature is measured in one of the three air chambers of the main frame box while the outlet air temperature is measured in the suppression cavity above the upper plate.

Output from the thermistors and thermocouples used in the experiment are collected and measured by a Monitor Labs 9300 data logger.

Power input to the fluid cell is varied by means of a Staco 140 V x 50 A variac. Applied power measurements are made using Simpson 0-300 V and 0-750 V dynamometer type wattmeters with rated accuracies of $\pm$ 2% of full scale.

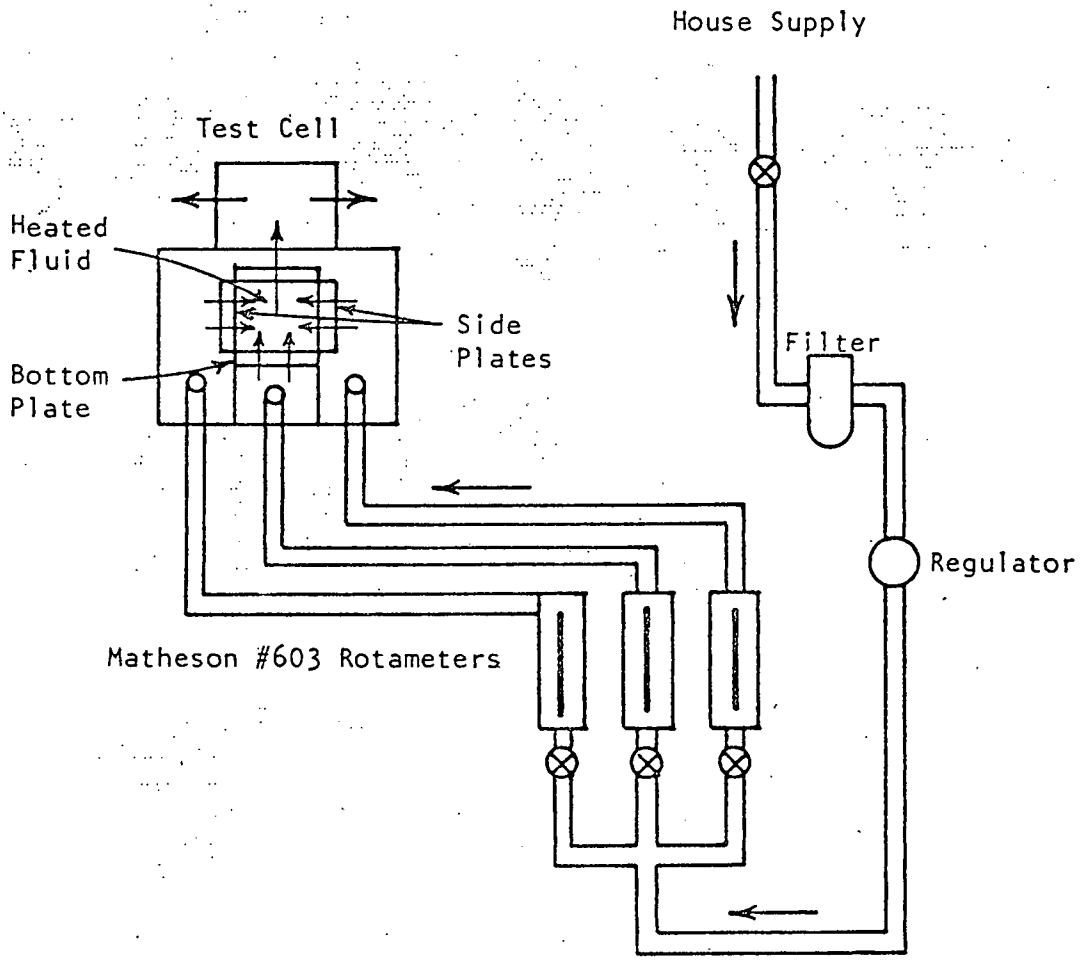

Figure 21. Air Flow Circuit.

The entire cell is thermally insulated using a 2.5 cm thick layer of styrofoam.

III.2 Experimental Procedure

Two modes of experiments have been conducted using this test cell. In the first type of experiments, the top plate is held in contact with the copper sulfate solution, while in the second type the top plate is held at a level 1.9 cm higher than the free surface of the electrically heated fluid. For the free surface case a brass wire mesh grid electrode (1.25 cm pitch) was suspended just below the surface of the pool and current was passed from the grid to the lower porous surface. The side plates were covered with the Mylar film. For the solid upper surface case, test runs were made with both a side-to-side electrode configuration and a bottom-to-top electrode configuration in order to investigate the characteristics of both porous side and porous lower boundaries as compared with the discrete holes of the Mylar covered boundaries. In addition, two different methods were used in the bottom-to-top electrode configuration in order to investigate the effects on power application of the observed partial unwetting of the upper plate with gas injection. Experiments were run with the current passed from a brass wire mesh grid electrode held slightly below the top plate to the bottom porous plate and from the upper cooling plate to the bottom porous plate. Results from the two methods showed little difference.

For the different boundary conditions discussed above, experiments have been conducted with different values of power input, pool height (i.e. aspect ratio), and superficial gas velocity. The range of experimental variables and the corresponding non-dimensional parameters are listed in Table 5.

Preparation for a test run begins with selection of aspect ratio and power level. The aspect ratio is set by installing the corner supports in the test cell and setting the upper plate in position. The constant temperature baths are brought to the proper temperature and cooling water flow to the plates is initiated. Once power is applied to the pool, flow rates are adjusted to the four cooling plates to produce a temperature difference of approximately 3°C across the plates in order to maintain the plates in a nearly-isothermal state. The pool center temperature and the water flow temperature differences across the cooling plates are monitored by the data logger during the experiment to determine when steady state conditions are reached. The power level is kept constant throughout the experiment. A period of 15 - 30 minutes is required for the test cell to reach steady state (experiments with gas injection reach steady state much faster than experiments without gas injection). At that point the water flow rates, inlet and exit water temperatures, air flow rates, inlet and exit air temperatures, plate temperatures, and maximum pool temperatures are recorded.

The initial run at each power level and aspect ratio is made without gas injection. Other experiments with different gas injection

TABLE 5

Ranges of Experimental Variables

And Non-Dimensional Parameters

Power Input (watt)	100 - 600
Pool Height (cm)	1.9 - 9.7
Superficial Gas Velocity (cm/min)	0.0 - 24.8
Internal Rayleigh Number	1.1×10^{5} - 1.1×10^{9}
Aspect Ratio (w/L)	1.05 - 5.31
Nondimensional Gas Velocity $(\frac{V^3\rho}{\mu g})$	5×10^{-10} - 5×10^{-3}

rates at the same power level and aspect ratio follow. The gas injection rate is increased for each of the succeeding runs. For each gas injection velocity, the pool center temperature and cooling water temperatures are monitored until steady state conditions are reached (usually within 15 - 30 minutes). A series of 10 experiments at the same power level and aspect ratio with different gas velocities usually takes about 3-1/2 hours to complete.

A total of 300 experiments have been conducted; 160 experiments with a porous bottom and free upper surface, 60 experiments with porous sides, 144 experiments with porous bottom and an electrode grid, and 35 experiments with a porous bottom and the upper plate serving as the electrode.

A complete listing of the data obtained and calculated values is contained in Appendix A.

Chapter IV

EXPERIMENTAL RESULTS

Results from experiments conducted in this investigation using three different test cell configurations are presented in this chapter. These are: 1) test cell with a porous lower boundary, discrete holes in the side boundaries, and a solid upper boundary, 2) test cell with discrete holes in the lower boundary, porous side boundaries, and a solid upper boundary, and 3) test cell with a porous lower boundary, discrete holes in the side boundaries, and a free upper surface. A total of 399 experiments have been conducted. Of these, there are 179 of type 1 boundary conditions, 60 of type 2, and 160 of type 3.

Values of the sideward, downward, and upward power fractions, Nusselt numbers, and maximum pool temperatures are reported. Nusselt type correlations are given for the sideward, downward, and upward heat transfer rates as functions of the governing parameters. These represent the main results of this investigation. The data for all of the experiments conducted in this investigation are listed in Appendix A.

Visual observation of the flow pattern resulting from gas injection into the volumetrically heated pool shows conditions ranging from a gentle bubbly flow at the low range of gas flow rate to vigorous pool mixing at the high end of the range. Flow of gas from the side walls appears as a widening plume of bubbles rising to the surface at low gas velocities. Visual observation of this effect is not possible at higher velocities due to the vigorous mixing created in the

pool. For experiments with a solid upper boundary, the upper surface is observed to become partially unwetted as gas rising up through the pool inpinges on it and accumulates before escaping through the holes to the suppression chamber above.

The vigorous mixing produced by the percolating gases through the pool alters the temperature distribution within the pool from the distorted parabolic shape with above centerline maximum which develops in the natural convection case to a nearly isothermal distribution throughout the pool. Figure 22 from previous work [A1] shows a comparison of the measured temperature distribution along the pool centerline for experiments with and without gas injection. The effective boundary layer thickness is reduced considerably with the injection of gas. As gas injection rates into the pool are increased, the maximum pool temperature decreases. A non-dimensional parameter, M, which is inversely proportional to the pool temperature rise, may be defined to allow comparison of the effect of gas injection on pool temperature for various boundary conditions, aspect ratios, and volumetric heating rates. The pool temperature rise is normalized in terms of the maximum temperature difference that would appear using a one-dimensional conduction model for pools with isothermal upper and lower surfaces $(\frac{QL^2}{8k})$;

$$M = \frac{QL^2}{8k\Delta T}$$

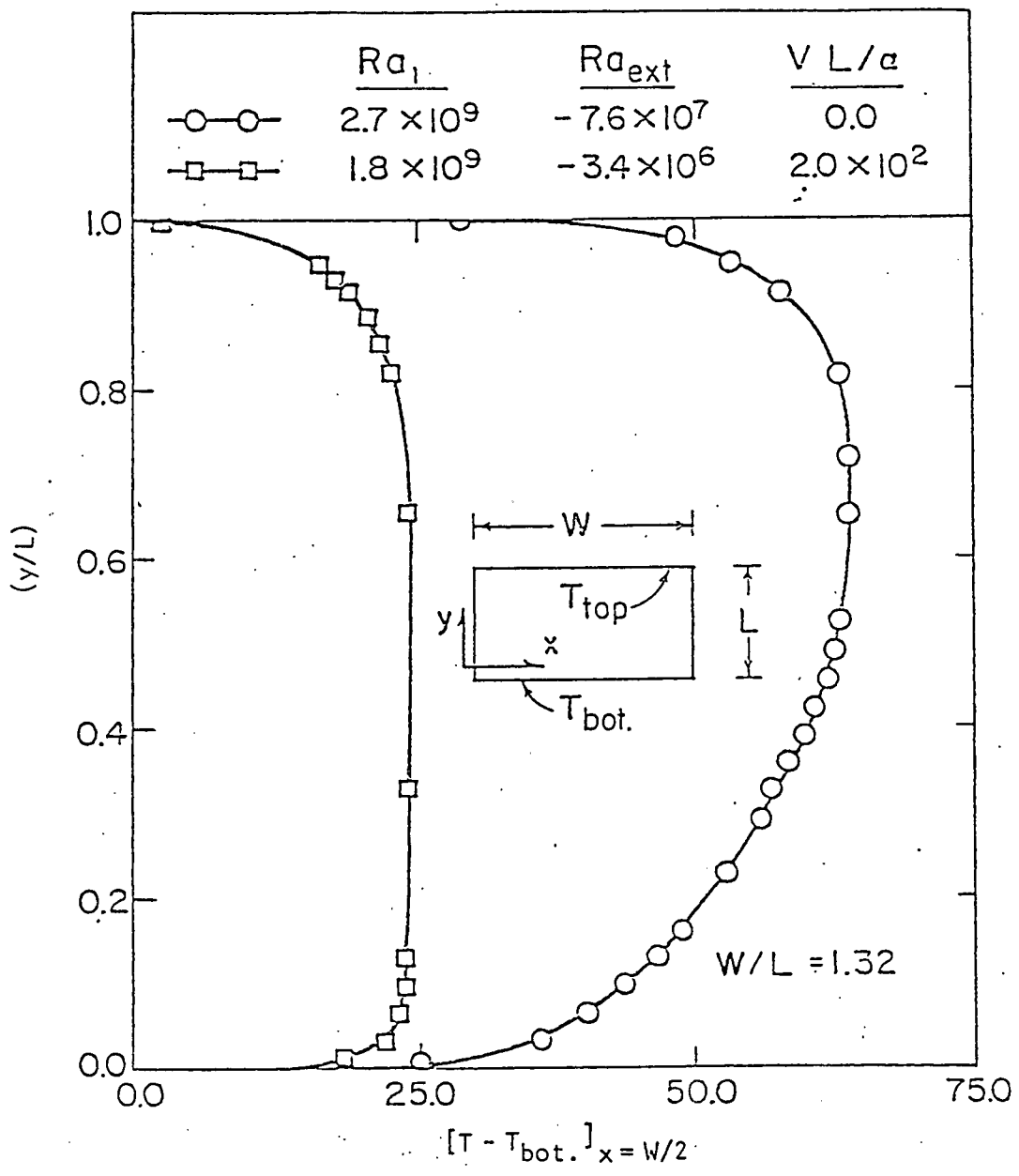

Figure 22. Temperature Distribution along the Pool Centerline for Two Experiments with and without Gas Injection.

where

Q = volumetric heat generation (W/cm^3)

and

ΔT = maximum temperature difference between the pool and boundaries (°C)

Figures 23, 24 and 25 show the effects of aspect ratio, W/L, and superficial gas velocity, V, on M for the three experimental configurations investigated. These figures clearly show that for the same power input, gas injection will considerably decrease the maximum pool temperature from the corresponding natural convection value. Reductions by factors of 2 to 4 as compared with natural convection are obtained as the superficial gas velocity is increased to the upper limit of the examined range. The pool temperatures are reduced rapidly (i.e. M increases) as gas is introduced at the boundaries. As the gas injection rate is increased, its effect on M begins to saturate and the maximum pool temperature appears to level off. As would be expected due to the smaller pool volume, pools of higher aspect ratio, W/L, saturate at lower superficial gas velocities.

A comparison of M values at similar aspect ratios for different test cell configurations is shown in Figure 26 and reveals a pronounced effect. Significantly higher reductions in pool temperature are observed for the solid surface model with a porous lower boundary and discrete hole side boundaries than for the solid surface model with a discrete hole lower boundary and porous side boundaries. The reasons for this behavior are not clear. It is possible that randomly

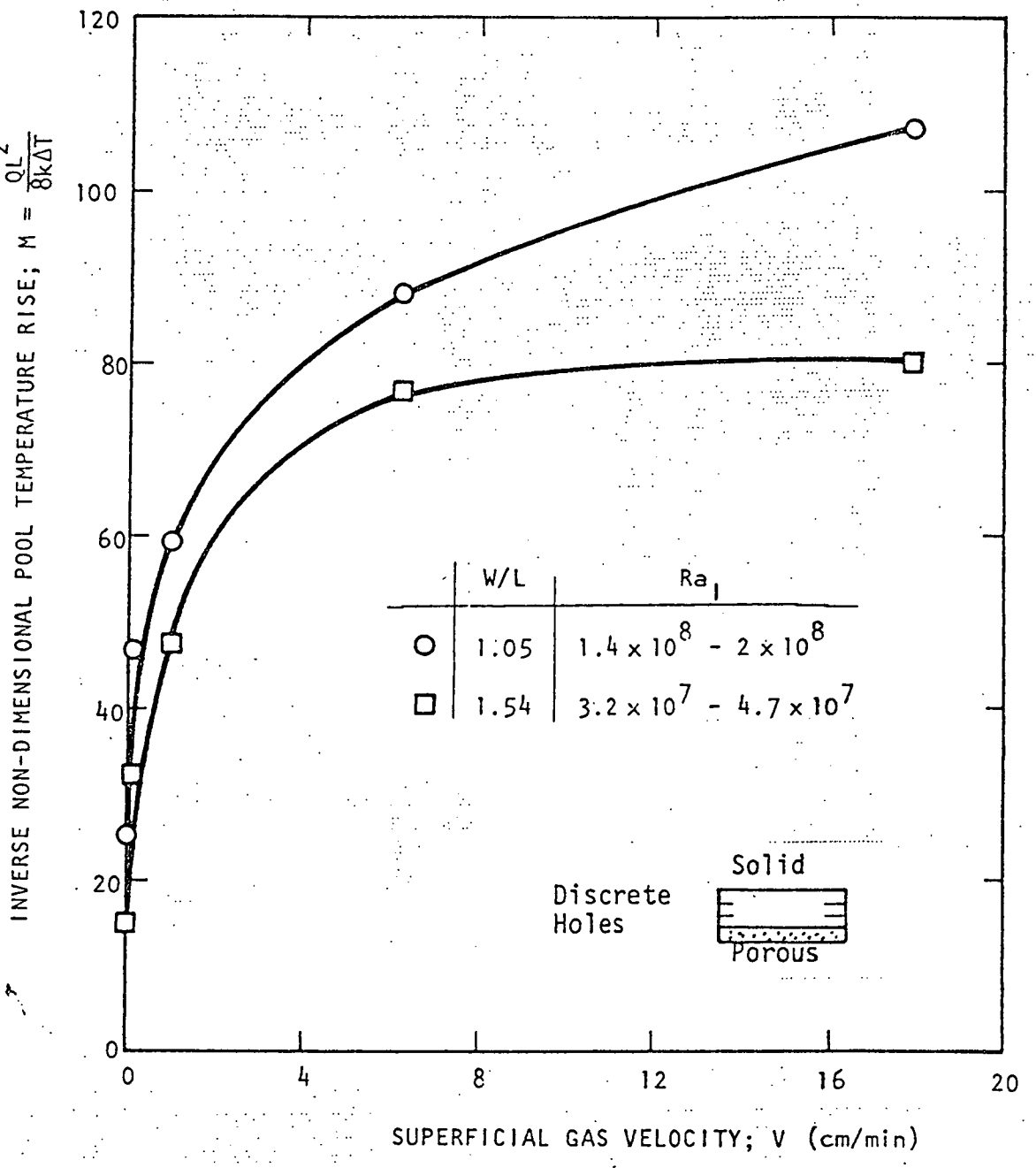

Figure 23. Effect of Aspect Ratio and Superficial Gas Velocity on the Inverse Non-dimensional Pool Temperature Rise for a Porous Lower Boundary and Solid Upper Boundary.

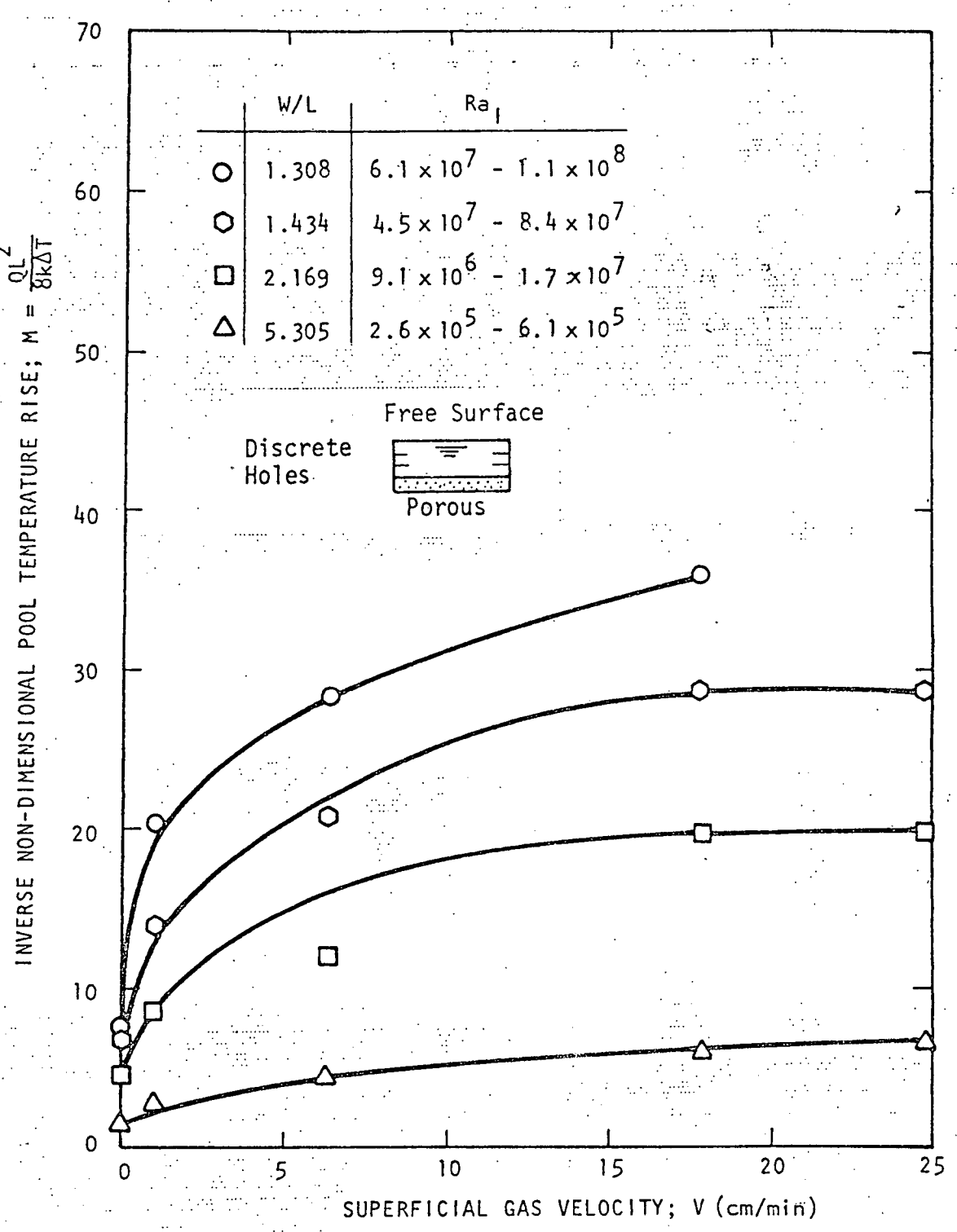

Figure 24. Effect of Aspect Ratio and Superficial Gas Velocity on the Inverse Non-dimensional Pool Temperature Rise for a Porous Lower Boundary and Free Upper Surface.

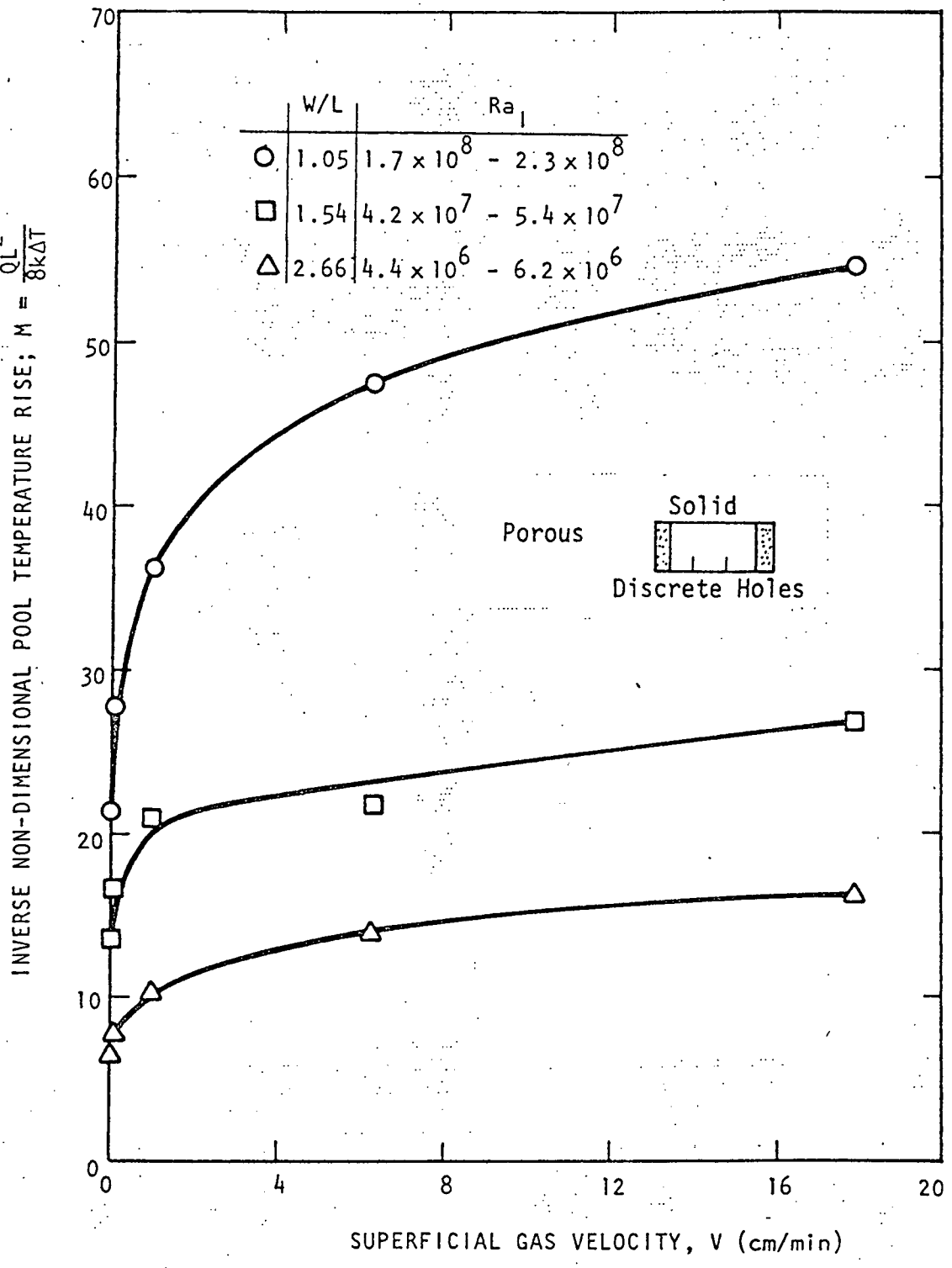

Figure 25. Effect of Aspect Ratio and Superficial Gas Velocity on the Inverse Non-dimensional Pool Temperature Rise for Porous Side Boundaries and a Solid Upper Boundary.

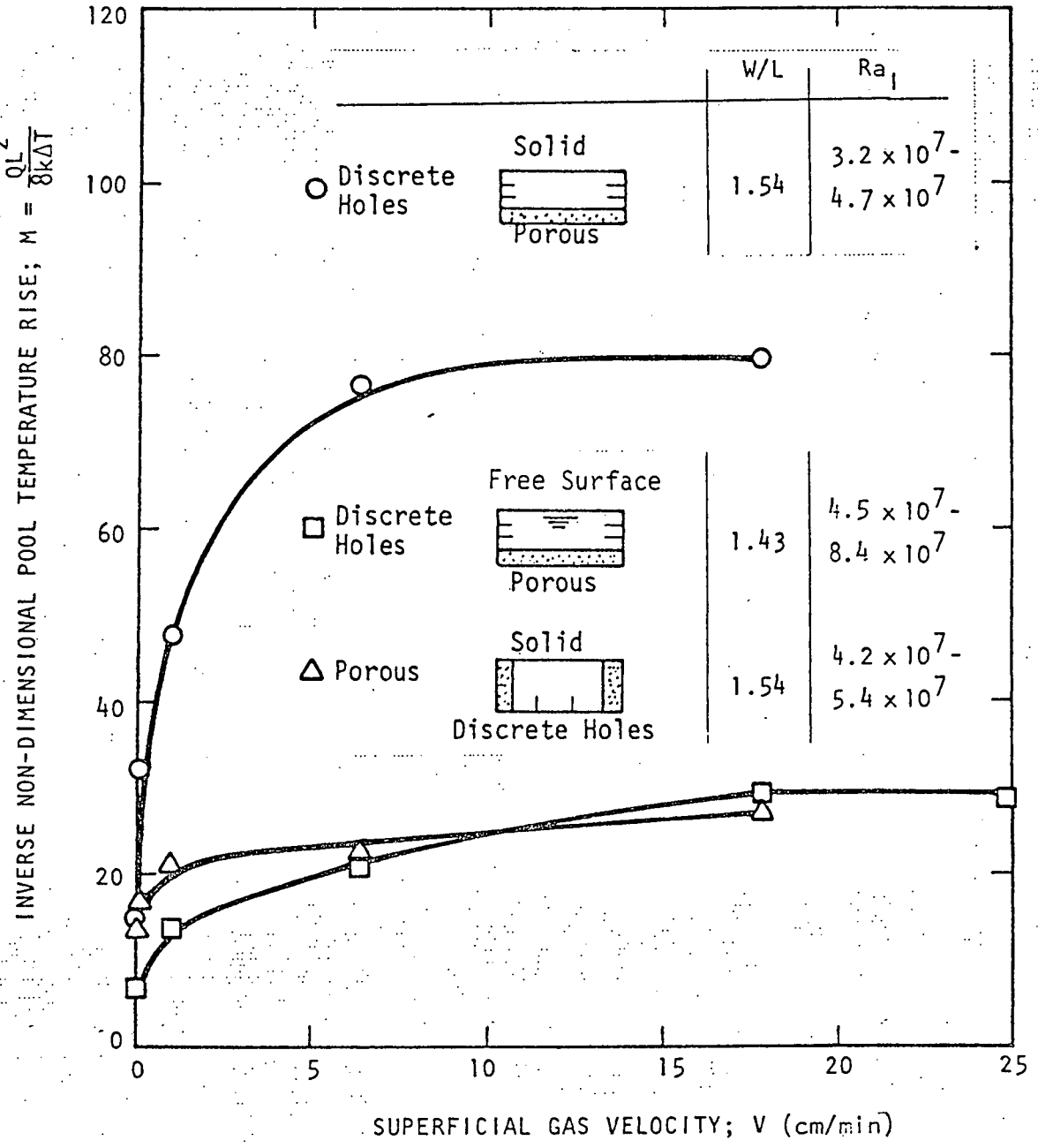

Figure 26. Effect of Boundary Conditions and Superficial Gas Velocity on the Inverse Non-dimensional Pool Temperature Rise.

rising air bubbles from a porous bottom plate produce greater mixing effects than air flowing up from discrete holes on the bottom plate. The manner in which air is injected from the side may not be as important in terms of total pool mixing. The higher pool temperatures observed for the free surface experiments are reasonable because of the lower heat transfer rates through the upper surface. Further discussion of this variation will be postponed until later in this chapter when the upward Nusselt numbers for different boundary conditions are compared.

The heat transfer rates to the pool boundaries are significantly affected by gas injection. Figure 27 shows the effect of increasing gas injection rates on the downward Nusselt number. Nusselt numbers are plotted in this figure and in the figures to follow with the dependence on layer depth (i.e. aspect ratio) removed by multiplying the defined Nusselt numbers, $Nu \equiv \frac{hL}{k}$, by the aspect ratio, W/L. The downward, sideward, and upward Nusselt numbers are plotted as $Nu_0 \cdot \frac{W}{L} = \frac{h_0 L}{k} \cdot \frac{W}{L}$, $Nu_s \cdot \frac{W}{L} = \frac{h_s L}{k} \cdot \frac{W}{L}$, and $Nu_1 \cdot \frac{W}{L} = \frac{h_1 L}{k} \cdot \frac{W}{L}$, respectively, where

h_0 = downward heat transfer coefficient ($W/cm^2°C$)

h_s = sideward heat transfer coefficient ($W/cm^2°C$)

h_1 = upward heat transfer coefficinet ($W/cm^2°C$), and

L = layer depth (cm).

This method allows easier examination of any layer depth dependence on the heat transfer coefficient.

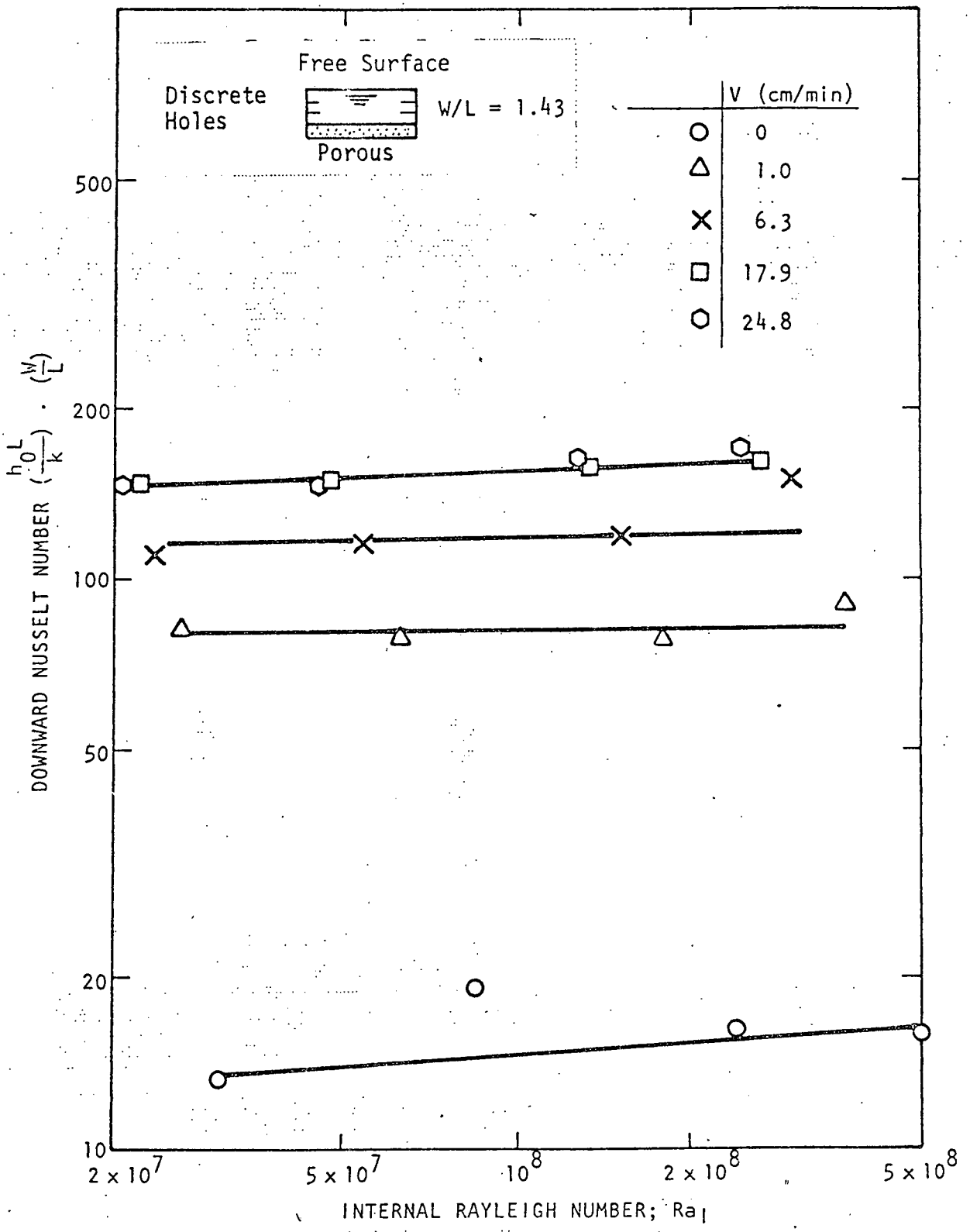

Figure 27. Effect of Superficial Gas Velocity and Internal Ra_I Number on the Downward Nusselt Number for a Porous Lower Boundary.

The downward Nusselt numbers shown in Figure 27 show a marked increase with superficial gas velocity for low values of V, however, this effect seems to saturate at higher velocities. The Nusselt numbers at the lower boundary of a volumetrically heated pool with gas injection appear to be independent of the internal Rayleigh number. The lack of natural convection effects is not surprising in view of the strong mixing produced by the gas bubbles percolating through the pool.

The effects of aspect ratio, gas injection, and Rayleigh number on the sideward Nusselt numbers for porous side boundaries are shown in Figure 28. The natural convection cases show the dependence on Rayleigh number discussed in the background section of this report. Gas injection is observed to increase the sideward Nusselt number significantly while seemingly eliminating natural convection influences (i.e. dependence on the internal Rayleigh number). For pools with gas injection at the boundaries, the effect of aspect ratio on the normalized sideward Nusselt number, $\frac{h_s L}{k} \cdot \frac{W}{L}$, appears to be negligible. Similar trends are shown in Figure 29 for the downward Nusselt number for the case of a porous lower boundary. The magnitude of the Nusselt numbers with gas injection are on the same order for both the side and lower porous boundaries.

A clear picture of the effect of gas injection on the Nusselt number can be seen from Figures 30 and 31. Figure 30 shows a plot of the downward Nusselt number vs. the superficial gas velocity, V.

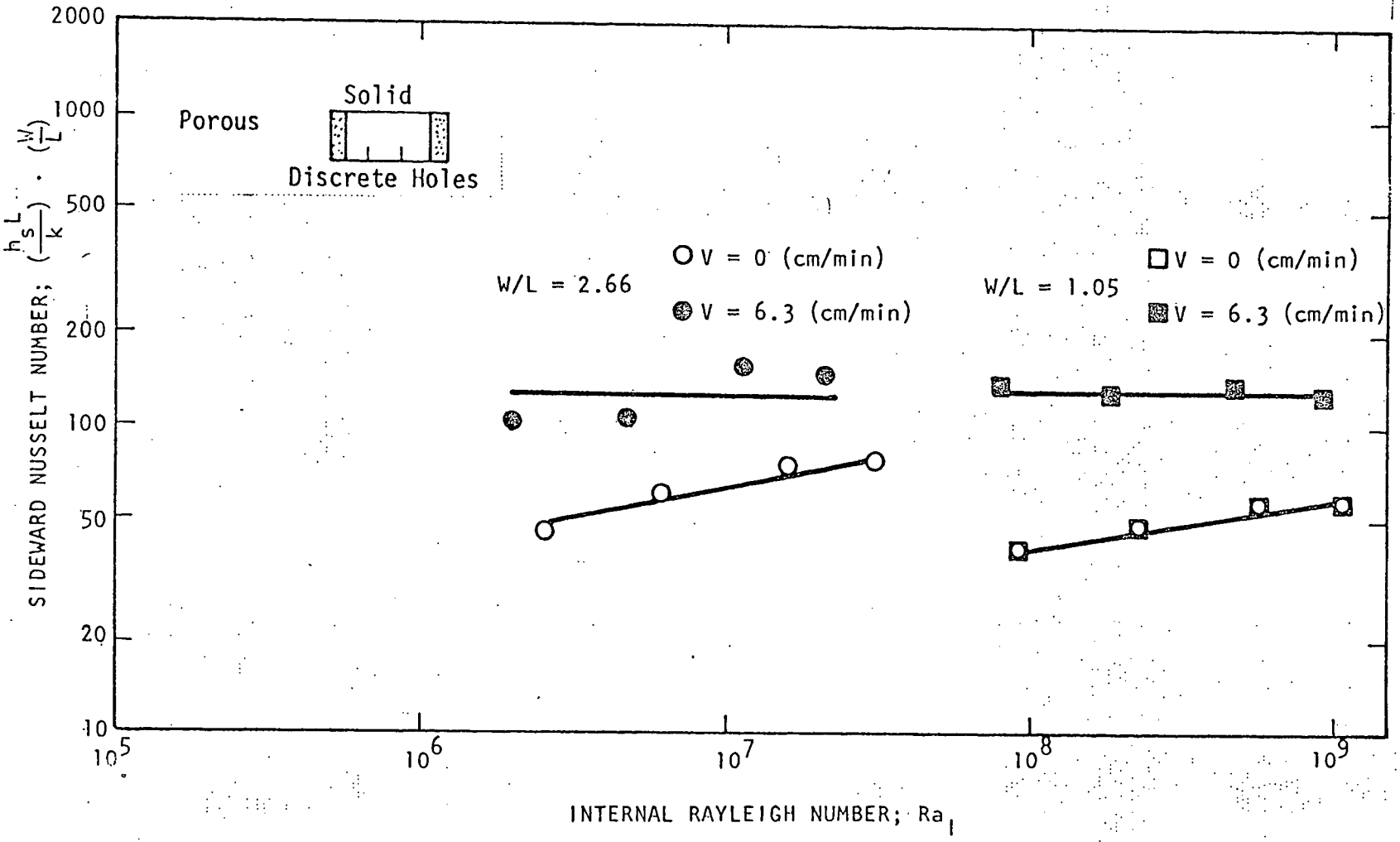

Figure 28. Effect of Aspect Ratio, Gas Injection, and Internal Rayleigh Number on the Sideward Nusselt Number for Porous Side Boundaries.

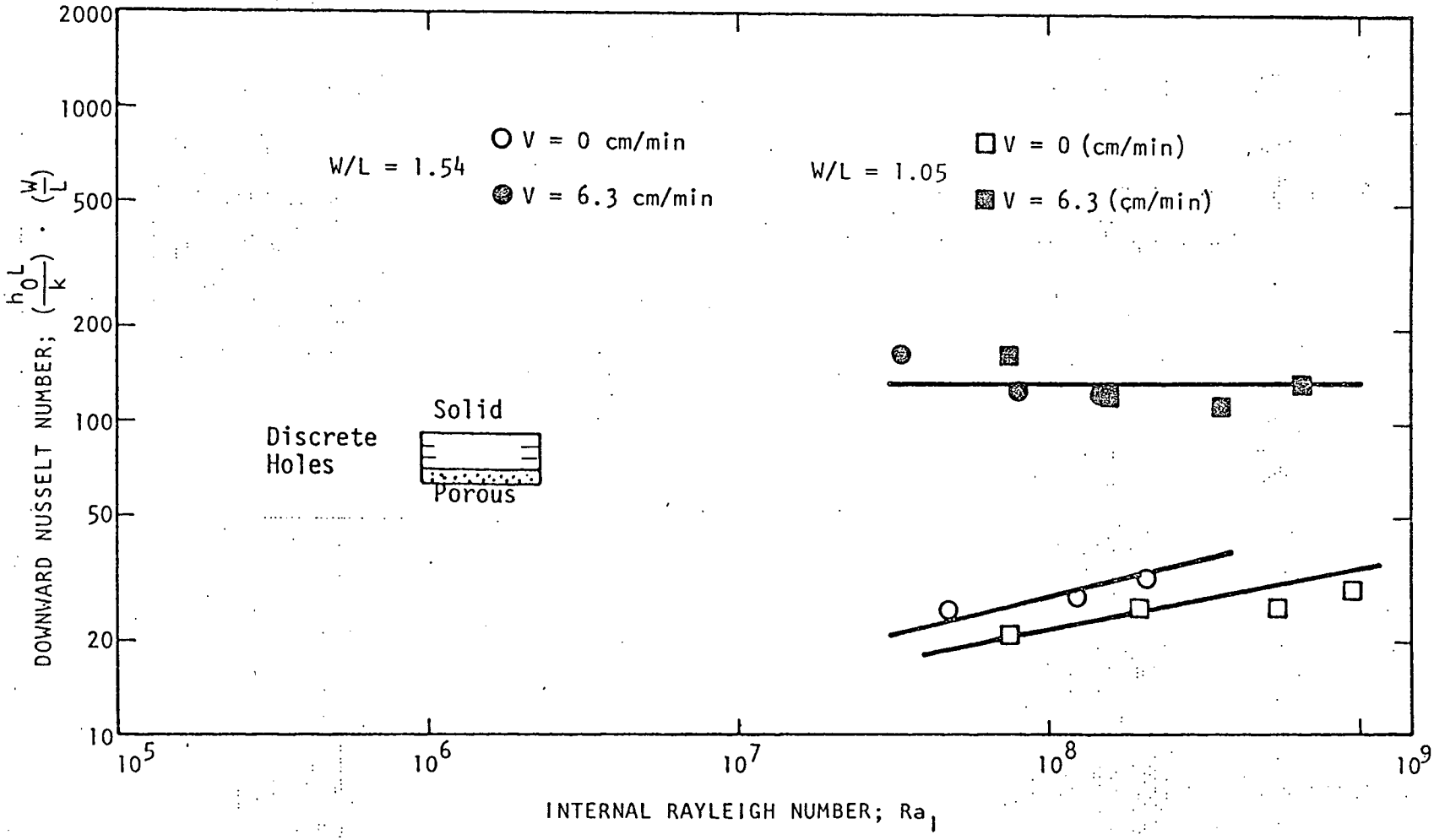

Figure 29. Effect of Aspect Ratio, Gas Injection, and Internal Rayleigh Number on the Downward Nusselt Number for a Porous Lower Boundary.

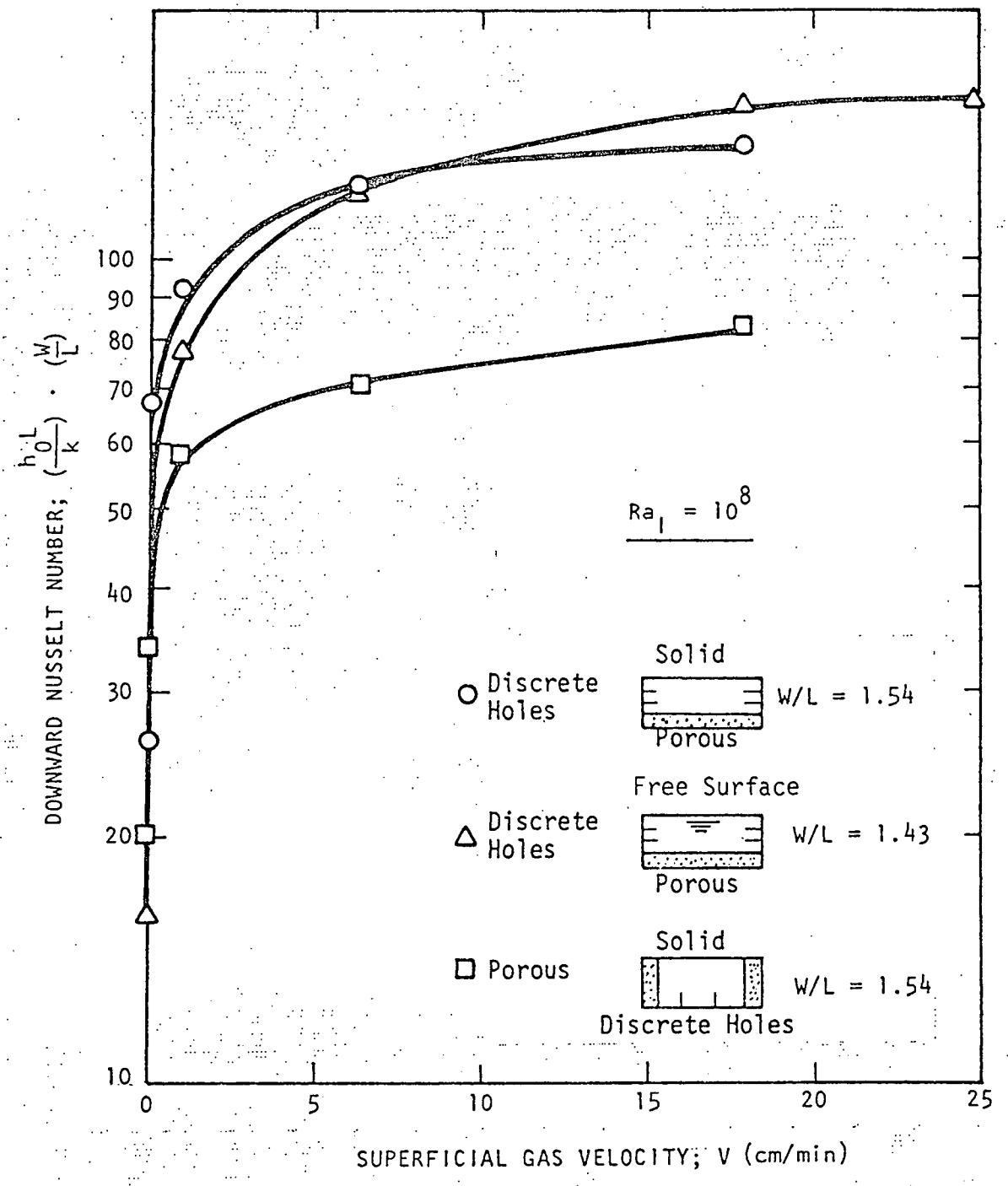

Figure 30. Effect of Boundary Conditions and Superficial Gas Velocity on the Downward Nusselt Number.

A steep increase with V from the natural convection values is seen as gas injection is initiated, with a levelling off of this increase for higher V. Similar results are shown in Figure 31 for the sideward Nusselt number.

The sideward and downward Nusselt numbers in Figures 30 and 31 show these effects for all of the different boundary conditions investigated. It is observed that the Nusselt numbers for porous boundary surfaces are considerably higher than those for the discrete hole boundaries. Sideward Nusselt numbers taken over a range of Ra_l at a medium range gas injection rate are shown in Figure 32 for the different boundary conditions. The porous side boundary shows sideward Nusselt number increases of approximately 40-50% over the discrete hole side boundaries. This behavior is in agreement with the work of Kutateladze and Malenkov [K7]. Figure 33, taken from [K7], shows the influence of the number of holes on heat transfer in the nitrogen bubbling of water. The figure also shows that the effect of hole distribution remains to be significant up to very high superficial gas velocities ($V \approx 6000$ cm/min). In the range of superficial gas velocities investigated in this study, 0-24.8 cm/min, increases in the heat transfer coefficient in the range of 30-50% are predicted by extrapolating Figure 33 which are comparable to the results obtained in this investigation. A similar comparison of the effect of boundary conditions is shown in Figure 34 for the downward Nusselt number at a medium range superficial gas velocity. The two cases with porous lower boundaries, both the free and solid upper surface

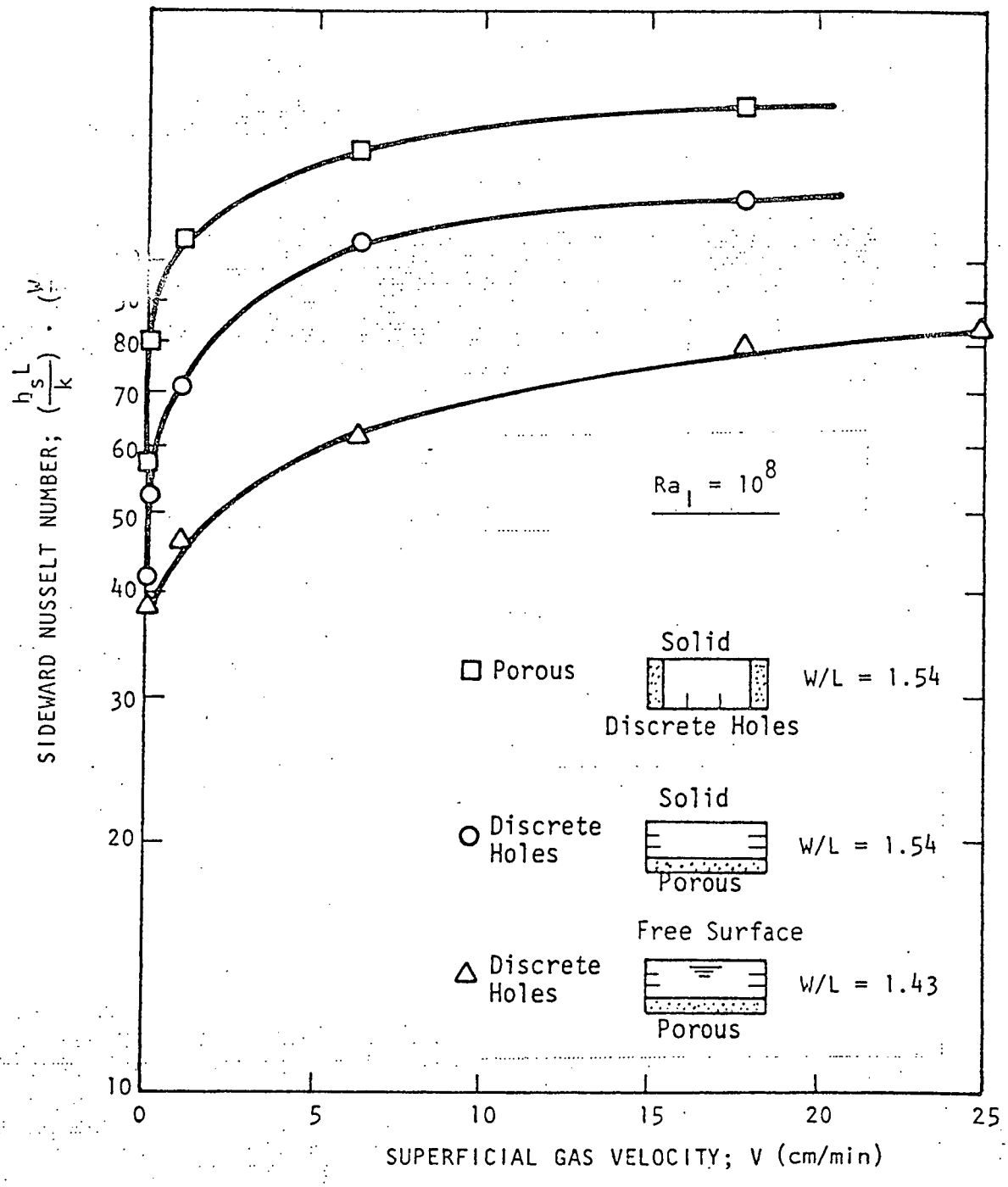

Figure 31. Effect of Boundary Conditions and Superficial Gas Velocity on the Sideward Nusselt Number.

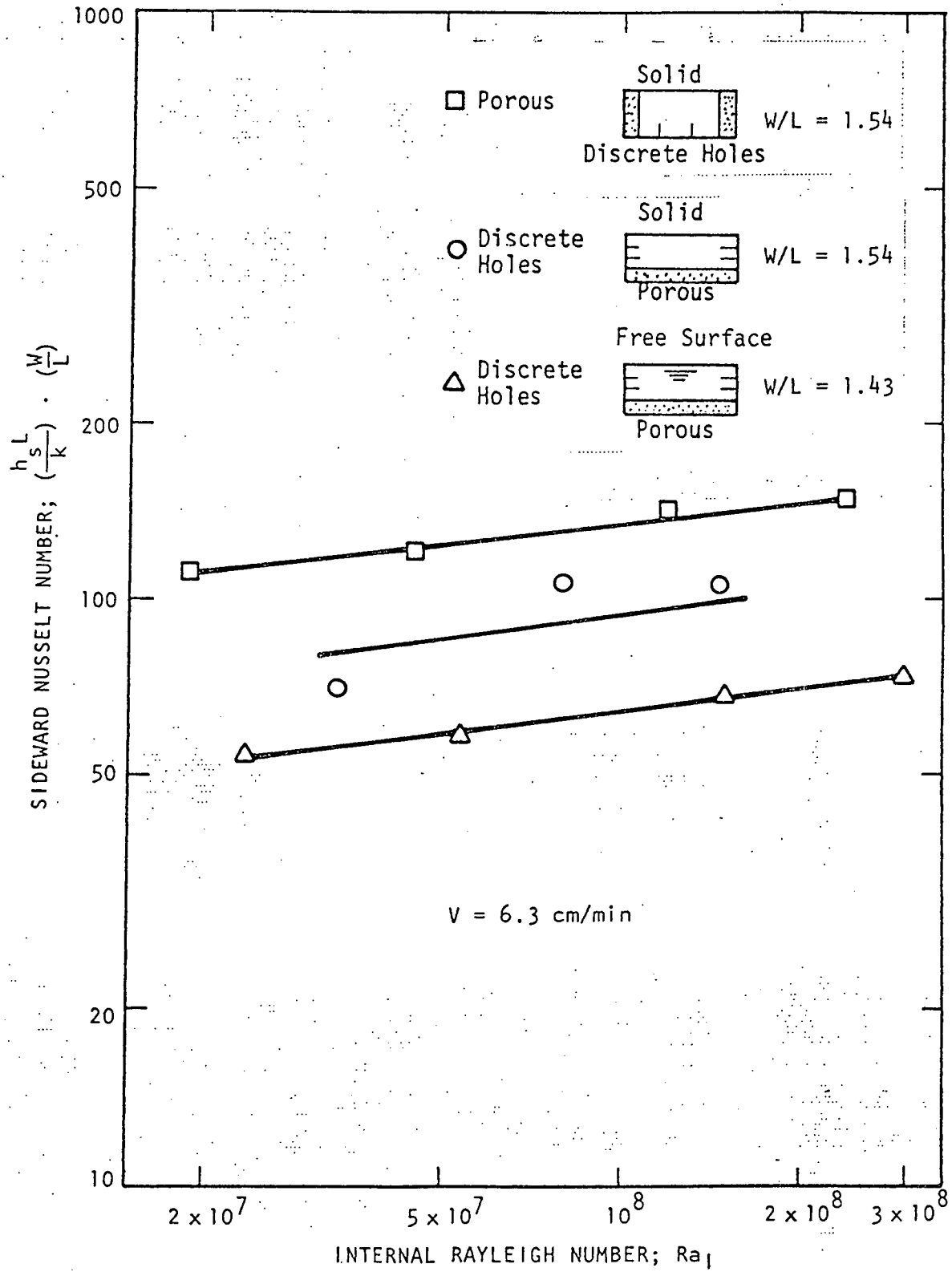

Figure 32. Effect of Boundary Conditions and Internal Rayleigh Number on the Sideward Nusselt Number.

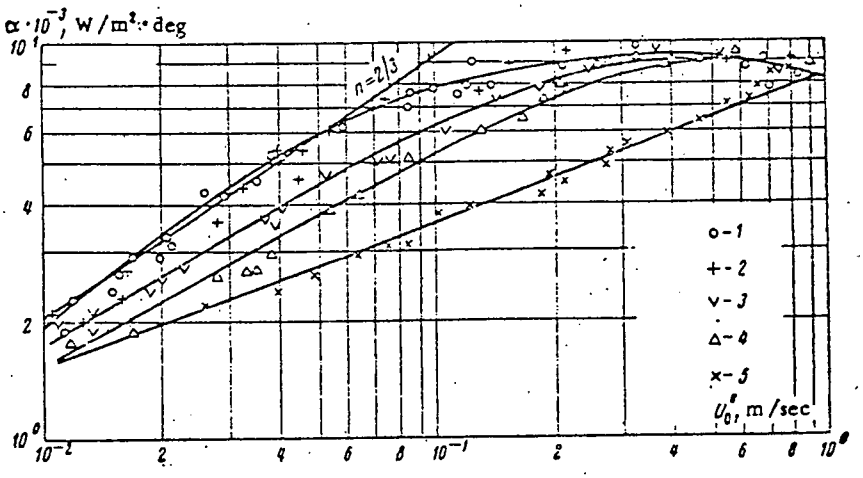

Influence of the number of holes on heat transfer (hole diameter 0.2 mm) in the nitrogen bubbling of water, $P = 9.81 \cdot 10^4$ N/m^2. 1) Plate of porous material; 2) plate with 2000 drillholes; 3) 1000 holes; 4) 480; 5) 20.

Figure 33. Influence of the Number of Holes on Heat Transfer in the Nitrogen Bubbling of Water (Taken from Kutateladze and Malenkov [K7]).

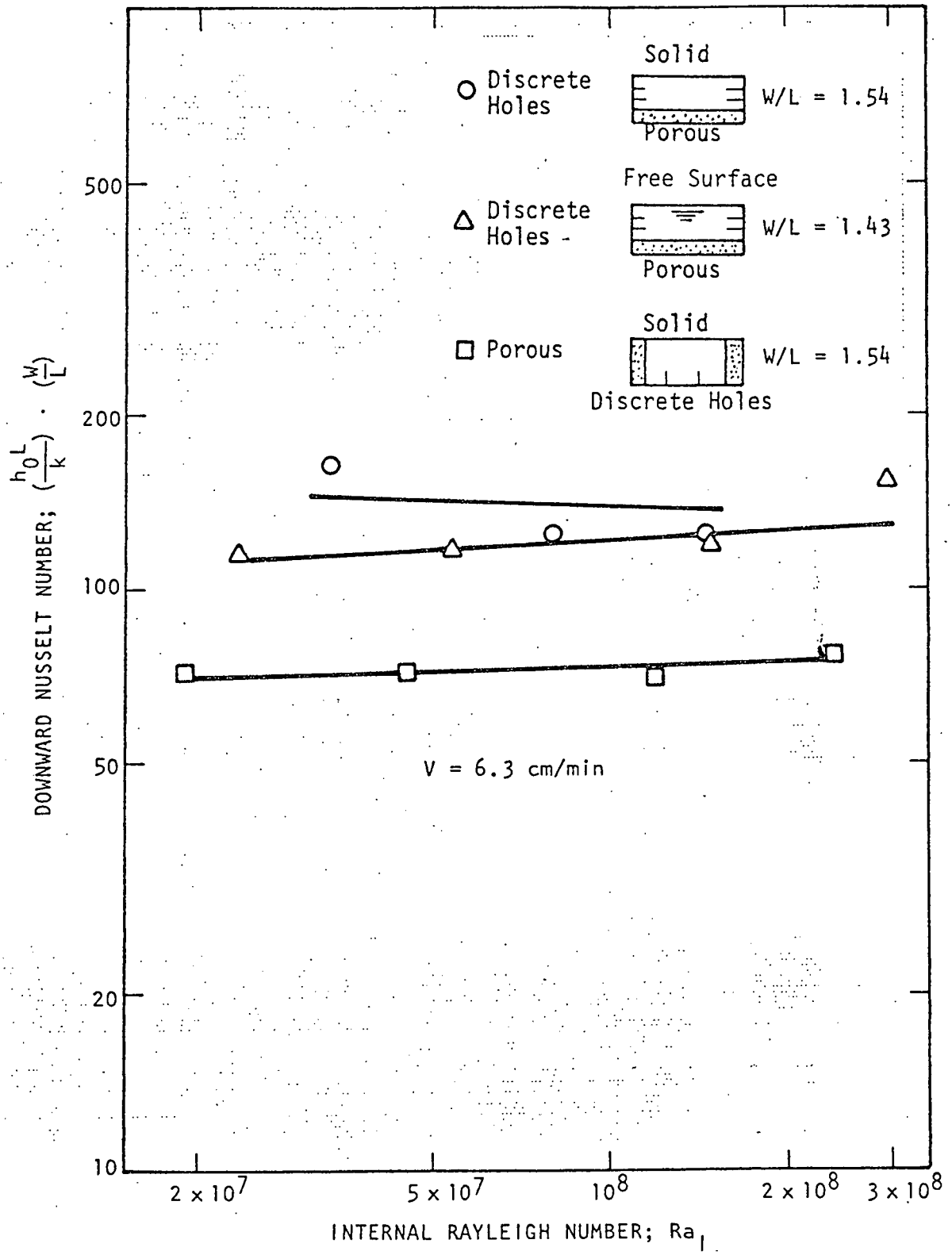

Figure 34. Effect of Boundary Conditions and Internal Rayleigh Number on the Downward Nusselt Number.

cases, show significant increases over the discrete hole lower boundary, solid upper surface case.

The effect of boundary conditions on the upward Nusselt number for a medium range superficial gas velocity is shown in Figure 35. The upward Nusselt number for the free surface case is comparatively very low as expected. The surprising result is the large difference in values for the experiments with porous side boundaries and the experiments where the lower boundary is porous, both experiments having solid upper surfaces. It is not clear from the experimental results as to the cause of this wide variation. Although the upper surface is insulated with a Mylar film in the porous side boundary case, it would not be expected to cause these large differences. A possible explanation is that the test cell configuration with the different arrangements of the porous plates may be producing a vapor film below the upper plate in the case with porous side boundaries (i.e. the escape of air is impeded in that case) while not forming a film in the case of the porous lower boundary. Gas injected at the surface of porous plates may have different mixing effects or rise to the upper plate in a different manner than gas injected from discrete holes. A plot of upward Nusselt number vs. superficial gas velocity for the different boundary conditions is shown in Figure 36 which tends to support this reasoning. The upward Nusselt number for the porous side boundary is seen to decrease as gas injection is increased from the natural convection values (which approach the same value). The inverse non-dimensional pool temperature rise indicated in Figure 26 for the

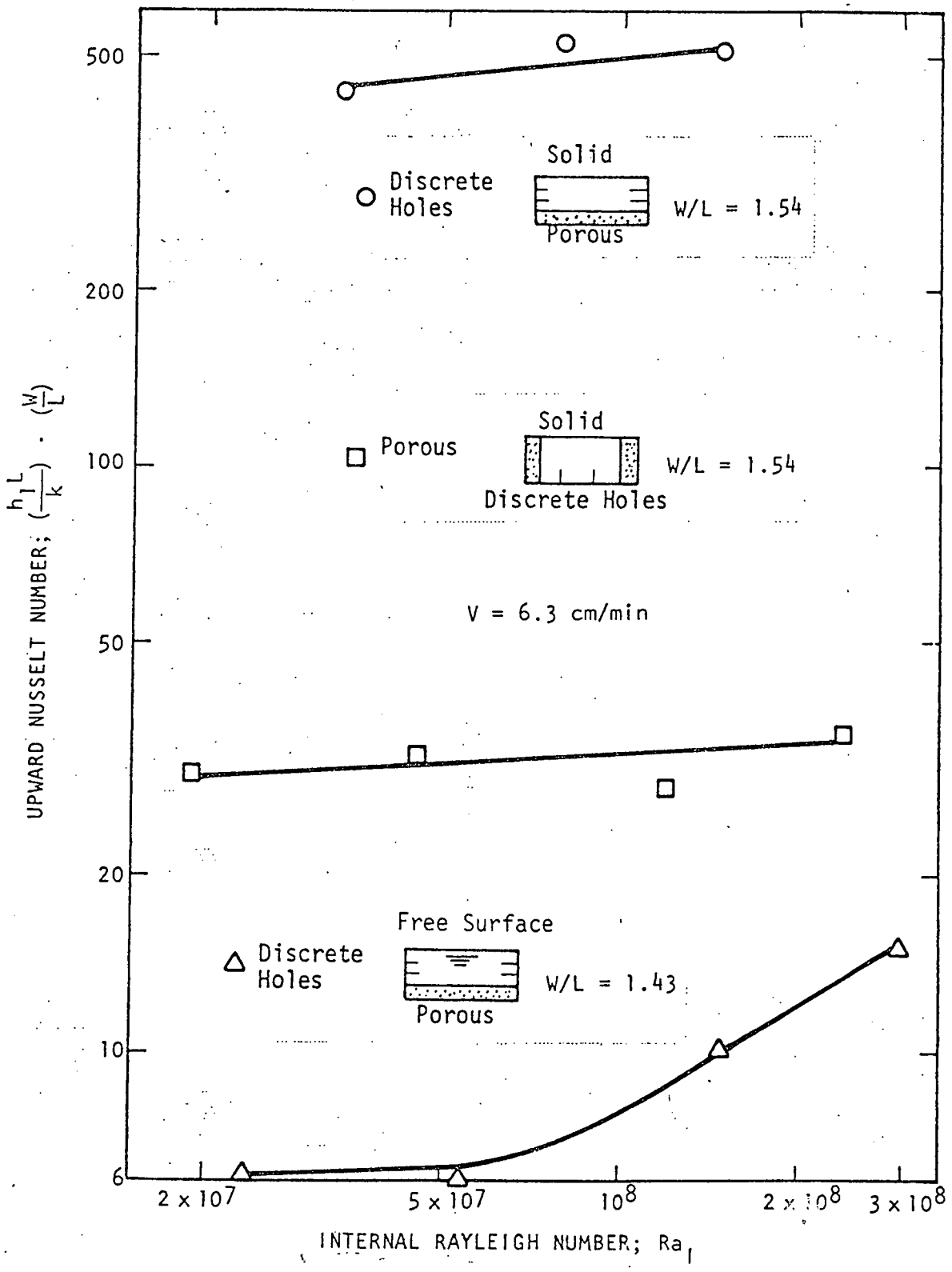

Figure 35. Effect of Boundary Conditions and Internal Rayleigh Number on the Upward Nusselt Number.

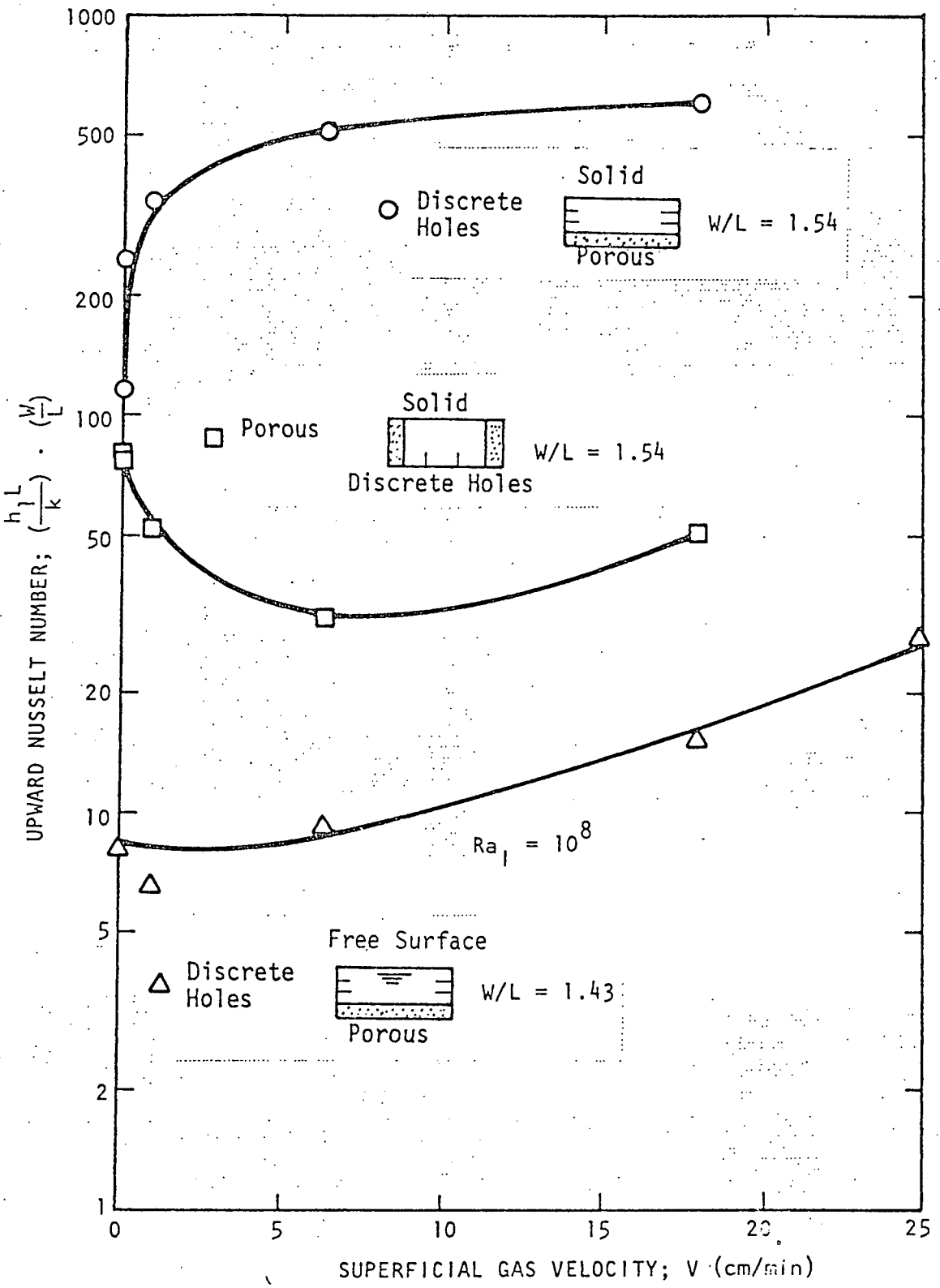

Figure 36. Effect of Boundary Conditions and Superficial Gas Velocity on the Upward Nusselt Number.

different boundary conditions shows consistent results with the effect on the upward Nusselt numbers. The pool temperature is reduced considerably more for the porous lower boundary case than for the porous side boundary case, which is consistent with the higher heat transfer coefficient at the upper surface for the porous lower boundary case.

Interesting results are observed, which incorporate the major findings of this investigation, when the sideward and downward Nusselt numbers are plotted vs. the superficial gas velocity on a log scale. Figures 37 and 38 show these results as a function of aspect ratio, W/L, and boundary conditions.

Looking at Figure 37, the data for the different boundary conditions are seen to fall along straight lines. For the experiments with a porous lower boundary and solid upper surface the data points for different aspect ratios show the same behavior, indicating that their is no dependence of the normalized downward Nusselt number on the aspect ratio. The free surface experiments show a slightly higher slope than the solid upper surface experiments. The discrete hole boundary case shows a fairly similar slope to that of the porous lower boundary although the magnitude is decreased.

Similar observations may be made for the sideward Nusselt numbers shown in Figure 38. The effect of aspect ratio on the normalized sideward Nusselt number appears to be insignificant. The free surface experiments again show a slightly higher dependence on the superficial gas velocity.

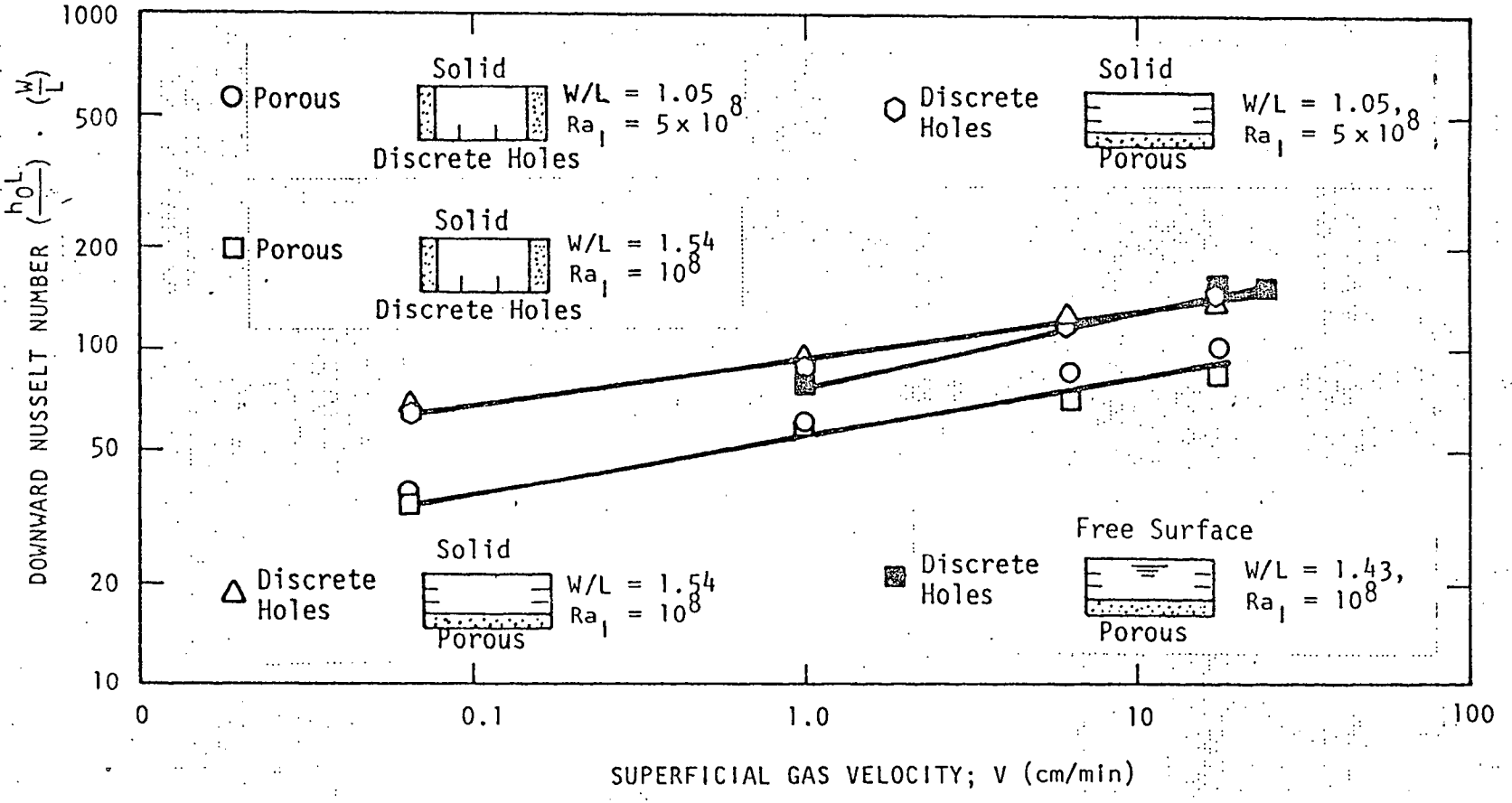

Figure 37. Effect of Boundary Conditions, Aspect Ratio and Superficial Gas Velocity on the Downward Nusselt Number.

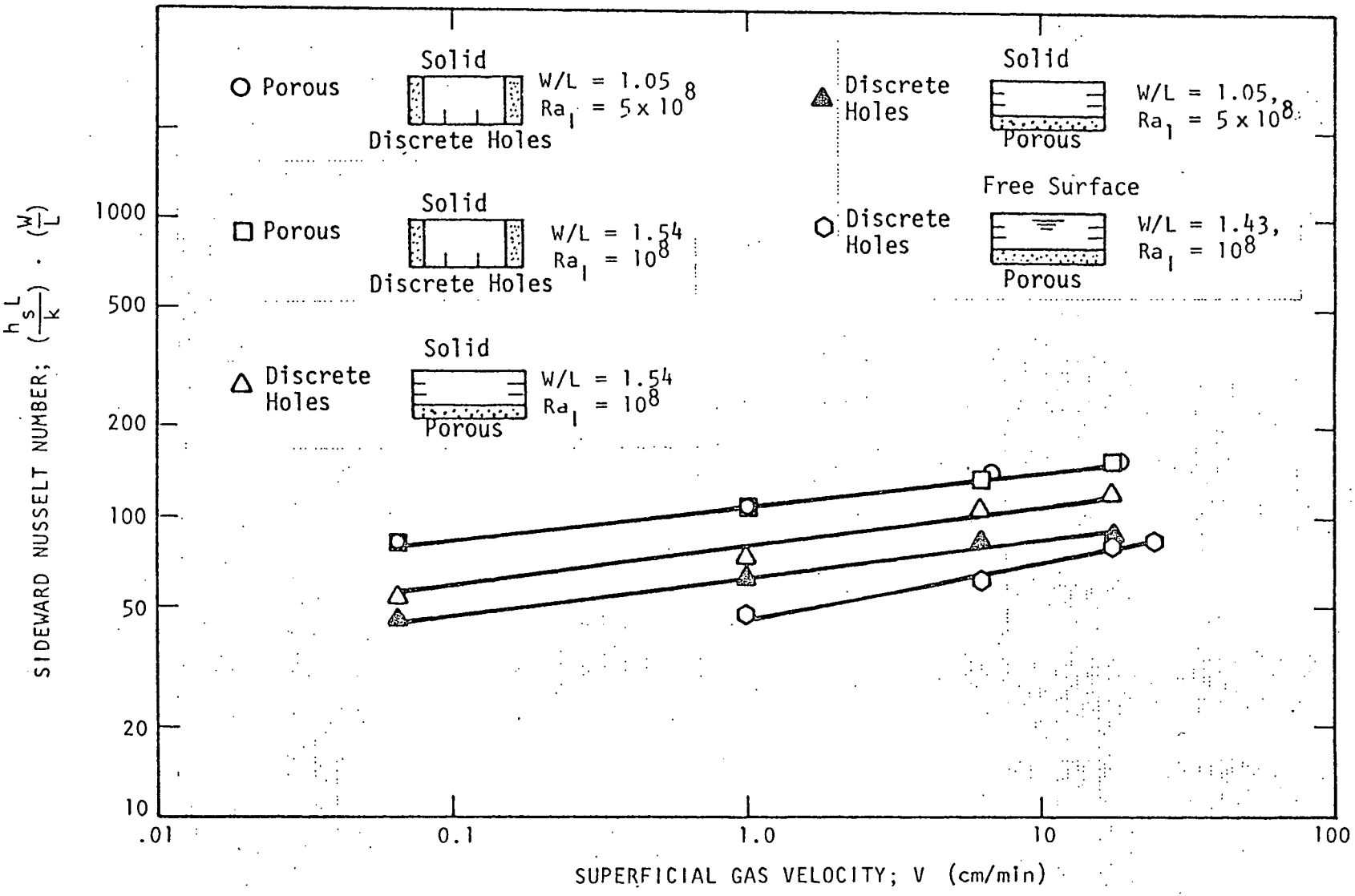

Figure 38. Effect of Boundary Conditions, Aspect Ratio, and Superficial Gas Velocity on the Sideward Nusselt Number.

With the insight gained from Figures 37 and 38, a least squares fit of the data was made to obtain a correlation that is primarily dependent on the superficial gas velocity, V, and independent of the internal Rayleigh number, Ra_I, and aspect ratio, W/L. A correlation using a non-dimensional form of the superficial gas velocity employed by Hart [H1] in an experiment where a liquid column is agitated by gas bubbles describes the data very well; the non-dimensional quantity V^* defined by

$$V^* \equiv \left[\frac{V^3\rho}{\mu g}\right]$$

is the only independent variable on which the Nusselt numbers depend.

This quantitity may also be written in terms of the Reynolds and Froude numbers where the velocity, V, is that of the gas and the other properties are those of the volumetrically-heated liquid

$$\left(\frac{V^3\rho}{\mu g}\right) = \left(\frac{\rho V L_g}{\mu}\right)\left(\frac{V^2}{gL_g}\right)$$

$$= Re \cdot Fr,$$

where

ρ = density of the liquid (kg/cm^3)

μ = viscosity of the liquid (poise)

g = gravitational constant (cm/s^2)

L_g = characteristic dimension for the gas bubbles (cm).

The quantity (Re · Fr) represents the ratio of the

$$\left(\frac{\text{inertial forces}}{\text{viscous forces}}\right) \cdot \left(\frac{\text{inertial forces}}{\text{gravity forces}}\right).$$

The Froude number is generally not of importance except for systems which include a free surface. It also appears to be important in the two-phase, two component system examined here even though the liquid may not have a free surface.

The following Nusselt-type correlations have been obtained.

1. Downward Nusselt Number

For a porous lower boundary with the current passed between the upper plate and lower porous plate, the downward Nusselt number is given by:

$$Nu_0 \cdot \frac{W}{L} = 204[ReFr]^{0.05} \quad (5 \times 10^{-10} \leq ReFr \leq 5 \times 10^{-3})$$

This correlation fits the data (28 points) with a standard deviation of 19.1. A comparison between the experimental and predicted values of Nusselt number is given in Figure 39. This correlation is recommended for use in actual molten core debris/concrete systems since the boundary conditions closely simulate the gas release process at the lower boundary.

For the same case with the current passed between a wire grid electrode placed immediately below the top plate and the lower porous plate, the downward Nusselt number is given by:

$$Nu_0 \cdot \left(\frac{W}{L}\right) = 193[ReFr]^{0.048} \quad (5 \times 10^{-10} \leq ReFr \leq 5 \times 10^{-3})$$

This correlation fits the data (128 points) with a standard deviation of 29.7. A comparison between the experimental and predicted values of Nusselt number is given in Figure 40.

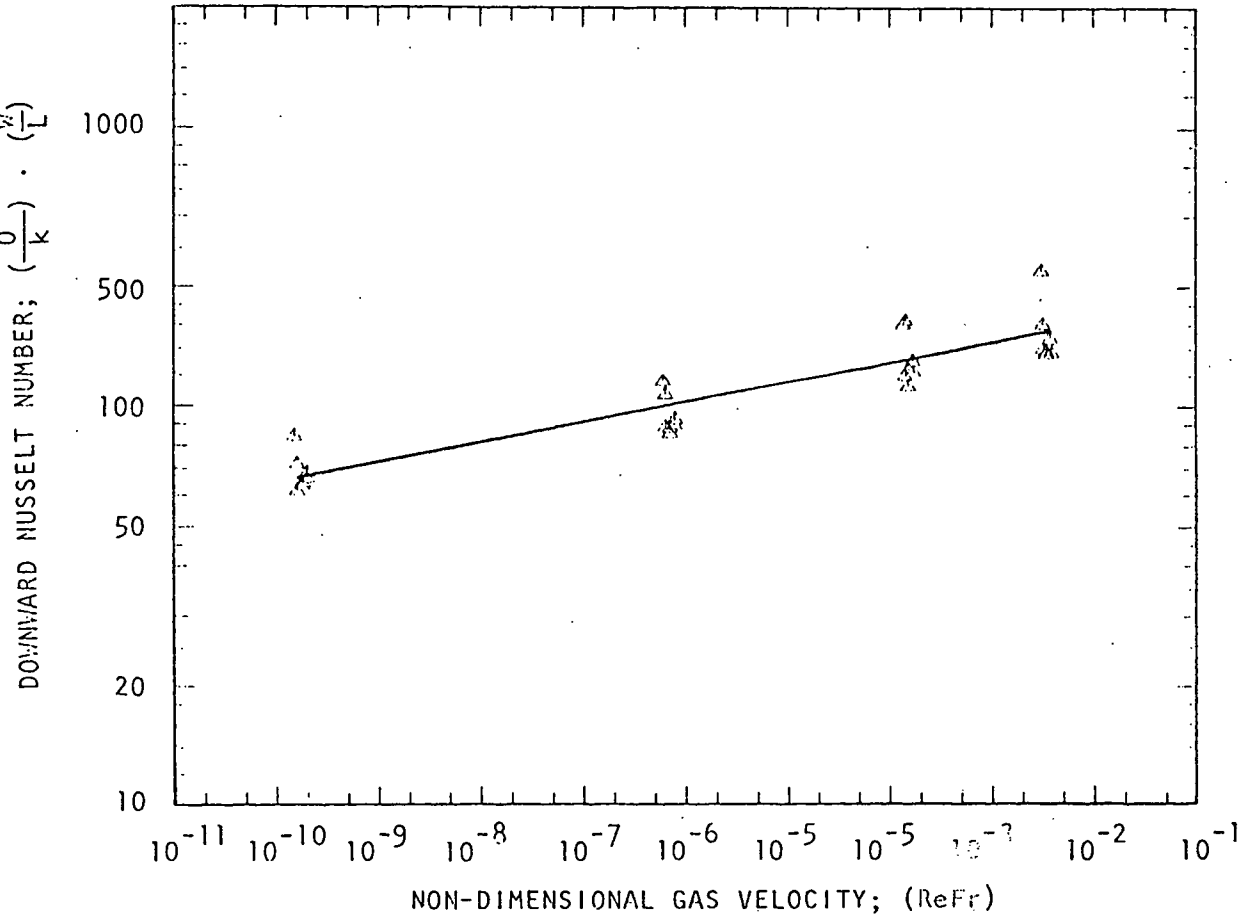

Figure 39. Comparison of Experimental and Predicted Downward Nusselt Numbers for a Porous Lower Boundary with Upper and Lower Plate Electrodes.

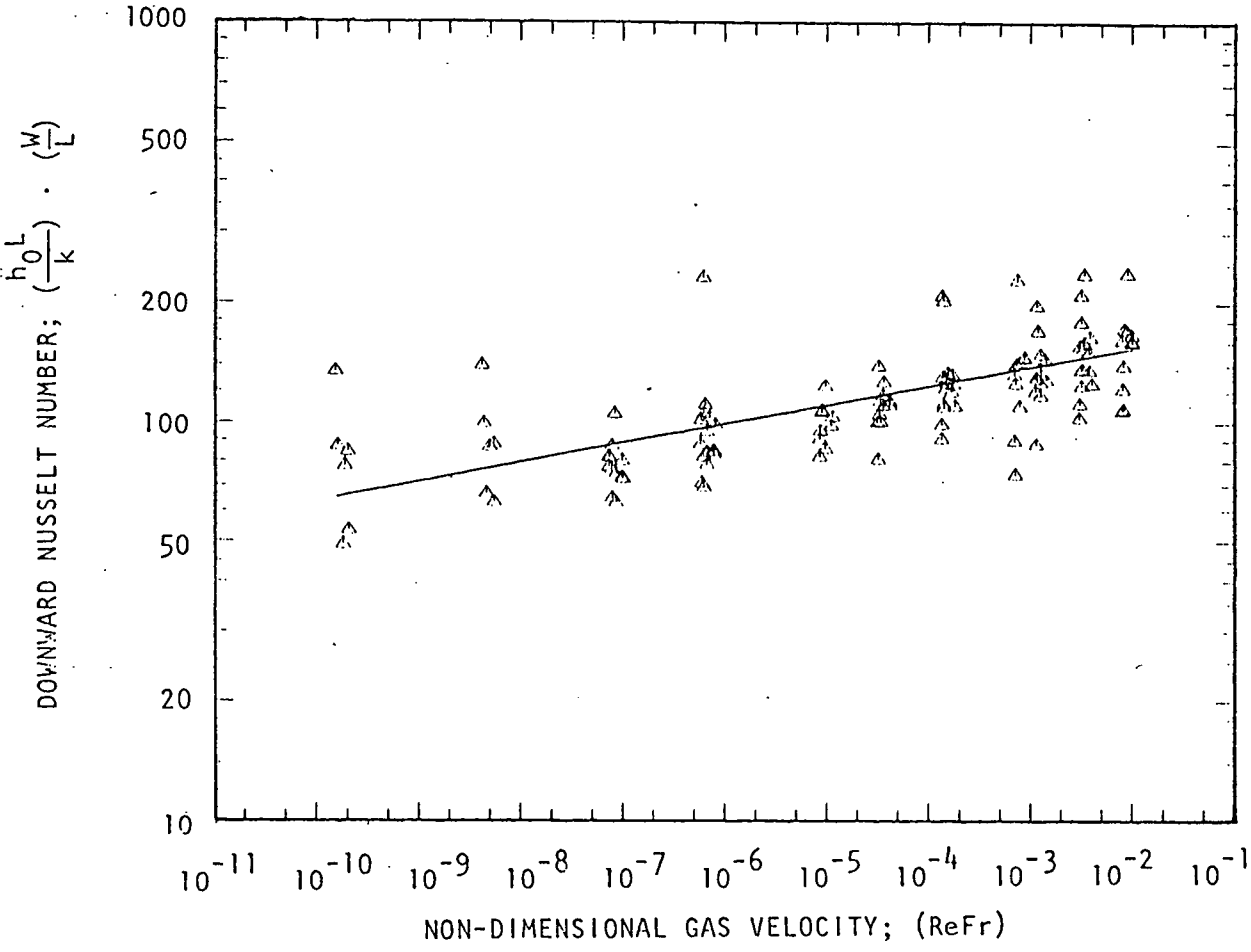

Figure 40. Comparison of Experimental and Predicted Downward Nusselt Numbers for a Porous Lower Boundary with Upper Grid and Lower Plate Electrodes.

The data obtained for the case without the grid electrode shows less scatter (Fig. 39), although the number of data points is significantly lower than those with the grid electrode (Fig. 40). However, the two correlations agree quite well, indicating that the existence of the intermittent gas layer below the upper plate does not significantly affect the application of power to the cell since sufficient contact is always maintained between the liquid and the solid surface.

The correlation of downward Nusselt number for a porous lower boundary and a free upper surface is given by:

$$Nu_0 \cdot \frac{W}{L} = 231[ReFr]^{0.074} \qquad (5 \times 10^{-10} \leq ReFr \leq 5 \times 10^{-3})$$

This correlation fits the data (144 points) with a standard deviation of 10.6. A comparison between experimental and predicted values is given in Figure 41. As indicated in previous plots, the downward Nusselt number is seen to have a higher dependence on the velocity for a free surface upper boundary than for a solid upper boundary.

2. Sideward Nusselt Numbers

The sideward Nusselt number for test cells with porous side boundaries and solid upper boundary is given by:

$$Nu_s \cdot \left(\frac{W}{L}\right) = 194[ReFr]^{0.043} \qquad (5 \times 10^{-10} \leq ReFr \leq 5 \times 10^{-3})$$

This correlation fits the data (48 points) with a standard deviation of 7.0. A comparison between experimental and predicted values is given in Figure 42. This correlation is recommended for use in

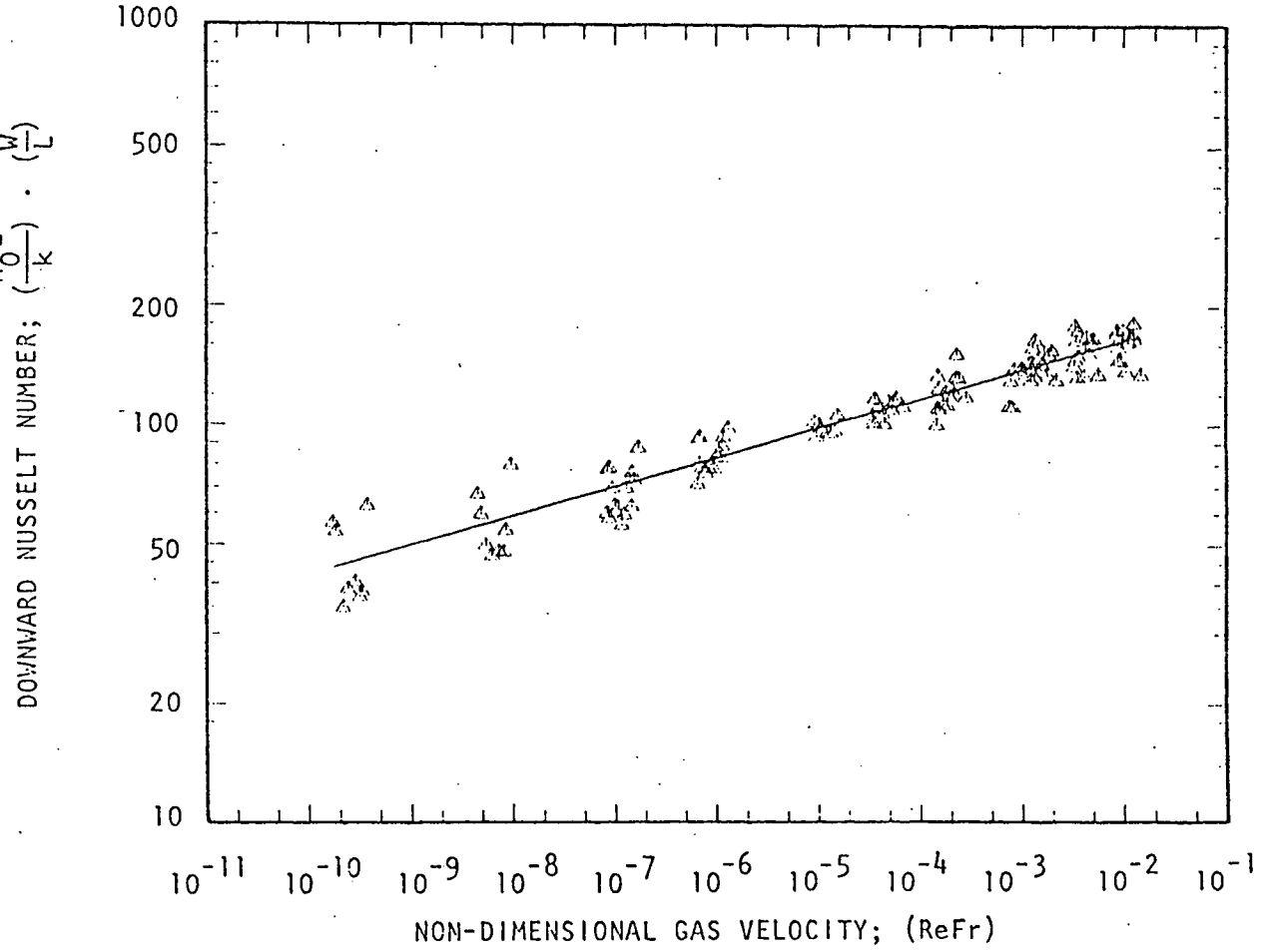

Figure 41. Comparison of Experimental and Predicted Downward Nusselt Numbers for a Porous Lower Boundary and a Free Upper Surface.

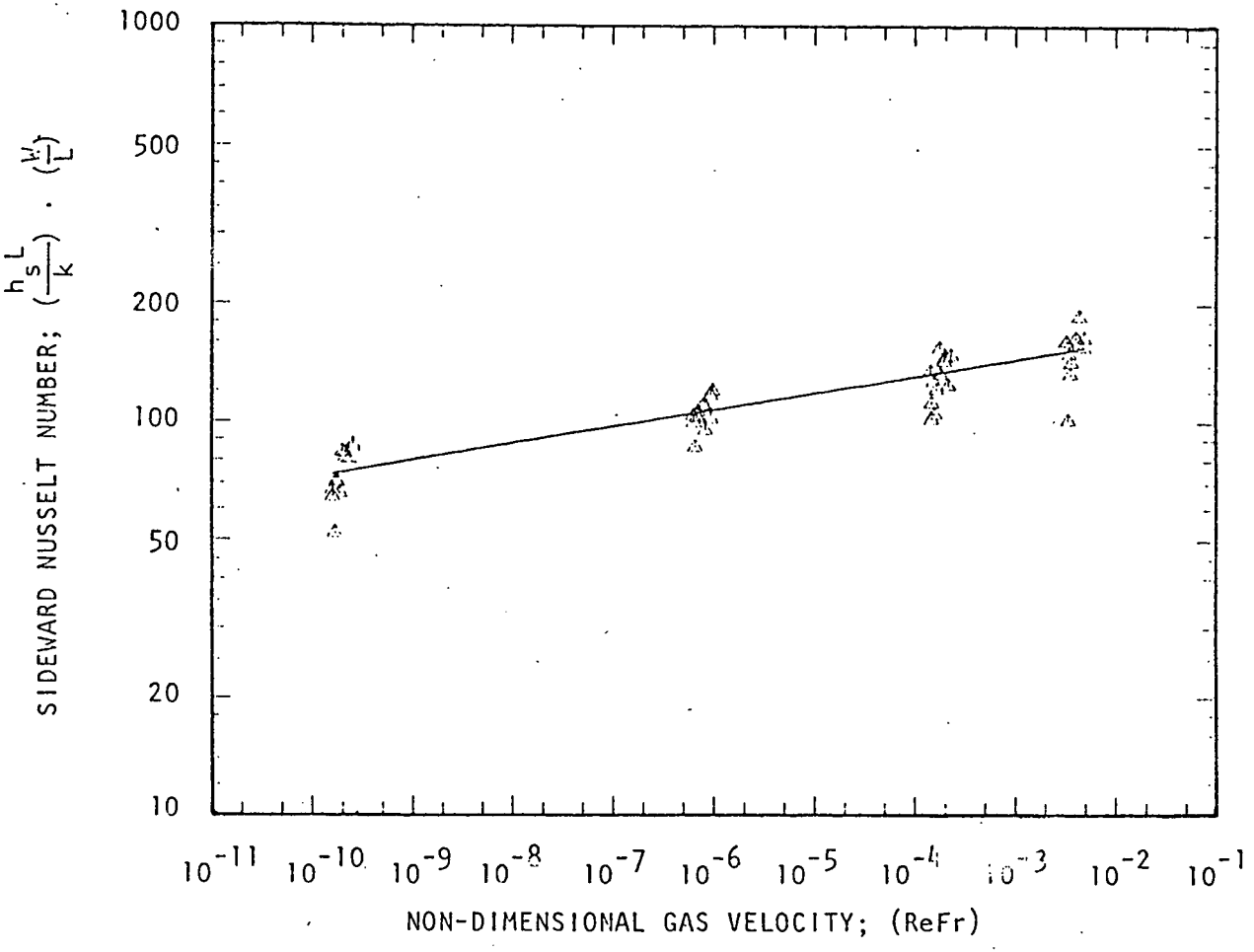

Figure 42. Comparison of Experimental and Predicted Sideward Nusselt Numbers for Porous Side Boundaries.

actual molten core debris concrete systems since the boundary conditions closely simulated the gas release process at the boundaries.

The sideward and downward Nusselt numbers to porous boundaries have a fairly similar dependence on the superficial gas velocity. The above correlations are the main results of this investigation.

In order to determine the relative fractions of power that are transferred in the sideward, downward, and upward directions for the molten debris/concrete system the upward Nusselt number must also be determined. Limitations on the experiment prevented measurements in the case where both side and lower boundaries are porous simultaneously. In addition, the variation in upward Nusselt number for the porous side and porous lower boundary experiments, both with solid upper boundaries, casts uncertainties on the upper boundary modelling.

An approximate method of combining the results of the porous side model and the porous bottom model into a model with both porous sides and bottom may be made using the known values of the sideward Nusselt number for the porous side, the downward Nusselt number for the porous bottom, and the averaged values of the inverse non-dimensional temperature rise, M. By averaging the values of M, the upward Nusselt number will essentially be determined by the average pool-to-boundary temperature difference between the two models (porous side boundary model and porous lower boundary model). An energy balance over the test cell gives

$$1 = Nu_s \cdot \left(\frac{L}{W}\right) \cdot \frac{1}{4M^*} + Nu_0 \cdot \frac{1}{8M^*} + Nu_1 \cdot \frac{1}{8M^*}$$

where

$$M^* = \frac{M(\text{Porous Lower Boundary}) + M(\text{Porous Side Boundary})}{2}$$

The upward Nusselt number is the only unknown in the equation and may be solved for. By matching data points (equivalent power input, aspect ratio, and superficial gas velocity) from the porous lower boundary model and from the porous side boundary model a set of upward Nusselt numbers may be generated. A least squares fit of these data points produced a correlation of the form:

$$Nu_1 \cdot \frac{W}{L} = 565[ReFr]^{0.048}.$$

This correlation fits the data (28 points) with a standard deviation of 81. A comparison of the calculated values and the values predicted by the correlation is shown in Figure 43. There is a good deal of scatter in the data. The above method would obviously work better if the pool temperatures for the two models combined were closer (i.e. the upper boundary conditions showed similar trends with gas injection). The above approximation is intended merely to illustrate a method for combining the results of the two experiments and the result is not presented as a solution to the problem. Future work should address the problem of upper surface modelling in order to closely simulate the actual system.

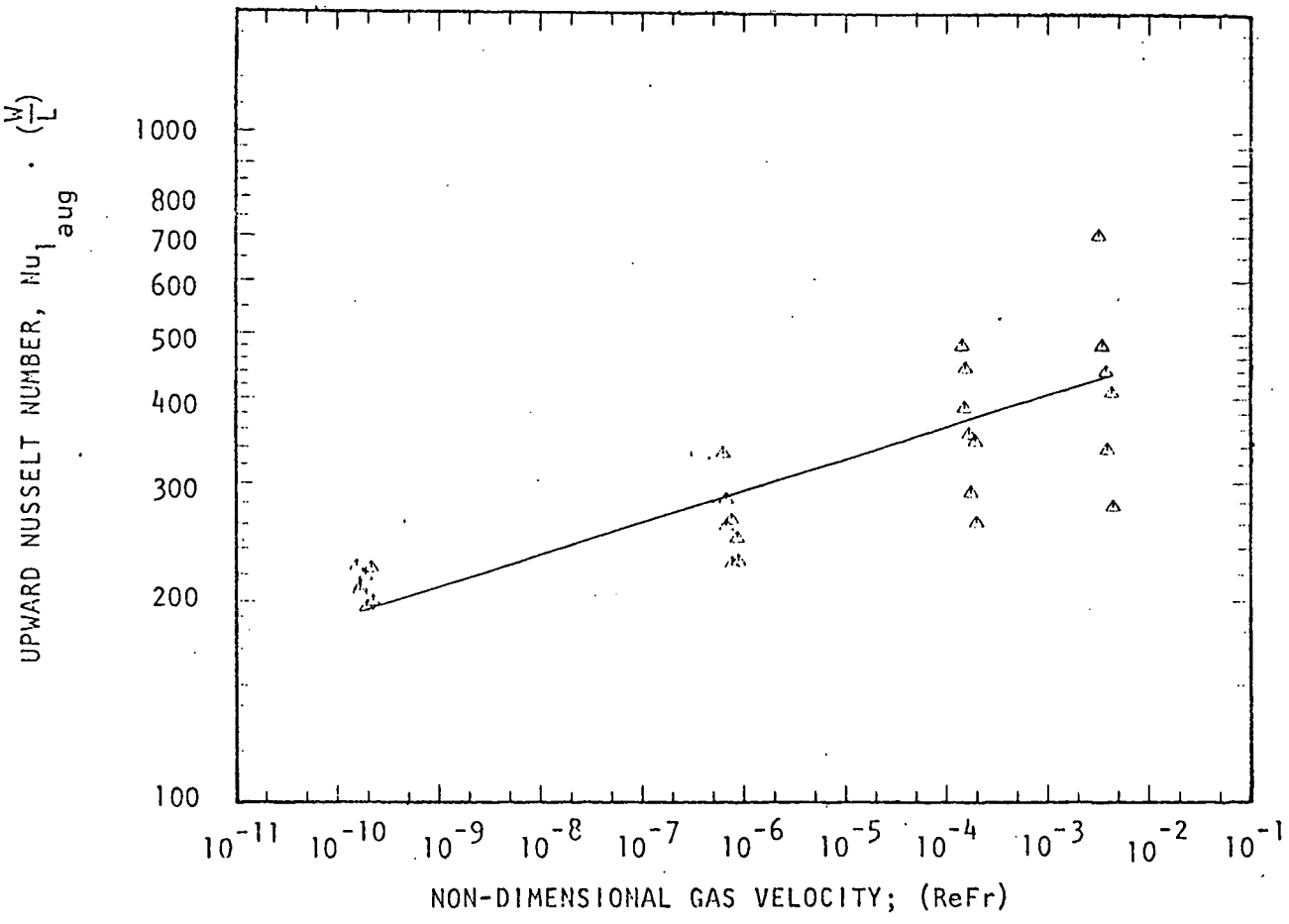

Figure 43. Comparison of Calculated and Predicted Nusselt Numbers.

Chapter V

CONCLUSIONS AND RECOMMENDATIONS

V.1 Conclusions

Gas injection at the boundaries of a volumetrically-heated pool is found to have a significant effect on the heat transfer rates at the pool boundaries. Pool maximum temperatures are reduced considerably with gas injection as compared to natural convection. The pools are well-stirred by the gas and show nearly isothermal temperature distributions.

Natural convection effects are found to be negligible in the gas mixed pool; the sideward, downward, and upward Nusselt numbers are independent of the internal Rayleigh number.

The pool layer depth (i.e. aspect ratio) has a negligible effect on the normalized Nusselt numbers and heat transfer coefficient around the pool boundaries.

Correct modelling of the pool boundaries so that they would simulate debris pool/concrete systems is found to be very important. Nusselt numbers to porous boundaries where the gas emanates from random locations along the surface are significantly higher than those with discrete holes.

Small gas injection rates are found to cause steep increases in Nusselt number from the natural convection values. The rate of increase with increasing superficial gas velocities decreases, however, as the initial mixing effects and boundary layer reduction effect saturate.

For volumetrically heated pools with gas injection at the boundaries, the downward and sideward Nusselt numbers for porous plates are comparable. This is in contrast to the natural convection case where sideward Nusselt numbers are significantly higher than the downward Nusselt numbers (see Figures 7 and 11). Although the sideward and downward Nusselt numbers are well correlated, the upper boundary condition will be very important in determining the relative power distribution upward and into the concrete.

The Nusselt numbers to porous plates with gas evolution are directly correlated to the product of Reynolds and Froude numbers; $(Re \cdot Fr) \equiv (\frac{v^3\rho}{\mu g})$ which is a measure of the buoyancy and viscous drag effects produced by the gas as it mixes the liquid.

The downward Nusselt number in a free upper surface model shows a higher dependence on the non-dimensional parameter, $(Re \cdot Fr)$, and the superficial gas velocity than models with a solid upper surface.

V.2 Recommendations

In terms of the PAHR problem, further work is required to allow adequate description of the molten core debris/concrete system. As a result of this work, several investigations are recommended; these include:

(1) Measurement of sideward Nusselt numbers to a porous side boundary for a free upper surface model is recommended.

(2) Experiments with liquid and gas injection at the sides and lower boundaries are recommended since they simulate the

combined heat and mass transfer processes taking place in the actual system where molten oxides of concrete mix with and continually dilute the core debris pool.

(3) The effects of gas injection on two-layer pools to simulate an immiscible steel layer above the core debris are also of interest. As the pool is continually diluted by the dissolved concrete its density decreases below that of the initially lighter steel layer. The inversion process which may follow will significantly affect the pool growth pattern.

(4) In terms of the Nusselt type correlations presented in this thesis, follow-up investigations over a wider range of the physical constants, density and viscosity, would provide added confidence in extrapolating the correlations to the molten debris/concrete system.

(5) In order to determine the relative power distribution into the concrete and upward into containment for the PAHR problem, modelling of the upper boundary must be improved. Large scale tests with upper boundaries such as overlying steel layers would be useful in outlining the gross characteristics of these systems.

BIBLIOGRAPHY

[A1] S.I. Abdel-Khalik and D.K. Felde, "Heat Transfer in Volumetrically Heated Pools with Gas Injection at the Boundaries," Proc. 3rd PAHR "Information Exchange", Argonne National Lab, ANL-78-10, Nov. 2-4, 1977.

[B1] L. Baker, Jr., F.B. Cheung, M.G. Chasanov, E.S. Sowa, J.D. Bingle, G. Staahl, J.R. Pavlik, W. Holloway, "Interactions of LMFBR Core Debris with Concrete", Argonne National Laboratory, Argonne, Illinois.

[B2] R.F. Bergholz and R. Bjorge, "Bubble-Induced Heat Transfer in a Heat Generating Liquid Layer", Proc. of 3rd PAHR "Information Exchange", Argonne National Laboratory, ANL-78-10, (Nov. 1977).

[B3] L. Baker, Jr., M.G. Chasanov, J.D. Gabor, W.H. Gunther, J.C. Cassulo, J.D. Bingle, G.A. Mansoori, "Heat Removal from Molten Fuel Pools", Argonne National Laboratory, Argonne, Illinois.

[C1] Catton, I., Erdmann, R.C., "PACR for LMFRB's", (UCLA-ENG-7343) July 1972 - June 1973.

[F1] G. Fieg, "Experimental Investigations of Heat Transfer Characteristics in Liquid Layers with Internal Heat Sources", Kernforschungszentrum Karlsruhe, Institut für Neutronenphysik und Reaktortechnik.

[F2] Fiedler, H.E. and Wille, R., "Turbulante Freie Konvektion in Einer Horizontalen Flussigkeitsschicht mit Volumen-Warmequolls", Paper NC 4.5, Proceedings Fourth Int. Heat Transfer Conf., Paris, Versailles, 1970.

[F3] R. Farhadieh and L. Baker, Jr., "Simulation Experiments of the Growth of a Hot Fuel Pool in a Sacrificial Bed", Argonne National Laboratory, ANL/RAS 76-27 (Sept. 1976).

[F4] D.K. Felde, Z. Musicki, and S.I. Abdel-Khalik, "Growth of Volumetrically-Heated Pools in Miscible Gas-Releasing Solid Beds", Proc: Post Accident Heat Removal Mtg, Ispra, Italy (Oct. 1978).

[F5] G. Fieg and H. Werle, "Heat Transfer Measurements from Internally Heated Liquids Enclosed by Nonmelting and Melting Boundaries", Proc. of the 3rd PAHR "Information Exchange", Argonne National Laboratory, ANL-78-10, (Nov. 1977).

[G1] E.L. Gluekler and A. Dayan, "Considerations of the Third Line of Assurance-Post-Accident Heat Removal and Core Retention in Containment", General Electric Company, Sunnyvale, California.

[G2] G.A. Greene, O.C. Jones, Jr., and C.E. Schwarz, "Thermo-Fluid Mechanics of Volume-Heated Boiling Pools", Brookhaven National Laboratory, BNL-NUREG-50759, (Dec. 1977).

[G3] A. Ganguli, A. Luk, and S.G. Bankoff, "Heat Transfer Characteristics of a Non-Boiling Pool with Spatially Uniform Gas Injection", Northwestern University, Evanston, Illinois (Dec. 1978).

[H1] W.F. Hart, "Heat Transfer in Bubble Agitated Systems. A General Correlation', Ind. Eng. Chem., Vol. 15 (1), 109 (1976).

[J1] M. Jahn and H.H. Reineke, "Free Convection Heat Transfer with Internal Heat Sources Calculations and Measurements", 5th Int. Heat Transfer Conf., Tokyo (Sept. 1974), Vol. III, pp. 74-78.

[K1] M.S. Kazimi, J.C. Chen, "A Condensed Review of the Technology of Post-Accident Heat Removal for the Liquid Metal Fast Breeder Reactor", American Nuclear Society Critical Reviews, Nuclear Technology, Vol. 38, No. 3 (May 1978).

[K2] F.A. Kulacki and R.J. Goldstein, "Thermal Convection in a Horizontal Fluid Layer with Uniform Volumetric Energy Sources", J. Fluid Mechanics, 55. 2. 271 (1972).

[K3] F.A. Kulacki, A.A. Emara, S.A. Korpela, N.K. Cambha, and J.H. Min, "Natural Convection with Internal Energy Sources: Some Recent Experimental and Numerical Results with Post-Accident Heat Removal Applications", Proceedings of the Third PAHR Information Exchange, ANL-78-10, Argonne National Lab, (Nov. 1977).

[K4] F.A. Kulacki, M.E. Nagle, "Natural Convection in a Horizontal Fluid Layer with Volumetric Energy Sources", ASME Transactions Journal of Heat Transfer, Vol. 97, Series C, 1975, pp. 204-211.

[K5] A.A. Kudirka, "Two Phase Heat Transfer with Gas Injection through a Porous Boundary Surface", Argonne National Laboratories, ANL 6862, (March 1964).

[K6] M.S. Kazimi, "Thermohydraulic LMFBR Safety Experiments", Brookhaven National Laboratory, BNL-NUREG-50544, (Sept. 1976).

[K7] S.S. Kutateladze and I.G. Malenkov, "Fluid and Gas Dynamical Aspects of Heat Transfer in the Injection Bubbling and Boiling of Liquids", Trans. from Teplofizika Vysokikh Temperatue, Vol. 14 (4), July - Aug. 1976, p. 703.

[M1] J.D. McCormack and A.K. Postma, "Water and Gas Release from Heated Concrete", HEDL-SA-1117, Sept. 1976.

[M2] J.F. Muir, D.A. Powers and D. A. Dahlgren, "Studies on Molten Fuel-Concrete Interactions", Sandia Laboratories, Albuquerque, New Mexico.

[M3] F. Mayinger, H.H. Reineke, R. Schramm, U. Steinberner, "Behavior of the Core Melt-Down in Case of a Hypothetical Malfunction", Institute for Processing Techniques of the Institute of Technology, Hannover, 1976, NRC Translation #427.

[P1] D.A. Powers, D.A. Dahlgren, J.F. Muir, W.D. Murefin, "Exploratory Study of Molten Core Material/Concrete Interaction, July 1975 - March 1977", Sandia Laboratories, SAND77-2042 (Feb. 1978).

[P2] R.S. Peckover, "The Thermal Containment of Reactor Core Material after Shutdown", Proc. Fast Reactor Safety Conf, Conf.-740401, p. 802, U.W. Atomic Energy Commission (1974).

[S1] Schwab, J.R. and Schwiderski, E.W., "Convection Experiments with Electrolytically Heated Fluid Layers", J. Fluid Mech., Vol. 48, 1971, p. 703.

[S2] R.J. Slember, "Safety-Related Design Considerations for the Clinch River Breeder Reactor Plant", Westinghouse Electric Corporation, Oak Ridge, TN 37830.

[T1] Tritton, D.J. and Zarraga, M.N., "Convection in Horizontal Fluid Layers with Heat Generation Experiments", J. Fluid Mech. Vol. 30. 1967, p. 21.

Data for Discrete Hole Lower Boundary, Porous Side Boundaries, and Solid Upper Boundary.

RUN NO.	INPUT POWER (W)	POWER(WATTS) LEFT SIDE	RIGHT SIDE	BOTTOM	TOP	AIR	ENERGY BALANCE ERROR(%)	POOL TEMP (C)	PLATE TEMP(C) L	R	B	T	SUPERFITIAL GAS VELOCITY (CM/MIN)	(ReFr)
501.	100.	27.7	26.4	7.4	33.2	.00	-5.4	33.9	26.7	25.4	26.7	27.4	.000	.0000
502.	100.	31.5	29.4	14.7	24.6	.01	.2	31.3	26.6	25.9	26.6	26.3	.065	.1587-09
503.	100.	33.2	31.5	16.4	14.9	.21	-3.8	30.5	27.0	27.0	27.0	26.6	1.033	.6400-06
504.	100.	33.9	31.7	16.6	13.6	1.28	-3.2	29.8	27.1	27.1	27.0	26.4	6.329	.1451-03
505.	100.	32.8	29.9	15.4	11.2	3.46	-7.2	29.2	27.1	26.8	26.9	25.9	17.955	.3256-02
506.	200.	52.1	49.3	14.3	80.9	.00	-1.4	38.8	27.0	26.3	27.2	27.3	.000	.0000
507.	200.	59.8	54.2	27.8	47.8	.02	-5.2	36.1	27.8	26.2	27.0	26.6	.065	.1739-09
508.	200.	62.0	59.4	33.9	34.5	.24	-4.9	34.8	29.1	27.1	28.2	26.8	1.033	.6950-06
509.	200.	63.3	60.1	37.7	30.1	1.43	-3.7	33.6	28.6	27.7	28.4	26.9	6.329	.1557-03
510.	200.	63.6	59.1	37.7	23.1	3.69	-6.3	32.7	28.6	27.4	28.3	25.8	17.955	.3495-02
511.	400.	98.0	90.1	27.6	168.0	.00	-4.1	46.3	29.4	26.2	28.7	27.1	.000	.0000
512.	400.	115.6	105.9	53.1	96.1	.04	-7.3	44.0	31.2	27.4	30.1	26.6	.065	.2017-09
513.	400.	118.6	112.5	63.2	83.2	.62	-5.5	42.5	32.4	29.3	31.7	26.4	1.033	.8061-06
514.	400.	115.6	109.5	68.6	75.4	1.77	-7.3	40.8	32.7	30.0	32.6	26.8	6.329	.1803-03
515.	400.	122.2	110.7	70.1	62.6	4.88	-7.3	40.4	33.8	30.8	33.1	27.1	17.955	.4088-02
516.	600.	143.4	130.7	42.1	229.8	.00	-9.1	57.3	34.0	28.6	33.9	28.3	.000	.0000
517.	600.	147.1	136.8	64.2	173.0	.04	-13.2	52.9	35.9	31.7	35.7	28.1	.065	.2339-09
518.	600.	155.0	151.9	91.4	139.3	-.15	-10.4	52.7	37.6	35.7	36.7	29.0	1.033	.9550-06
519.	600.	154.4	147.7	98.8	132.4	-.92	-11.4	52.1	40.1	37.9	40.6	31.1	6.329	.2175-03
520.	600.	153.8	146.5	95.7	120.9	-2.63	-14.3	50.9	42.2	38.1	41.3	28.6	17.955	.4885-02
521.	100.	21.4	21.0	13.4	46.7	.00	2.5	33.2	26.3	24.3	25.8	25.0	.000	.0000
522.	100.	21.6	21.2	18.5	43.3	.01	4.6	31.6	26.7	25.4	25.9	25.0	.065	.1593-09
523.	100.	25.2	25.4	23.7	28.2	.22	2.8	30.6	27.2	25.9	26.6	24.7	1.033	.6439-06
524.	100.	27.0	27.6	27.4	18.9	1.28	2.3	30.8	26.9	26.7	26.7	23.6	6.329	.1478-03
525.	100.	24.8	24.6	25.8	24.8	3.48	3.5	29.4	27.2	26.5	26.4	24.9	17.955	.3279-02
526.	200.	43.5	43.5	23.5	89.6	.00	.0	40.3	28.3	25.0	27.6	27.1	.000	.0000
527.	200.	43.5	42.1	31.7	79.0	.02	-1.9	37.5	28.9	25.9	27.4	26.8	.065	.1792-09
528.	200.	46.7	47.5	45.2	54.7	.26	-1.8	36.2	29.8	27.6	28.2	25.3	1.033	.7147-06
529.	200.	53.4	52.3	52.3	36.5	1.49	-2.0	36.6	30.0	28.9	28.9	24.1	6.329	.1653-03
530.	200.	47.4	48.9	49.2	44.1	4.22	-3.1	34.6	29.8	28.1	28.4	24.6	17.955	.3629-02
531.	400.	85.6	85.0	41.9	168.8	.00	-4.7	50.2	30.2	26.7	29.3	28.4	.000	.0000
532.	400.	88.3	88.8	57.5	148.6	.04	-4.2	46.7	31.1	28.3	29.8	27.1	.065	.2114-09
533.	400.	95.3	98.0	79.2	103.2	.62	-5.9	45.0	31.5	30.6	30.6	25.7	1.033	.8404-06
534.	400.	112.5	110.9	97.7	56.0	1.83	-5.3	46.0	34.3	33.0	31.7	24.9	6.329	.1965-03
535.	400.	100.7	101.7	94.3	76.2	10.75	-4.2	43.0	33.1	32.0	31.0	25.2	17.955	.4263-02
536.	600.	123.9	113.2	57.6	272.0	.00	-5.6	56.8	32.4	27.4	30.6	26.8	.000	.0000
537.	600.	141.3	135.1	86.3	196.8	.04	-6.7	58.9	35.4	32.4	34.7	28.1	.065	.2570-09
538.	600.	161.4	147.0	117.0	144.2	.63	-5.0	55.6	36.5	34.8	36.0	25.3	1.033	.9987-06
539.	600.	175.2	159.5	143.3	100.3	5.83	-3.0	56.2	39.1	38.1	37.3	25.9	6.329	.2315-03
540.	600.	153.3	143.9	137.0	119.1	-2.61	-8.2	51.9	37.6	37.8	36.0	25.8	17.955	.4952-02
541.	100.	15.2	13.2	17.7	45.8	.00	-8.1	38.1	29.6	28.5	28.7	26.9	.000	.0000
542.	100.	13.2	11.7	22.6	47.2	.01	-5.4	34.2	27.2	27.8	28.2	27.3	.065	.1676-09
543.	100.	12.0	11.4	24.1	44.2	.21	-8.0	32.6	28.3	29.1	28.0	26.4	1.033	.6649-06
544.	100.	11.9	11.0	23.5	46.5	1.22	-6.0	31.3	27.6	28.5	27.9	26.8	6.329	.1492-03
545.	100.	10.7	9.9	21.0	44.6	3.32	-10.4	30.7	28.1	27.4	27.3	26.8	17.955	.3371-02
546.	200.	32.7	30.1	31.5	97.6	.00	-4.1	42.8	28.3	28.3	28.1	27.9	.000	.0000
547.	200.	30.9	27.5	38.6	97.6	.01	-2.7	40.3	27.4	28.7	28.0	26.8	.065	.1901-09
548.	200.	27.3	25.9	42.2	93.0	.22	-5.7	36.9	29.8	29.4	27.7	27.8	1.033	.7246-06

549.	200.	26.2	24.4	42.6	97.6	1.37	-3.9	34.9	27.4	28.9	28.1	27.6	6.329	.1600-03
550.	200.	25.4	23.9	40.4	93.4	3.75	-6.6	33.8	28.0	29.1	28.0	28.0	17.955	.3571-02
551.	400.	59.7	55.3	59.2	200.5	.00	-6.3	52.8	32.2	31.1	29.4	27.9	.000	.0000
552.	400.	53.4	51.6	73.8	191.9	.04	-7.3	48.2	29.4	31.5	29.6	28.1	.065	.2169-09
553.	400.	49.6	49.7	77.7	191.9	.30	-7.7	44.9	29.3	31.9	29.3	28.6	1.033	.8396-06
554.	400.	50.8	48.4	80.6	189.5	1.74	-7.2	40.7	31.9	31.7	29.3	28.4	6.329	.1799-03
555.	400.	49.9	48.4	78.1	183.2	4.62	-8.9	39.4	29.4	32.2	29.3	27.3	17.955	.4009-02
556.	600.	88.4	91.4	85.5	298.3	.00	-6.0	63.6	33.1	31.5	30.7	30.3	.000	.0000
557.	600.	85.5	84.0	103.2	297.2	.04	-5.0	58.9	32.2	33.7	30.2	29.8	.065	.2570-09
558.	600.	73.6	78.1	118.3	300.7	.63	-4.8	52.2	33.7	35.6	29.6	32.2	1.033	.9488-06
559.	600.	74.1	78.1	124.2	293.9	3.84	-4.3	48.1	33.1	34.6	29.8	31.7	6.329	.2037-03
560.	600.	76.1	82.1	117.8	280.2	10.83	-5.5	44.9	30.9	34.8	30.1	27.9	17.955	.4400-02

Data for Discrete Hole Lower Boundary, Porous Side Boundaries, and Solid Upper Boundary.

RUN NO.	POWER FRACTION SIDE	BOTTOM	TOP	NUSSELT NUMBER SIDE	BOTTOM	TOP	ASPECT RATIO	RAYLEIGH NO.	M	SUPERFICIAL GAS VELOCITY (CM/MIN)	(ReFr)
501.	.571	.078	.351	36.4	10.7	53.8	1.051	.9209+08	.1631+02	.000	.0000
502.	.607	.147	.246	63.6	32.8	52.3	1.051	.8813+08	.2649+02	.065	.1587-09
503.	.672	.170	.157	98.3	49.8	40.8	1.051	.8187+08	.3479+02	1.033	.6400-06
504.	.676	.171	.153	128.1	62.3	46.7	1.051	.8012+08	.4334+02	6.329	.1451-03
505.	.676	.166	.158	152.2	72.1	47.8	1.051	.7416+08	.5176+02	17.955	.3256-02
506.	.515	.075	.410	43.7	13.4	73.7	1.051	.2309+09	.2116+02	.000	.0000
507.	.601	.147	.252	66.8	34.3	52.8	1.051	.2001+09	.2784+02	.065	.1739-09
508.	.639	.178	.183	97.5	54.0	45.5	1.051	.1916+09	.3602+02	1.033	.6950-06
509.	.641	.196	.164	120.7	77.8	49.9	1.051	.1846+09	.4732+02	6.329	.1557-03
510.	.655	.201	.144	141.8	92.0	41.5	1.051	.1737+09	.5446+02	17.955	.3495-02
511.	.490	.072	.438	52.6	16.0	89.4	1.051	.5657+09	.2644+02	.000	.0000
512.	.597	.143	.259	79.4	39.4	56.7	1.051	.5108+09	.3268+02	.065	.2017-09
513.	.611	.167	.222	105.0	60.3	53.9	1.051	.4990+09	.4289+02	1.033	.8061-06
514.	.607	.185	.208	125.8	86.0	56.9	1.051	.4662+09	.5527+02	6.329	.1603-03
515.	.628	.189	.182	155.8	100.0	52.9	1.051	.4601+09	.6291+02	17.955	.4088-02
516.	.503	.077	.420	53.6	18.0	79.2	1.051	.1075+10	.2773+02	.000	.0000
517.	.545	.123	.332	76.2	37.6	70.5	1.051	.9185+09	.3633+02	.065	.2339-09
518.	.571	.170	.259	96.9	65.9	59.4	1.051	.9422+09	.4612+02	1.033	.9550-06
519.	.568	.184	.247	118.0	86.1	63.5	1.051	.9178+09	.5559+02	6.329	.2175-03
520.	.584	.186	.230	147.1	100.8	53.5	1.051	.8636+09	.6446+02	17.955	.4885-02
521.	.414	.131	.455	28.8	19.0	60.0	1.542	.2093+08	.1180+02	.000	.0000
522.	.410	.176	.414	41.7	34.6	70.1	1.542	.2003+08	.1569+02	.065	.1593-09
523.	.493	.231	.276	64.7	59.0	48.9	1.542	.1912+08	.2071+02	1.033	.6439-06
524.	.535	.268	.197	72.4	70.8	29.7	1.542	.1898+08	.2145+02	6.329	.1478-03
525.	.478	.249	.273	104.0	91.6	55.4	1.542	.1811+08	.2986+02	17.955	.3279-02
526.	.435	.117	.448	33.7	19.5	70.7	1.542	.5339+08	.1346+02	.000	.0000
527.	.436	.161	.403	45.4	32.9	77.0	1.542	.4723+08	.1655+02	.065	.1792-09
528.	.490	.230	.280	68.7	59.3	52.9	1.542	.4500+08	.2088+02	1.033	.7147-06
529.	.539	.267	.194	78.4	71.5	32.0	1.542	.4548+08	.2172+02	6.329	.1653-03
530.	.497	.254	.249	91.8	84.0	50.6	1.542	.4173+08	.2682+02	17.955	.3629-02
531.	.447	.110	.443	40.1	20.4	78.8	1.542	.1355+09	.1504+02	.000	.0000
532.	.462	.150	.388	53.6	34.7	77.5	1.542	.1232+09	.1874+02	.065	.2114-09
533.	.514	.211	.276	71.0	56.3	55.1	1.542	.1151+09	.2168+02	1.033	.8406-06
534.	.590	.258	.153	92.6	69.8	28.0	1.542	.1193+09	.2194+02	6.329	.1965-03
535.	.528	.245	.227	100.6	80.8	50.5	1.542	.1107+09	.2672+02	17.955	.4263-02
536.	.418	.102	.480	44.7	22.0	90.8	1.542	.2379+09	.1754+02	.000	.0000
537.	.494	.154	.352	55.6	35.6	63.9	1.542	.2475+09	.1873+02	.065	.2570-09
538.	.541	.205	.254	77.9	60.0	48.1	1.542	.2321+09	.2369+02	1.033	.9987-06
539.	.575	.246	.179	95.9	76.4	34.5	1.542	.2403+09	.2516+02	6.329	.2315-03
540.	.540	.249	.212	105.8	87.2	45.1	1.542	.2042+09	.2841+02	17.955	.4952-02
541.	.309	.192	.498	16.7	19.6	42.8	2.660	.2549+07	.4601+01	.000	.0000
542.	.263	.238	.499	19.5	39.6	72.2	2.660	.2267+07	.7812+01	.065	.1676-09
543.	.255	.262	.483	32.4	56.1	76.9	2.660	.2006+07	.1004+02	1.033	.6649-06
544.	.243	.250	.507	38.2	73.6	112.6	2.660	.2009+07	.1385+02	6.329	.1492-03
545.	.230	.234	.535	38.1	65.9	129.3	2.660	.1873+07	.1321+02	17.955	.3371-02
546.	.327	.164	.509	22.4	22.2	67.6	2.660	.6214+07	.6344+01	.000	.0000
547.	.300	.198	.502	24.7	32.5	74.8	2.660	.5869+07	.7696+01	.065	.1901-09
548.	.282	.224	.494	38.4	47.9	107.1	2.660	.5063+07	.1006+02	1.033	.7246-06
549.	.263	.222	.515	39.5	65.6	140.9	2.660	.4735+07	.1391+02	6.329	.1600-03

550.	.264	.216	.520	49.8	73.8	177.4	2.660	.4400+07	.1604+02	17.955	.3571-02
551.	.307	.158	.535	27.5	25.5	81.2	2.660	.1666+06	.7602+01	.000	.0000
552.	.283	.199	.518	30.3	40.4	97.5	2.660	.1404+08	.9537+01	.065	.2169-09
553.	.269	.211	.521	35.7	51.1	120.4	2.660	.1273+06	.1141+02	1.033	.8396-06
554.	.267	.218	.515	57.8	74.0	162.3	2.660	.1131+06	.1597+02	6.329	.1799-03
555.	.270	.214	.516	61.2	80.9	162.1	2.660	.1063+08	.1772+02	17.955	.4009-02
556.	.319	.152	.529	28.6	25.9	89.3	2.660	.3132+06	.8011+01	.000	.0000
557.	.297	.181	.522	32.7	36.0	102.1	2.660	.2847+06	.9344+01	.065	.2570-09
558.	.266	.207	.527	43.8	52.7	152.2	2.660	.2412+08	.1197+02	1.033	.9488-06
559.	.265	.216	.519	55.0	69.2	185.1	2.660	.2167+06	.1504+02	6.329	.2037-03
560.	.279	.208	.513	69.8	81.9	175.8	2.660	.1952+06	.1852+02	17.955	.4400-02

$FIN

Data for Porous Lower Boundary, Discrete Hole Side Boundaries, and Solid Upper Boundary with Upper Plate to Lower Plate Electrodes.

RUN NO.	INPUT POWER (W)	POWER(WATTS) LEFT SIDE	RIGHT SIDE	BOTTOM	TOP	AIR	ENERGY BALANCE ERROR(%)	POOL TEMP (C)	PLATE TEMP(C) L	R	B	T	SUPERFITIAL GAS VELOCITY (CM/MIN)	(ReFr)
401.	100.	8.8	9.9	11.2	46.8	.00	-23.3	34.4	27.9	26.9	28.7	27.4	.000	.0000
402.	100.	7.8	9.0	20.6	64.1	.01	1.5	29.4	26.1	26.7	26.8	25.4	.065	.1524-09
403.	100.	5.8	6.3	18.6	64.5	.18	-4.6	28.7	26.4	26.7	27.0	26.0	1.033	.6138-06
404.	100.	5.3	5.9	18.2	69.5	1.11	-.0	28.0	26.4	26.4	26.8	26.2	6.329	.1385-03
405.	100.	4.3	4.8	15.9	65.9	3.14	-6.0	27.4	26.6	26.1	26.7	26.3	17.955	.3119-02
406.	200.	28.2	28.4	21.5	99.3	.00	-11.3	37.8	28.3	27.2	28.9	25.2	.000	.0000
407.	200.	17.6	19.9	31.0	127.4	.01	-2.0	32.2	26.0	26.9	26.9	26.4	.065	.1613-09
408.	200.	15.8	18.9	33.9	120.8	.20	-5.2	31.4	26.9	27.3	27.3	25.8	1.033	.6505-06
409.	200.	14.1	16.5	31.0	129.6	1.25	-3.8	29.8	26.2	26.9	27.0	26.3	6.329	.1449-03
410.	200.	11.5	13.5	27.7	121.6	3.42	-11.1	29.2	26.2	27.0	27.1	26.2	17.955	.3261-02
411.	400.	61.8	61.8	41.6	211.0	.00	-6.0	46.1	29.4	27.6	29.3	27.3	.000	.0000
412.	400.	38.1	41.2	60.5	251.3	.02	-2.2	37.8	27.0	28.7	27.8	25.1	.065	.1602-09
413.	400.	37.5	41.2	64.9	240.8	.24	-3.8	35.9	27.2	29.2	28.0	27.0	1.033	.7106-06
414.	400.	33.9	38.7	60.1	248.7	1.49	-4.3	33.3	27.2	28.8	27.7	28.1	6.329	.1551-03
415.	400.	31.8	37.8	59.0	252.6	4.08	-3.7	32.5	26.4	28.9	27.9	28.1	17.955	.3484-02
416.	600.	85.5	89.5	64.1	322.9	.00	-6.3	53.2	30.2	28.8	30.6	28.7	.000	.0000
417.	600.	61.8	66.4	94.8	346.7	.02	-5.0	43.8	27.9	30.1	29.1	30.7	.065	.2012-09
418.	600.	60.9	66.4	108.3	331.8	.29	-5.4	41.3	27.9	31.3	26.9	30.4	1.033	.7911-06
419.	600.	58.2	66.9	104.7	345.2	1.84	-3.9	38.2	28.0	31.2	29.8	30.6	6.329	.1710-03
420.	600.	49.0	62.0	102.9	348.2	5.19	-5.5	37.1	28.4	31.1	29.8	31.1	17.955	.3614-02
421.	200.	25.4	25.9	25.9	112.8	.00	-5.0	38.4	28.0	27.4	27.6	26.7	.000	.0000
422.	200.	13.5	14.6	35.7	132.9	.01	-1.6	32.3	26.7	27.2	27.0	25.9	.065	.1615-09
423.	200.	12.9	14.5	35.7	132.0	.17	-2.3	30.7	26.5	27.2	27.1	26.2	1.033	.6420-06
424.	200.	10.4	11.6	33.1	135.7	1.08	-4.1	29.4	26.5	27.0	27.2	26.0	6.329	.1435-03
425.	200.	9.3	10.2	30.8	135.8	3.05	-5.4	28.7	26.1	26.7	26.7	25.8	17.955	.3220-02
426.	400.	51.9	51.4	49.5	223.7	.00	-5.9	47.3	29.1	28.5	28.7	28.0	.000	.0000
427.	400.	32.1	33.3	66.3	248.0	.01	-5.1	38.4	27.8	29.1	27.7	28.2	.065	.1828-09
428.	400.	31.0	34.5	69.4	245.7	.19	-4.8	36.0	27.4	29.3	27.8	27.7	1.033	.7114-06
429.	400.	30.5	33.4	66.0	254.2	1.17	-3.7	33.6	28.0	29.3	28.0	26.4	6.329	.1559-03
430.	400.	29.4	31.3	63.6	247.4	3.32	-6.2	32.6	27.6	28.9	27.7	28.6	17.955	.3488-02
431.	600.	74.7	75.8	72.7	339.3	.00	-6.2	54.1	30.9	30.0	30.7	29.3	.000	.0000
432.	600.	49.9	52.0	101.1	364.2	.01	-5.5	44.2	28.1	30.7	29.0	30.4	.065	.2025-09
433.	600.	51.2	55.2	108.4	348.6	.21	-6.1	41.7	29.1	31.5	29.7	31.8	1.033	.7960-06
434.	600.	52.1	58.1	109.6	353.3	1.35	-4.2	39.1	29.1	31.9	29.8	31.9	6.329	.1745-03
435.	600.	51.2	54.9	108.3	339.3	3.99	-7.1	37.9	30.2	31.9	29.7	31.6	17.955	.3686-02

Data for Porous Lower Boundary, Discrete Hole Side Boundaries, and Solid Upper Boundary with Upper Plate to Lower Plate Electrodes.

RUN NO.	POWER FRACTION SIDE	BOTTOM	TOP	NUSSELT NUMBER SIDE	BOTTOM	TOP	ASPECT RATIO	RAYLEIGH NO.	M	SUPERIFICAL GAS VELOCITY (CM/MIN)	(ReFr)
401.	.244	.146	.611	14.0	20.4	70.5	1.051	.7610+08	.1664+02	.000	.0000
402.	.165	.203	.632	30.2	84.4	173.6	1.051	.8209+08	.4938+02	.065	.1524-09
403.	.127	.195	.678	30.0	115.7	254.2	1.051	.7454+08	.7051+02	1.033	.6138-06
404.	.112	.182	.706	38.5	159.8	425.6	1.051	.7520+08	.1043+03	6.329	.1385-03
405.	.097	.169	.735	45.3	218.9	667.6	1.051	.6870+08	.1545+03	17.955	.3119-02
406.	.319	.121	.560	29.5	25.1	82.3	1.051	.2004+09	.2465+02	.000	.0000
407.	.191	.158	.650	34.7	61.6	233.6	1.051	.1764+09	.4630+02	.065	.1613-09
408.	.183	.179	.638	43.4	88.7	228.9	1.051	.1672+09	.5907+02	1.033	.6505-06
409.	.159	.161	.680	51.5	119.1	405.0	1.051	.1568+09	.8786+02	6.329	.1449-03
410.	.141	.156	.703	53.1	140.0	444.9	1.051	.1425+09	.1070+03	17.955	.3261-02
411.	.328	.111	.561	36.0	25.4	115.0	1.051	.5509+09	.2730+02	.000	.0000
412.	.203	.155	.643	42.1	63.2	271.6	1.051	.4409+09	.4861+02	.065	.1602-09
413.	.205	.169	.627	54.7	85.8	282.8	1.051	.4043+09	.6045+02	1.033	.7106-06
414.	.190	.157	.653	74.2	112.1	506.1	1.051	.3641+09	.8494+02	6.329	.1551-03
415.	.181	.153	.666	83.3	135.5	619.2	1.051	.3547+09	.1053+03	17.955	.3484-02
416.	.311	.114	.575	37.3	28.9	133.0	1.051	.9976+09	.3013+02	.000	.0000
417.	.225	.166	.609	44.9	66.3	271.1	1.051	.7813+09	.4740+02	.065	.2012-09
418.	.224	.191	.585	57.9	90.1	315.9	1.051	.7242+09	.5622+02	1.033	.7911-06
419.	.217	.181	.602	80.2	130.2	476.0	1.051	.6600+09	.8539+02	6.329	.1710-03
420.	.196	.181	.623	84.4	147.9	622.3	1.051	.6221+09	.9706+02	17.955	.3814-02
421.	.270	.136	.594	24.9	24.8	99.9	1.542	.4739+08	.1476+02	.000	.0000
422.	.143	.182	.675	28.1	71.7	220.4	1.542	.3874+08	.3203+02	.065	.1615-09
423.	.140	.183	.677	38.8	106.9	316.3	1.542	.3610+08	.4737+02	1.033	.6420-06
424.	.115	.173	.713	45.4	163.2	430.7	1.542	.3346+08	.7663+02	6.329	.1435-03
425.	.103	.163	.734	45.6	160.3	504.3	1.542	.3186+08	.7979+02	17.955	.3220-02
426.	.274	.131	.594	28.5	27.1	118.4	1.542	.1230+09	.1674+02	.000	.0000
427.	.172	.174	.653	34.2	64.1	253.1	1.542	.9472+08	.2980+02	.065	.1628-09
428.	.172	.182	.646	45.8	88.6	309.7	1.542	.8653+08	.3941+02	1.033	.7114-06
429.	.166	.171	.663	69.1	124.2	521.8	1.542	.7966+08	.5877+02	6.329	.1559-03
430.	.162	.170	.668	76.5	138.2	663.4	1.542	.7465+08	.6586+02	17.955	.3488-02
431.	.268	.129	.603	32.1	31.2	138.0	1.542	.2205+09	.1960+02	.000	.0000
432.	.180	.178	.642	35.8	68.3	271.9	1.542	.1697+09	.3107+02	.065	.2025-09
433.	.189	.192	.619	48.8	93.0	363.0	1.542	.1568+09	.3922+02	1.033	.7960-06
434.	.192	.191	.617	68.8	122.3	511.4	1.542	.1470+09	.5197+02	6.329	.1745-03
435.	.190	.194	.616	81.5	136.7	561.1	1.542	.1365+09	.5705+02	17.955	.3686-02

aFIN

Data for Porous Lower Boundary, Discrete Hole Side Boundaries, and Free Surface Upper Boundary.

RUN NO.	INPUT POWER (W)	POWER(WATTS) LEFT SIDE	RIGHT SIDE	BOTTOM	TOP	AIR	ENERGY BALANCE ERROR(%)	POOL TEMP (C)	PLATE TEMP(C) L	R	B	T	SUPERFITIAL GAS VELOCITY (CM/MIN)	(ReFr)
41.	100.	34.4	33.4	15.3	3.1	.00	-13.8	39.1	27.8	28.0	25.3	28.9	.000	.0000
42.	100.	24.6	26.3	35.3	2.8	.08	-10.9	32.6	25.9	26.9	26.3	25.0	.517	.8312-07
43.	100.	24.6	26.4	35.1	2.6	.16	-11.2	31.7	25.8	26.7	26.4	25.0	1.033	.6539-06
44.	100.	24.7	26.0	35.1	2.8	.40	-11.0	31.0	26.0	26.8	27.3	25.4	2.519	.9354-05
45.	100.	24.7	25.9	35.6	3.0	.62	-10.2	30.7	25.7	26.6	27.0	25.4	3.907	.3474-04
46.	100.	24.5	24.7	35.1	3.1	1.04	-11.5	30.2	26.1	26.4	26.4	25.4	6.329	.1462-03
47.	100.	24.0	24.0	34.3	3.2	1.81	-12.5	29.7	26.0	26.4	26.4	25.6	10.979	.7553-03
48.	100.	24.2	23.9	34.1	3.4	2.20	-12.2	29.6	26.0	26.4	26.8	25.6	12.885	.1215-02
49.	100.	23.4	23.1	33.1	4.2	3.09	-13.2	29.2	25.8	26.3	26.7	25.8	17.955	.3256-02
50.	100.	21.9	21.6	31.0	5.5	4.42	-15.6	28.7	25.6	26.0	26.8	26.3	24.801	.8485-02
51.	200.	70.6	69.8	26.8	13.2	.00	-9.8	47.4	27.6	28.2	24.3	24.7	.000	.0000
52.	200.	53.4	59.7	68.9	5.6	.08	-6.2	38.6	25.7	27.2	26.2	24.7	.517	.9381-07
53.	200.	51.6	58.2	67.8	6.0	.15	-8.1	37.1	25.8	26.9	28.0	24.7	1.033	.7271-06
54.	200.	50.2	56.4	68.3	6.5	.38	-9.1	35.6	26.0	26.7	28.4	25.0	2.519	.1022-04
55.	200.	50.6	55.7	68.4	6.9	.62	-8.9	35.1	25.6	26.8	28.6	25.0	3.907	.3778-04
56.	200.	50.2	54.6	66.2	7.2	1.01	-10.4	34.3	25.6	26.6	27.9	25.0	6.329	.1579-03
57.	200.	50.2	53.1	65.1	7.4	1.82	-11.2	33.5	25.6	26.2	27.3	25.3	10.979	.8121-03
58.	200.	50.2	52.0	65.1	9.6	2.22	-10.4	33.2	25.6	26.4	28.3	25.0	12.885	.1304-02
59.	200.	48.4	49.8	61.9	11.6	3.23	-12.5	32.5	25.6	26.0	27.6	25.6	17.955	.3484-02
60.	200.	36.7	38.3	43.6	55.1	4.29	-11.0	29.8	24.7	24.9	26.9	24.7	24.801	.8730-02
61.	400.	135.0	139.8	50.3	43.6	.00	-7.8	64.8	30.0	31.0	27.4	25.6	.000	.0000
62.	400.	99.8	117.2	120.4	17.3	.08	-11.3	51.3	27.9	29.9	29.7	25.2	.517	.1171-06
63.	400.	96.4	112.8	132.7	16.4	.16	-10.4	48.2	27.7	29.4	31.3	25.2	1.033	.8892-06
64.	400.	97.1	109.9	134.8	17.1	.40	-10.2	45.7	27.9	28.9	31.2	25.2	2.519	.1231-04
65.	400.	99.8	109.8	133.7	17.6	.62	-9.6	44.5	27.8	28.9	30.9	25.2	3.907	.4505-04
66.	400.	99.1	107.6	130.6	17.1	1.06	-11.1	43.3	27.4	29.0	31.3	25.2	6.329	.1876-03
67.	400.	99.7	103.3	131.6	18.6	2.01	-11.2	41.9	28.1	28.7	32.0	25.3	10.979	.9574-03
68.	400.	98.4	103.3	129.6	19.4	2.37	-11.8	41.8	27.3	28.8	32.0	25.3	12.885	.1544-02
69.	400.	95.6	100.4	127.5	26.2	3.58	-11.7	40.4	27.0	28.2	30.6	25.8	17.955	.4091-02
70.	400.	87.4	90.9	113.1	46.7	5.16	-14.2	38.4	26.4	27.4	29.9	27.7	24.801	.1035-01
71.	600.	185.8	191.3	75.3	84.6	.00	-10.5	76.6	33.9	35.1	28.7	25.3	.000	.0000
72.	600.	146.9	163.3	199.9	39.5	.07	-8.4	63.1	31.8	34.0	35.8	23.9	.517	.1395-06
73.	600.	152.4	163.0	201.3	36.2	.15	-7.8	59.7	30.9	32.9	36.3	23.8	1.033	.1067-05
74.	600.	152.2	165.6	206.1	35.3	.36	-6.7	56.5	30.6	33.0	35.1	24.8	2.519	.1467-04
75.	600.	152.2	167.7	206.1	35.9	.57	-6.2	54.8	30.7	32.6	35.9	25.1	3.907	.5335-04
76.	600.	152.3	160.0	202.4	35.9	1.01	-8.1	52.6	30.6	32.0	35.7	24.7	6.329	.2191-03
77.	600.	152.3	158.1	197.3	37.6	2.02	-8.8	50.6	30.2	31.4	35.8	24.7	10.979	.1112-02
78.	600.	148.6	155.2	197.3	40.5	2.46	-9.3	49.8	30.3	31.7	34.9	25.1	12.885	.1774-02
79.	600.	142.2	143.7	184.7	60.9	4.01	-10.7	47.4	29.9	30.8	35.0	26.2	17.955	.4600-02
80.	600.	119.3	121.5	145.5	58.0	5.58	-25.0	43.6	27.9	29.2	34.3	25.9	24.801	.1134-01
121.	100.	29.1	29.7	19.7	6.5	.00	-15.1	40.8	27.0	27.2	25.4	26.7	.000	.0000
122.	100.	22.5	25.7	44.6	3.7	.08	-3.4	35.6	26.2	26.3	27.6	25.4	.517	.8813-07
123.	100.	20.9	23.4	45.7	3.1	.17	-6.8	33.9	25.6	26.1	27.9	25.6	1.033	.6822-06
124.	100.	21.0	22.1	47.4	3.0	.41	-6.1	33.2	25.8	25.9	27.9	25.3	2.519	.9753-05
125.	100.	21.6	22.4	45.6	2.8	.61	-7.0	32.9	25.6	25.7	28.1	25.1	3.907	.3618-04
126.	100.	21.0	21.3	44.6	2.9	1.02	-9.7	32.0	26.0	26.0	27.8	25.1	6.329	.1512-03
127.	100.	21.5	22.1	43.6	3.1	1.77	-8.0	31.3	25.6	25.8	27.8	25.2	10.979	.7795-03
128.	100.	21.5	21.6	41.8	3.1	2.08	-9.9	30.9	25.7	25.9	27.7	25.3	12.885	.1250-02

129.	100.	21.3	20.5	40.5	3.4	2.91	-11.4	30.5	25.8	25.9	27.6	25.7	17.955	.3357-02
130.	100.	20.6	19.7	38.1	3.6	4.02	-13.9	30.1	25.6	25.9	27.3	25.4	24.801	.8785-02
131.	200.	59.3	61.2	44.3	17.0	.00	-9.1	49.5	26.3	27.0	25.9	25.2	.000	.0000
132.	200.	43.0	47.5	83.5	5.7	.08	-10.1	41.8	24.9	25.8	28.1	25.8	.517	.9968-07
133.	200.	40.3	45.1	86.4	5.0	.16	-11.5	40.1	24.6	25.4	28.6	25.4	1.033	.7759-06
134.	200.	41.0	45.1	89.9	4.9	.38	-9.4	38.2	24.9	25.4	28.7	25.1	2.519	.1079-04
135.	200.	41.7	43.7	89.9	4.8	.63	-9.6	37.2	25.1	25.3	28.8	25.2	3.907	.3940-04
136.	200.	41.7	43.3	85.6	5.2	1.00	-11.5	36.1	24.8	25.4	28.3	25.3	6.329	.1638-03
137.	200.	43.4	44.7	85.8	5.4	1.73	-9.5	35.1	24.8	25.4	28.6	25.6	10.979	.8373-03
138.	200.	43.1	43.3	82.3	5.2	2.03	-12.0	34.6	24.9	25.2	28.1	25.3	12.685	.1341-02
139.	200.	42.3	42.9	79.3	5.5	2.86	-13.5	33.5	25.0	25.3	27.9	26.0	17.955	.3551-02
140.	200.	42.0	40.9	75.2	6.0	4.10	-15.9	33.0	24.6	25.1	27.6	26.2	24.801	.9270-02
141.	400.	113.9	113.4	60.9	70.4	.00	-10.3	64.6	29.1	29.3	26.7	25.9	.000	.0000
142.	400.	88.5	98.9	145.0	27.3	.07	-10.0	55.3	27.3	28.0	30.9	23.2	.517	.1243-06
143.	400.	83.4	90.9	159.3	24.1	.15	-10.5	52.6	26.4	27.4	31.9	23.2	1.033	.9535-06
144.	400.	86.3	86.5	164.5	23.6	.37	-9.7	49.8	26.7	27.3	32.3	22.8	2.519	.1325-04
145.	400.	87.0	86.5	161.4	22.7	.57	-10.5	47.6	26.4	27.2	32.6	23.1	3.907	.4755-04
146.	400.	87.0	90.2	159.4	21.8	.93	-10.2	46.3	27.0	27.4	32.6	23.0	6.329	.1974-03
147.	400.	87.0	88.7	157.3	23.9	1.68	-10.3	44.1	27.1	27.7	32.6	23.6	10.979	.9930-03
148.	400.	87.0	88.7	154.2	23.6	1.90	-11.1	43.7	26.8	27.4	32.6	23.0	12.685	.1593-02
149.	400.	87.0	86.5	151.2	29.3	2.76	-10.8	42.1	27.0	27.6	32.1	23.8	17.955	.4198-02
150.	400.	83.5	82.9	140.9	39.1	3.65	-12.5	40.8	26.7	27.1	31.8	24.4	24.801	.1085-01
151.	600.	170.2	176.1	82.0	115.1	.00	-9.4	79.7	30.4	31.2	28.9	27.0	.000	.0000
152.	600.	128.8	143.6	222.8	45.9	.08	-9.8	66.6	28.2	29.8	37.6	25.1	.517	.1463-06
153.	600.	128.6	137.0	233.0	42.5	.15	-9.8	65.1	28.9	29.8	39.0	26.8	1.033	.1146-05
154.	600.	126.7	133.0	233.0	43.5	.38	-8.9	60.9	28.3	29.6	39.0	24.6	2.519	.1570-04
155.	600.	128.4	141.7	232.8	43.0	.58	-8.1	59.0	26.9	29.9	38.8	24.3	3.907	.5701-04
156.	600.	127.5	141.7	231.5	46.5	1.03	-8.6	55.8	28.9	30.0	40.4	23.7	6.329	.2303-03
157.	600.	132.1	139.8	231.4	44.6	1.97	-8.4	54.1	28.4	30.4	37.9	24.1	10.979	.1171-02
158.	600.	131.2	138.8	231.5	43.5	2.40	-8.8	53.2	28.7	30.1	37.8	24.2	12.685	.1667-02
159.	600.	129.3	135.0	226.4	49.2	3.35	-9.5	51.3	28.4	29.9	37.0	24.2	17.955	.4912-02
160.	600.	122.9	127.3	211.3	79.8	5.08	-8.9	48.3	28.2	29.7	35.7	26.2	24.801	.1232-01
201.	100.	24.1	25.0	27.9	7.6	.00	-15.4	41.0	26.3	28.5	27.0	23.9	.000	.0000
202.	100.	18.1	21.2	47.8	5.1	.01	-7.8	36.2	26.5	27.2	27.3	23.8	.065	.1743-09
203.	100.	17.1	20.0	48.1	5.3	.03	-9.5	35.0	26.1	26.7	27.4	24.0	.194	.4596-08
204.	100.	15.7	18.7	48.9	4.5	.08	-12.1	34.1	25.7	26.5	27.4	24.0	.517	.8564-07
205.	100.	15.5	18.9	51.1	4.8	.16	-9.5	33.6	26.1	26.7	27.8	24.2	1.033	.6785-06
206.	100.	16.2	18.0	52.3	5.4	.59	-7.6	32.7	26.1	26.3	26.0	24.3	3.907	.3606-04
207.	100.	15.7	17.8	51.1	5.5	.95	-8.9	31.8	25.9	26.5	27.8	24.2	6.329	.1507-03
208.	100.	15.5	17.5	49.2	5.6	1.94	-10.2	31.1	25.9	26.5	27.4	24.6	12.685	.1253-02
209.	100.	15.7	16.8	47.5	6.0	2.69	-11.4	30.3	26.3	26.9	27.4	24.0	17.955	.3344-02
210.	100.	14.5	15.5	42.7	8.1	3.71	-15.5	29.5	25.4	26.1	26.9	24.6	24.801	.8655-02
211.	200.	55.9	57.5	52.6	17.9	.00	-8.0	51.3	27.4	28.0	26.9	25.8	.000	.0000
212.	200.	45.1	52.7	71.7	9.2	.01	-10.6	48.2	26.1	27.6	27.2	26.0	.065	.2171-09
213.	200.	41.5	49.8	81.3	7.9	.03	-9.7	44.9	26.1	27.2	26.1	25.9	.194	.5534-08
214.	200.	39.6	46.1	89.9	7.5	.08	-8.4	43.6	26.1	27.2	28.3	25.6	.517	.1026-06
215.	200.	36.8	42.8	93.2	6.4	.16	-10.3	41.1	25.9	26.7	28.3	25.4	1.033	.7676-06
216.	200.	36.1	37.3	97.7	5.9	.61	-11.2	38.4	26.1	26.5	26.7	25.2	3.907	.4046-04
217.	200.	35.5	36.8	95.0	5.7	.99	-13.0	37.3	25.9	26.5	28.6	25.2	6.329	.1680-03
218.	200.	34.7	38.5	89.6	6.2	2.00	-14.5	35.2	25.9	26.7	29.4	25.4	12.685	.1356-02
219.	200.	34.7	37.1	84.9	7.1	2.78	-16.8	34.3	25.9	26.7	29.1	25.4	17.955	.3606-02
220.	200.	34.7	37.1	84.9	7.1	2.78	-16.8	34.3	25.9	26.7	29.1	25.4	17.955	.3606-02
221.	400.	100.4	102.7	94.4	55.6	.00	-11.7	70.7	29.4	32.0	28.7	23.9	.000	.0000
222.	400.	86.9	100.9	140.0	37.4	.01	-8.7	66.4	28.5	31.9	32.0	23.7	.065	.2651-09
223.	400.	82.8	94.5	149.7	34.2	.03	-9.7	63.1	28.0	30.6	32.1	23.7	.194	.7359-08
224.	400.	78.8	86.4	169.6	29.2	.07	-9.0	58.5	27.4	29.4	34.1	22.6	.517	.1307-06
225.	400.	80.5	82.9	177.9	24.7	.14	-8.5	55.7	27.0	29.1	34.2	23.3	1.033	.9996-06

226.	400.	79.2	86.4	182.1	23.9	.56	-7.0	50.1	26.9	29.1	34.1	23.6	3.907	.4971-04
227.	400.	74.8	84.0	176.9	22.9	.94	-10.1	48.6	27.4	29.4	34.1	23.8	6.329	.2056-03
228.	400.	77.0	84.5	174.9	25.0	1.91	-9.2	45.7	27.2	29.1	34.0	23.0	12.885	.1648-02
229.	400.	76.4	82.9	166.6	23.1	2.82	-10.8	43.8	28.0	29.6	33.6	23.4	17.955	.4318-02
230.	400.	75.4	80.2	159.4	39.3	4.24	-10.3	42.7	27.6	29.4	33.0	24.7	24.801	.1118-01
231.	600.	144.9	156.2	118.1	103.2	.00	-12.9	84.8	31.3	34.1	36.3	25.8	.000	.0000
232.	600.	132.1	151.4	179.2	74.2	.01	-10.5	79.4	30.9	33.7	33.4	25.2	.065	.3380-09
233.	600.	124.8	144.7	210.2	61.4	.03	-9.8	74.9	30.2	32.8	36.9	25.4	.194	.8602-08
234.	600.	119.3	136.0	234.4	54.7	.07	-9.3	70.9	30.6	33.3	39.2	23.2	.517	.1555-06
235.	600.	120.3	129.3	251.6	49.0	.15	-8.3	67.6	30.0	32.6	40.9	24.3	1.033	.1187-05
236.	600.	116.4	133.2	252.8	110.5	.56	2.6	61.8	30.2	32.8	40.6	24.3	3.907	.5935-04
237.	600.	120.3	133.2	248.2	106.5	.91	1.5	59.0	30.9	33.7	40.2	23.4	6.329	.2423-03
238.	600.	123.0	131.2	243.7	120.4	2.21	3.4	56.4	29.8	33.0	40.7	24.6	12.885	.1961-02
239.	600.	116.6	122.6	227.6	156.7	3.65	4.5	53.4	30.0	33.0	39.6	25.3	17.955	.5064-02
240.	600.	105.6	109.1	201.2	148.0	5.30	-5.2	48.8	30.2	33.7	37.6	29.4	24.801	.1243-01
281.	100.	16.2	17.5	42.8	10.7	.00	-12.8	43.1	25.6	26.3	25.9	23.0	.000	.0000
282.	100.	12.4	14.9	56.4	6.9	.01	-9.4	38.7	24.8	25.6	27.8	23.1	.065	.1837-09
283.	100.	11.5	14.6	59.0	6.8	.03	-8.1	38.1	24.6	25.9	27.8	23.0	.194	.4906-08
284.	100.	11.0	13.4	60.4	6.6	.08	-8.5	35.9	24.6	25.6	27.8	23.1	.517	.8873-07
285.	100.	10.7	13.0	60.4	6.5	.15	-9.2	34.9	24.4	25.2	28.1	22.9	1.033	.6965-06
286.	100.	10.2	12.8	63.8	6.5	.57	-6.2	34.1	24.4	25.7	28.3	22.9	3.907	.3700-04
287.	100.	9.7	11.8	57.9	5.8	.92	-14.0	32.6	24.4	25.2	27.7	23.1	6.329	.1530-03
288.	100.	10.4	12.9	58.6	6.6	1.87	-9.6	31.8	24.6	25.6	27.9	22.9	12.885	.1272-02
289.	100.	10.8	13.0	57.5	7.2	2.60	-8.9	31.2	24.4	25.4	27.4	23.0	17.955	.3398-02
290.	100.	10.5	12.4	54.2	7.8	3.59	-11.5	30.8	24.4	25.0	27.3	23.4	24.801	.8902-02
291.	200.	37.2	39.9	77.4	30.8	.00	-7.3	60.8	26.9	27.8	26.1	26.3	.000	.0000
292.	200.	28.4	34.1	98.3	18.7	.01	-10.2	55.1	25.9	27.6	29.6	25.0	.065	.2419-09
293.	200.	26.1	33.2	104.7	16.2	.03	-9.8	52.4	25.2	26.9	29.8	24.4	.194	.6270-08
294.	200.	22.7	29.2	105.6	11.9	.08	-15.3	47.4	25.0	26.9	30.1	24.1	.517	.1096-06
295.	200.	21.5	27.2	113.2	11.2	.17	-13.4	45.6	25.7	26.9	30.8	24.4	1.033	.8492-06
296.	200.	20.9	24.9	114.9	7.5	.63	-15.6	41.7	25.2	26.1	30.6	25.4	3.907	.4300-04
297.	200.	21.7	24.5	118.4	8.5	1.01	-13.0	40.8	25.0	26.7	30.8	25.3	6.329	.1802-03
298.	200.	23.4	26.8	120.9	8.7	1.89	-9.2	39.4	25.0	26.5	30.9	25.4	12.885	.1481-02
299.	200.	22.6	26.3	119.2	9.1	2.75	-10.1	37.8	25.2	26.3	30.3	25.8	17.955	.3672-02
300.	200.	21.7	24.2	105.6	9.0	4.00	-17.8	35.9	24.8	26.1	29.6	25.7	24.801	.9813-02
301.	400.	60.4	67.7	130.9	96.6	.00	-11.1	78.7	28.7	31.3	30.7	26.0	.000	.0000
302.	400.	53.6	66.5	159.7	61.8	.01	-14.5	74.6	28.3	30.7	32.2	23.6	.065	.3173-09
303.	400.	51.8	63.6	180.4	48.8	.03	-13.9	71.3	27.4	29.8	34.1	23.7	.194	.8236-08
304.	400.	46.1	59.1	197.5	40.1	.08	-14.3	67.0	26.9	29.8	35.7	24.0	.517	.1472-06
305.	400.	43.7	54.2	209.0	34.1	.15	-14.7	61.9	26.7	29.3	36.6	23.9	1.033	.1099-05
306.	400.	42.0	52.1	218.9	28.4	.57	-14.5	56.8	26.3	28.7	37.9	24.2	3.907	.5504-04
307.	400.	44.1	48.8	220.0	26.9	.89	-14.8	54.3	26.5	28.3	37.7	24.0	6.329	.2250-03
308.	400.	45.7	52.1	209.1	25.7	1.63	-16.4	51.3	26.3	28.5	37.2	24.4	12.885	.1814-02
309.	400.	45.7	56.2	216.9	28.4	2.77	-12.5	49.1	26.5	29.1	35.8	24.3	17.955	.4740-02
310.	400.	45.7	56.2	216.9	28.4	3.83	-12.2	49.1	26.5	29.1	35.6	24.3	24.801	.1249-01
311.	600.	79.4	93.2	329.0	175.9	.00	12.9	90.0	34.4	33.9	38.7	28.9	.000	.0000
312.	600.	70.3	97.3	319.8	117.5	.01	51.2	88.9	33.7	36.9	39.4	27.2	.065	.3775-09
313.	600.	70.3	94.1	320.7	97.2	.03	5.4	84.4	33.1	38.9	39.0	26.1	.194	.9659-08
314.	600.	64.0	85.5	321.6	82.0	.08	.5	78.9	32.6	41.7	37.0	25.6	.517	.1719-06
315.	600.	62.7	86.4	392.9	74.3	.16	2.7	76.0	32.0	43.3	36.8	24.4	1.033	.1323-05
316.	600.	67.2	85.9	400.9	65.4	.62	3.3	71.8	32.4	44.3	36.6	24.4	3.907	.6796-04
317.	600.	68.1	88.7	400.9	64.8	.99	3.9	69.7	31.9	44.4	36.2	23.9	6.329	.2812-03
318.	600.	64.0	82.8	377.0	102.9	2.42	4.9	63.9	31.1	42.8	35.2	28.1	12.885	.2187-02
319.	600.	59.5	80.5	339.8	148.1	3.66	5.3	59.5	30.9	41.1	34.3	25.0	17.955	.5577-02
320.	600.	59.5	80.5	339.8	148.1	5.05	5.5	59.5	30.9	41.1	34.3	25.0	24.801	.1470-01

Data for Porous Lower Boundary, Discrete Hole Side Boundaries, and Free Upper Surface Boundary

RUN NO.	POWER FRACTION SIDE	BOTTOM	TOP	NUSSELT NUMBER SIDE	BOTTOM	TOP	ASPECT RATIO	RAYLEIGH NO.	M	M	Superficial Gas Velocity (CM/MIN)	(ReFr)
41.	.787	.178	.035	31.5	11.6	3.1	1.308	.4251+08		.6224+01	.000	.0000
42.	.572	.396	.032	44.1	60.0	4.0	1.308	.3419+08		.1449+02	.517	.8312-07
43.	.574	.396	.031	50.1	71.4	4.3	1.308	.3269+08		.1723+02	1.033	.6539-06
44.	.570	.395	.035	59.0	101.7	6.0	1.308	.3211+08		.2463+02	2.519	.9354-05
45.	.563	.397	.040	59.0	101.7	7.3	1.308	.3206+08		.2451+02	3.907	.3474-04
46.	.556	.397	.047	67.6	100.4	9.3	1.308	.3091+08		.2419+02	6.329	.1462-03
47.	.550	.393	.058	73.5	111.7	12.9	1.308	.2992+08		.2719+02	10.979	.7553-03
48.	.548	.388	.064	77.3	130.9	14.9	1.308	.2976+08		.3220+02	12.885	.1215-02
49.	.535	.381	.084	80.3	141.3	23.1	1.308	.2866+08		.3544+02	17.955	.3256-02
50.	.515	.368	.118	79.4	170.7	44.4	1.308	.2742+08		.4438+02	24.801	.8485-02
51.	.778	.149	.073	36.7	11.9	5.9	1.308	.1140+09		.7627+01	.000	.0000
52.	.603	.367	.030	49.1	69.5	4.3	1.308	.9063+08		.1810+02	.517	.9381-07
53.	.598	.369	.033	53.9	78.4	5.2	1.308	.8361+08		.2030+02	1.033	.7271-06
54.	.586	.376	.038	60.5	100.2	6.9	1.308	.7847+08		.2547+02	2.519	.1022-04
55.	.583	.375	.041	63.0	109.7	7.8	1.308	.7709+08		.2791+02	3.907	.3778-04
56.	.585	.370	.046	67.6	109.2	9.3	1.308	.7344+08		.2823+02	6.329	.1579-03
57.	.581	.367	.052	71.9	111.5	12.0	1.308	.7069+08		.2907+02	10.979	.8121-03
58.	.570	.364	.066	75.7	142.5	15.3	1.308	.7038+08		.3744+02	12.885	.1304-02
59.	.561	.354	.085	77.4	132.6	22.7	1.308	.6695+08		.3578+02	17.955	.3484-02
60.	.422	.245	.333	79.2	157.9	122.5	1.308	.6125+08		.6158+02	24.801	.8730-02
61.	.745	.136	.118	39.8	13.4	11.0	1.308	.3558+09		.9356+01	.000	.0000
62.	.612	.339	.049	49.2	56.2	6.7	1.308	.2561+09		.1583+02	.517	.1171-06
63.	.583	.370	.046	54.5	80.0	7.3	1.308	.2321+09		.2065+02	1.033	.8692-06
64.	.576	.375	.049	61.5	95.6	8.8	1.308	.2160+09		.2435+02	2.519	.1231-04
65.	.580	.370	.050	66.8	100.9	9.7	1.308	.2101+09		.2607+02	3.907	.4505-04
66.	.582	.367	.051	71.1	112.7	10.3	1.308	.1994+09		.2930+02	6.329	.1676-03
67.	.571	.370	.058	77.8	137.7	12.9	1.308	.1915+09		.3550+02	10.979	.9574-03
68.	.571	.367	.062	76.3	137.1	13.7	1.308	.1896+09		.3568+02	12.885	.1544-02
69.	.555	.361	.084	79.5	133.8	21.1	1.308	.1826+09		.3543+02	17.955	.4091-02
70.	.519	.329	.151	81.1	137.9	50.2	1.308	.1651+09		.3999+02	24.801	.1035-01
71.	.702	.140	.157	43.9	15.4	16.1	1.308	.6658+09		.1048+02	.000	.0000
72.	.564	.364	.072	51.3	72.9	10.0	1.308	.5158+09		.1915+02	.517	.1395-06
73.	.570	.364	.066	56.7	85.9	10.1	1.308	.4818+09		.2256+02	1.033	.1067-05
74.	.568	.368	.064	64.8	96.7	11.3	1.308	.4493+09		.2510+02	2.519	.1467-04
75.	.569	.366	.065	69.6	109.5	12.4	1.308	.4329+09		.2855+02	3.907	.5335-04
76.	.566	.367	.067	74.3	121.0	13.4	1.308	.4009+09		.3151+02	6.329	.2191-03
77.	.567	.360	.072	79.6	134.8	15.5	1.308	.3790+09		.3571+02	10.979	.1112-02
78.	.558	.363	.079	82.3	134.5	17.7	1.308	.3667+09		.3543+02	12.885	.1774-02
79.	.534	.345	.121	85.3	151.5	31.2	1.308	.3390+09		.4196+02	17.955	.4600-02
80.	.535	.323	.141	82.9	162.5	37.1	1.308	.2545+09		.4801+02	24.801	.1134-01
121.	.692	.231	.076	22.2	13.2	4.7	1.434	.3077+08		.4989+01	.000	.0000
122.	.499	.462	.040	27.3	58.6	4.0	1.434	.2884+08		.1106+02	.517	.8813-07
123.	.475	.490	.035	29.1	80.3	4.1	1.434	.2609+08		.1429+02	1.033	.6822-06
124.	.459	.505	.036	30.8	93.9	4.6	1.434	.2561+08		.1621+02	2.519	.9753-05
125.	.473	.490	.037	31.9	100.9	4.7	1.434	.2505+08		.1795+02	3.907	.3618-04
126.	.469	.487	.044	37.4	110.4	6.1	1.434	.2349+08		.1976+02	6.329	.1512-03
127.	.473	.474	.053	40.8	130.1	8.5	1.434	.2332+08		.2395+02	10.979	.7795-03
128.	.478	.464	.058	44.8	137.7	10.0	1.434	.2243+08		.2590+02	12.885	.1250-02
129.	.471	.457	.071	47.6	146.5	13.9	1.434	.2173+08		.2791+02	17.955	.3357-02

130.	.468	.443	.089	49.0	146.1	17.5	1.434	.2079+08	.2877+02	24.801	.8785-02
131.	.663	.244	.094	26.8	19.0	7.1	1.434	.8465+08	.6812+01	.000	.0000
132.	.504	.464	.032	28.4	62.9	3.7	1.434	.6702+08	.1181+02	.517	.9968-07
133.	.482	.488	.029	29.4	77.7	3.7	1.434	.6277+08	.1386+02	1.033	.7759-06
134.	.475	.496	.029	34.5	98.2	4.2	1.434	.5991+08	.1726+02	2.519	.1079-04
135.	.472	.498	.030	37.4	112.2	4.8	1.434	.5736+08	.1965+02	3.907	.3940-04
136.	.480	.485	.035	40.6	115.8	6.0	1.434	.5399+08	.2082+02	6.329	.1638-03
137.	.487	.474	.039	46.7	138.9	7.9	1.434	.5301+08	.2554+02	10.979	.8373-03
138.	.491	.468	.041	47.6	133.4	8.2	1.434	.5064+08	.2485+02	12.885	.1341-02
139.	.493	.459	.048	54.1	149.3	11.8	1.434	.4770+08	.2638+02	17.955	.3551-02
140.	.492	.447	.060	53.7	146.1	15.8	1.434	.4551+08	.2848+02	24.801	.9270-02
141.	.634	.170	.196	31.9	15.9	18.0	1.434	.2414+09	.8183+01	.000	.0000
142.	.521	.403	.076	34.1	59.7	8.6	1.434	.1944+09	.1290+02	.517	.1243-06
143.	.487	.445	.068	34.4	77.8	8.4	1.434	.1803+09	.1525+02	1.033	.9535-06
144.	.478	.455	.066	38.5	95.7	9.0	1.434	.1696+09	.1831+02	2.519	.1325-04
145.	.484	.451	.065	42.6	109.3	9.7	1.434	.1579+09	.2115+02	3.907	.4755-04
146.	.493	.443	.063	47.6	118.8	10.0	1.434	.1524+09	.2336+02	6.329	.1974-03
147.	.490	.439	.071	54.1	140.0	12.8	1.434	.1429+09	.2783+02	10.979	.9930-03
148.	.494	.434	.072	54.7	143.0	12.7	1.434	.1398+09	.2872+02	12.885	.1593-02
149.	.486	.424	.090	60.7	157.2	18.1	1.434	.1339+09	.3234+02	17.955	.4198-02
150.	.475	.402	.122	61.9	161.3	27.0	1.434	.1268+09	.3494+02	24.801	.1085-01
151.	.637	.151	.212	34.6	15.7	21.3	1.434	.4953+09	.9091+01	.000	.0000
152.	.503	.412	.085	36.0	76.2	11.0	1.434	.3804+09	.1613+02	.517	.1463-06
153.	.491	.430	.079	36.9	88.8	11.1	1.434	.3679+09	.1798+02	1.033	.1146-05
154.	.484	.426	.089	41.4	106.1	13.4	1.434	.3369+09	.2170+02	2.519	.1570-04
155.	.490	.422	.088	45.7	115.1	14.0	1.434	.3269+09	.2377+02	3.907	.5701-04
156.	.491	.422	.087	51.3	151.1	14.9	1.434	.2999+09	.3120+02	6.329	.2303-03
157.	.494	.421	.085	55.7	143.7	15.7	1.434	.2880+09	.2977+02	10.979	.1171-02
158.	.493	.423	.084	57.3	151.2	16.0	1.434	.2804+09	.3117+02	12.885	.1667-02
159.	.487	.417	.097	60.4	159.9	19.6	1.434	.2655+09	.3343+02	17.955	.4x12-02
160.	.458	.387	.155	65.8	169.8	39.1	1.434	.2460+09	.3826+02	24.801	.1232-01
201.	.580	.330	.090	20.2	20.6	4.6	2.169	.5867+07	.3610+01	.000	.0000
202.	.427	.518	.055	22.3	56.7	4.3	2.169	.5385+07	.6311+01	.065	.1743-09
203.	.410	.531	.059	22.8	66.9	5.1	2.169	.5056+07	.7266+01	.194	.4596-08
204.	.391	.556	.053	22.8	77.3	4.8	2.169	.4743+07	.8010+01	.517	.8564-07
205.	.380	.565	.055	25.3	92.6	5.6	2.169	.4791+07	.9439+01	1.033	.6785-06
206.	.370	.565	.064	27.8	117.1	7.5	2.169	.4729+07	.1194+02	3.907	.3606-04
207.	.368	.562	.070	31.7	133.7	8.9	2.169	.4510+07	.1372+02	6.329	.1507-03
208.	.368	.548	.084	36.4	144.7	12.4	2.169	.4305+07	.1523+02	12.885	.1x53-02
209.	.366	.536	.098	47.1	178.4	14.7	2.169	.4120+07	.1920+02	17.955	.3344-02
210.	.355	.505	.140	43.1	174.4	25.5	2.169	.3765+07	.1990+02	24.801	.8655-02
211.	.616	.287	.097	24.3	21.9	7.1	2.169	.1720+08	.4393+01	.000	.0000
212.	.547	.401	.052	23.4	34.8	4.2	2.169	.1534+08	.4998+01	.065	.2171-09
213.	.506	.451	.044	25.7	49.6	4.2	2.169	.1408+08	.6346+01	.194	.5534-08
214.	.468	.491	.041	26.2	60.6	4.3	2.169	.1376+08	.7122+01	.517	.1026-06
215.	.444	.519	.037	28.0	75.9	4.4	2.169	.1250+08	.8421+01	1.033	.7076-06
216.	.413	.550	.036	31.5	104.3	5.1	2.169	.1132+08	.1092+02	3.907	.4048-04
217.	.415	.546	.039	34.0	113.2	5.8	2.169	.1063+08	.1195+02	6.329	.1680-03
218.	.428	.524	.048	43.5	164.7	8.9	2.169	.9612+07	.1811+02	12.885	.1356-02
219.	.431	.510	.059	47.6	173.1	11.8	2.169	.9045+07	.1958+02	17.955	.3606-02
220.	.431	.510	.059	47.6	173.1	11.8	2.169	.9045+07	.1958+02	17.955	.3606-02
221.	.575	.267	.157	25.1	22.2	11.7	2.169	.5197+08	.4776+01	.000	.0000
222.	.514	.383	.102	25.9	40.4	8.7	2.169	.4890+08	.6269+01	.065	.2x51-09
223.	.491	.414	.095	26.2	48.1	8.6	2.169	.4497+08	.6683+01	.194	.7359-08
224.	.454	.466	.080	27.5	69.6	8.1	2.169	.4072+08	.8605+01	.517	.1307-06
225.	.446	.486	.068	29.8	83.4	7.7	2.169	.3813+08	.9890+01	1.033	.9996-06
226.	.445	.489	.066	38.2	115.8	9.4	2.169	.3368+08	.1364+02	3.907	.4971-04

227.	.442	.492	.066	40.4	124.7	9.8	2.169	.3115+08	.1460+02	6.329	.2056-03
228.	.444	.481	.074	47.5	153.6	12.2	2.169	.2894+08	.1839+02	12.885	.1648-02
229.	.446	.467	.087	55.0	167.8	15.7	2.169	.2693+08	.2072+02	17.955	.4318-02
230.	.434	.445	.122	56.9	169.3	24.9	2.169	.2624+08	.2195+02	24.801	.1118-01
231.	.576	.226	.197	28.1	21.1	17.0	2.169	.9967+08	.5373+01	.000	.0000
232.	.528	.334	.138	29.4	38.0	13.4	2.169	.9313+08	.6564+01	.065	.3380-09
233.	.498	.388	.113	30.6	54.3	12.2	2.169	.8606+08	.8055+01	.194	.8602-08
234.	.469	.430	.101	32.4	72.9	11.3	2.169	.8047+08	.9760+01	.517	.1555-06
235.	.453	.457	.089	34.2	93.4	11.3	2.169	.7563+08	.1178+02	1.033	.1187-05
236.	.409	.411	.180	41.5	118.4	29.5	2.169	.7449+08	.1661+02	3.907	.5935-04
237.	.416	.408	.176	47.7	132.2	30.2	2.169	.6902+08	.1869+02	6.329	.2423-03
238.	.410	.393	.198	51.2	155.0	38.6	2.169	.6590+08	.2275+02	12.885	.1961-02
239.	.381	.363	.256	55.4	165.9	57.7	2.169	.6168+08	.2636+02	17.955	.5064-02
240.	.377	.353	.269	59.4	181.4	80.4	2.169	.4971+08	.2958+02	24.801	.1243-01
241.	.386	.491	.123	10.1	25.6	5.5	5.305	.1801+06	.1230+01	.000	.0000
242.	.302	.622	.077	10.6	54.0	4.6	5.305	.1626+06	.2045+01	.065	.1837-09
243.	.284	.642	.075	10.7	59.6	4.7	5.305	.1614+06	.2187+01	.194	.4900-08
244.	.267	.660	.073	12.0	78.2	5.5	5.305	.1477+06	.2791+01	.517	.8673-07
245.	.261	.666	.073	12.4	93.1	5.8	5.305	.1412+06	.3293+01	1.033	.6965-06
246.	.245	.680	.075	13.7	117.5	6.7	5.305	.1410+06	.4071+01	3.907	.3700-04
247.	.249	.673	.078	14.6	123.9	7.5	5.305	.1223+06	.4338+01	6.329	.1530-03
248.	.258	.648	.094	18.6	157.6	10.0	5.305	.1247+06	.5726+01	12.885	.1272-02
249.	.261	.631	.107	20.5	164.1	12.7	5.305	.1224+06	.6125+01	17.955	.3398-02
250.	.259	.612	.129	20.1	164.6	16.4	5.305	.1174+06	.6336+01	24.801	.8902-02
251.	.416	.418	.166	11.5	23.6	8.9	5.305	.6127+06	.1331+01	.000	.0000
252.	.348	.548	.104	11.1	38.7	6.3	5.305	.5148+06	.1666+01	.065	.2419-09
253.	.329	.581	.090	11.4	46.8	5.9	5.305	.4829+06	.1898+01	.194	.6270-08
254.	.306	.623	.070	12.4	62.2	5.2	5.305	.3969+06	.2351+01	.517	.1096-06
255.	.281	.654	.065	13.0	78.2	5.5	5.305	.3847+06	.2821+01	1.033	.8492-06
256.	.271	.681	.048	14.8	107.1	5.2	5.305	.3345+06	.3706+01	3.907	.4300-04
257.	.265	.680	.055	16.1	122.7	6.4	5.305	.3361+06	.4254+01	6.329	.1602-03
258.	.276	.665	.058	19.3	148.0	7.9	5.305	.3350+06	.5241+01	12.885	.1481-02
259.	.272	.663	.066	21.3	167.3	10.3	5.305	.3119+06	.5949+01	17.955	.3672-02
260.	.279	.642	.079	23.2	175.0	13.4	5.305	.2652+06	.6421+01	24.801	.9613-02
261.	.360	.368	.272	12.9	26.6	17.9	5.305	.1696+07	.1704+01	.000	.0000
262.	.352	.467	.181	13.2	37.0	11.9	5.305	.1508+07	.1866+01	.065	.3173-09
263.	.335	.523	.142	13.4	47.8	10.1	5.305	.1432+07	.2151+01	.194	.8236-08
264.	.307	.576	.117	13.6	62.5	9.3	5.305	.1299+07	.2555+01	.517	.1472-06
265.	.287	.613	.100	14.5	82.9	9.0	5.305	.1154+07	.3186+01	1.033	.1099-05
266.	.275	.640	.085	16.2	115.9	8.9	5.305	.1024+07	.4266+01	3.907	.5504-04
267.	.273	.646	.081	17.4	132.9	9.2	5.305	.9576+06	.4850+01	6.329	.2250-03
268.	.293	.626	.082	20.8	150.6	10.3	5.305	.8705+06	.5671+01	12.885	.1614-02
269.	.291	.620	.089	24.5	165.3	12.8	5.305	.8602+06	.6285+01	17.955	.4740-02
270.	.290	.618	.092	24.5	165.3	13.2	5.305	.8628+06	.6304+01	24.801	.1249-01
271.	.255	.486	.260	14.9	62.0	27.9	5.305	.3966+07	.3009+01	.000	.0000
272.	.277	.529	.194	15.2	62.6	18.5	5.305	.3473+07	.2791+01	.065	.3775-09
273.	.260	.586	.154	16.7	79.4	16.2	5.305	.3345+07	.3190+01	.194	.9659-08
274.	.248	.616	.136	17.9	87.7	15.0	5.305	.2893+07	.3352+01	.517	.1719-06
275.	.242	.637	.121	19.9	98.2	14.2	5.305	.2795+07	.3629+01	1.033	.1323-05
276.	.247	.646	.107	23.8	112.0	13.7	5.305	.2661+07	.4081+01	3.907	.6796-04
277.	.251	.643	.106	26.3	118.4	14.2	5.305	.2558+07	.4339+01	6.329	.2612-03
278.	.233	.599	.167	29.2	130.7	29.3	5.305	.2224+07	.5140+01	12.885	.2187-02
279.	.222	.538	.240	32.3	134.9	43.9	5.305	.2024+07	.5906+01	17.955	.5577-02
280.	.221	.537	.242	32.3	134.9	44.3	5.305	.2028+07	.5919+01	24.801	.1470-01

$FIN

Data for Porous Lower Boundary, Discrete Hole Side Boundaries, and Solid Upper Boundaries with Upper Grid to Lower Plate Electrodes.

RUN NO.	INPUT POWER (W)	POWER(WATTS) LEFT SIDE	RIGHT SIDE	BOTTOM	TOP	AIR	ENERGY BALANCE ERROR(X)	POOL TEMP (C)	PLATE TEMP(C) L	R	B	T	SUPERFITIAL GAS VELOCITY (CM/MIN)	(ReFr)
1.	100.	17.8	16.7	10.8	45.1	.00	-9.6	32.2	25.8	26.2	25.4	25.0	.000	.0000
2.	100.	8.6	8.9	13.1	63.0	.09	-6.3	27.5	25.3	25.8	25.8	25.1	.517	.7443-07
3.	100.	6.4	6.8	11.0	56.8	.17	-18.9	27.0	25.3	25.7	25.7	25.1	1.033	.5883-06
4.	100.	5.2	5.4	11.4	61.7	.42	-16.0	27.5	25.9	26.3	26.2	25.4	2.519	.8624-05
5.	100.	5.6	5.8	13.7	70.1	.65	-4.1	27.6	26.4	26.6	26.6	25.4	3.907	.3228-04
6.	100.	5.1	5.1	11.9	71.4	1.09	-5.4	27.2	26.2	26.3	26.6	25.4	6.329	.1357-03
7.	100.	4.5	4.5	10.8	70.6	1.82	-7.9	27.0	26.1	26.1	25.4	25.4	10.979	.7056-02
8.	100.	4.2	4.5	10.6	70.2	2.21	-8.1	27.0	26.0	26.1	26.1	25.4	12.885	.1140-02
9.	100.	4.0	4.4	10.4	68.9	2.96	-9.4	26.9	25.6	25.9	25.9	25.3	17.955	.3077-02
10.	100.	3.5	4.1	10.1	67.7	4.24	-10.4	26.7	25.6	25.7	25.8	25.4	24.801	.8067-02
11.	200.	28.5	27.2	20.4	101.1	.00	-11.4	35.9	27.3	27.7	27.3	25.6	.000	.0000
12.	200.	19.4	19.9	26.8	123.8	.09	-3.9	30.1	25.1	26.7	25.3	25.2	.517	.7936-07
13.	200.	16.9	17.3	23.7	121.5	.18	-10.2	29.8	26.6	26.8	27.4	24.9	1.033	.6315-06
14.	200.	17.0	17.1	23.9	122.3	.43	-9.6	29.5	26.4	26.9	27.1	24.9	2.519	.9067-05
15.	200.	16.7	17.1	23.6	125.5	.69	-8.2	29.3	26.1	27.2	26.8	25.2	3.907	.3366-04
16.	200.	16.7	16.5	23.4	128.6	1.12	-6.8	29.1	26.0	26.9	26.8	25.2	6.329	.1422-03
17.	200.	14.4	14.4	22.6	131.8	1.95	-7.5	28.7	26.7	26.6	27.7	25.2	10.979	.7362-03
18.	200.	14.0	13.6	22.1	131.8	2.29	-8.1	28.6	26.6	26.6	27.2	25.2	12.885	.1187-02
19.	200.	13.2	12.8	21.2	129.4	3.17	-10.1	28.4	26.6	26.7	26.6	25.2	17.955	.3193-02
20.	200.	12.7	12.3	20.6	127.9	4.52	-11.0	28.3	25.7	27.0	27.0	25.2	24.801	.8391-02
21.	400.	59.5	59.5	34.3	211.0	.00	-8.9	43.4	27.4	27.4	27.9	25.8	.000	.0000
22.	400.	36.9	40.4	50.9	231.9	.12	-10.0	33.2	26.7	26.9	28.1	26.0	.517	.8418-07
23.	400.	35.6	39.9	49.8	237.9	.23	-9.2	33.9	26.3	28.1	27.7	26.0	1.033	.6822-06
24.	400.	36.6	40.3	51.6	232.0	.56	-9.7	33.4	26.2	27.7	29.0	25.7	2.519	.9784-05
25.	400.	37.0	39.9	52.0	239.4	.88	-7.7	33.2	27.7	27.3	28.9	25.4	3.907	.3641-04
26.	400.	35.9	37.5	50.5	242.4	1.42	-8.1	32.6	27.4	27.2	28.2	26.0	6.329	.1528-03
27.	400.	34.2	35.2	49.1	254.4	2.47	-6.2	31.7	26.3	27.6	28.0	26.0	10.979	.7843-03
28.	400.	34.2	35.4	49.1	245.4	2.87	-8.2	31.6	26.2	27.7	27.4	26.0	12.885	.1265-02
29.	400.	33.3	34.7	49.4	245.5	4.01	-8.3	31.2	26.6	26.4	29.0	25.8	17.955	.3402-02
30.	400.	31.4	33.5	48.3	244.0	5.54	-9.3	30.9	26.6	26.2	28.6	25.8	24.801	.8920-02
901.	600.	96.3	95.2	58.4	306.8	.00	-7.2	51.3	26.4	29.2	26.4	29.4	.000	.0000
902.	600.	72.1	82.9	89.9	308.2	.12	-7.8	41.4	27.1	27.4	28.7	31.8	.517	.9906-07
903.	600.	73.7	78.5	93.9	292.9	.28	-10.1	40.5	26.8	27.7	29.0	31.7	1.033	.7807-06
904.	600.	75.8	84.4	96.6	295.7	.70	-7.7	39.6	27.1	27.9	29.5	30.9	2.519	.1111-04
905.	600.	76.4	86.6	97.4	299.9	1.09	-6.4	38.3	26.6	28.1	29.3	31.3	3.907	.4033-04
906.	600.	74.8	80.7	96.3	299.9	1.76	-7.8	37.7	27.1	28.1	29.3	31.6	6.329	.1694-03
907.	600.	74.8	80.2	96.3	302.7	3.11	-7.2	36.7	27.0	27.7	29.8	31.4	10.979	.8661-03
908.	600.	74.3	81.3	96.3	305.5	3.57	-6.5	36.5	26.9	27.6	29.6	31.7	12.885	.1393-02
909.	600.	73.2	76.4	98.0	293.1	4.96	-9.0	36.5	26.9	27.7	29.7	31.4	17.955	.3770-02
910.	600.	72.6	78.0	98.6	291.7	6.85	-8.7	36.3	27.4	27.3	29.9	31.8	24.801	.9902-02
81.	100.	14.6	14.9	12.6	49.8	.00	-8.0	31.9	25.7	25.4	24.8	24.7	.000	.0000
82.	100.	7.3	8.0	16.5	57.7	.08	-10.3	27.6	25.2	25.9	25.4	25.2	.517	.7464-07
83.	100.	7.6	8.1	17.4	57.4	.17	-9.4	27.5	25.2	25.3	25.7	25.0	1.033	.5955-06
84.	100.	7.7	8.1	17.1	58.0	.42	-8.6	27.3	25.6	25.7	25.1	25.4	2.519	.8589-05
85.	100.	7.5	8.1	17.2	59.5	.65	-7.1	27.2	25.6	25.7	24.9	25.2	3.907	.3193-04
86.	100.	7.4	7.8	16.9	59.8	1.06	-7.0	26.8	25.3	25.4	25.0	25.4	6.329	.1346-03
87.	100.	6.8	7.4	16.4	59.1	1.63	-8.5	26.6	25.1	25.1	25.2	25.2	10.979	.6981-03
88.	100.	6.1	6.5	14.9	57.0	2.15	-13.4	26.6	25.4	25.3	25.2	25.3	12.885	.1128-02

89.	100.	4.0	4.4	16.1	60.5	2.98	-11.9	26.9	25.9	25.8	25.8	25.4	17.955	.3077-02
90.	100.	4.3	4.5	15.8	58.4	4.12	-12.8	26.6	25.3	25.4	25.6	25.4	24.801	.8057-02
91.	200.	27.9	26.0	20.7	112.0	.00	-6.7	37.4	26.8	27.2	27.0	25.4	.000	.0000
92.	200.	18.1	19.0	25.6	133.0	.10	-2.1	30.0	25.0	26.0	26.9	25.3	.517	.7928-07
93.	200.	17.0	18.0	23.9	131.0	.19	-4.9	29.6	25.1	25.6	25.9	24.9	1.033	.6270-06
94.	200.	18.1	17.8	25.7	130.1	.45	-3.9	29.2	25.3	25.9	26.7	25.4	2.519	.9003-05
95.	200.	17.4	17.8	24.7	129.2	.70	-5.1	29.1	25.3	25.7	26.8	25.3	3.907	.3351-04
96.	200.	17.8	17.3	24.4	131.9	1.13	-3.7	28.6	25.3	25.7	26.2	25.4	6.329	.1405-03
97.	200.	17.1	15.8	23.2	129.1	1.96	-6.4	28.1	24.9	25.6	26.3	25.3	10.979	.7251-03
98.	200.	16.2	15.7	22.4	131.0	2.29	-6.2	27.8	25.4	25.3	26.6	25.3	12.885	.1162-02
99.	200.	15.5	15.4	21.7	129.2	3.07	-7.6	27.7	25.2	25.3	26.6	25.3	17.955	.3136-02
100.	200.	14.8	14.2	21.2	125.5	4.24	-10.0	27.6	24.7	25.1	25.4	25.1	24.801	.8243-02
101.	400.	55.6	54.6	41.7	213.1	.00	-8.8	43.5	26.0	26.7	26.1	26.2	.000	.0000
102.	400.	37.1	40.2	50.8	232.7	.10	-9.8	34.4	24.4	25.6	25.9	26.4	.517	.8611-07
103.	400.	37.1	40.2	54.7	228.4	.21	-9.9	33.4	24.9	25.3	26.1	26.4	1.033	.6763-06
104.	400.	36.9	39.0	58.9	231.2	.50	-8.4	33.2	25.4	26.1	26.0	26.4	2.519	.9753-05
105.	400.	36.1	39.0	58.1	234.0	.81	-8.0	32.8	25.0	26.1	27.2	26.3	3.907	.3610-04
106.	400.	36.6	38.2	58.1	227.1	1.31	-9.7	32.1	25.2	26.2	27.2	26.7	6.329	.1515-03
107.	400.	35.5	36.2	57.0	232.6	2.17	-9.1	31.6	25.3	25.8	26.1	26.2	10.979	.7835-03
108.	400.	35.2	35.6	56.5	234.0	2.66	-9.0	31.1	25.1	25.8	26.0	26.4	12.885	.1255-02
109.	400.	35.2	34.2	56.5	236.7	3.69	-8.4	30.8	25.3	25.9	27.0	26.4	17.955	.3374-02
110.	400.	34.1	33.1	56.0	231.2	5.10	-10.1	30.5	25.1	25.4	27.0	26.4	24.801	.8848-02
111.	600.	83.5	82.5	59.6	304.2	.00	-11.7	51.2	28.1	28.8	27.2	29.3	.000	.0000
112.	600.	62.3	68.2	91.4	325.7	.13	-8.7	41.9	26.2	27.7	30.1	30.8	.517	.9977-07
113.	600.	64.5	70.5	98.2	316.8	.27	-8.3	41.2	26.3	28.2	29.0	31.7	1.033	.7897-06
114.	600.	68.6	71.4	103.0	312.3	.68	-7.4	40.7	26.7	27.8	30.4	30.6	2.519	.1135-04
115.	600.	69.5	72.8	103.0	303.3	1.06	-8.4	39.8	27.2	28.0	30.1	30.9	3.907	.4167-04
116.	600.	69.0	70.5	103.0	310.8	1.75	-7.5	38.6	26.9	28.0	30.4	30.8	6.329	.1725-03
117.	600.	67.7	67.8	100.3	309.3	3.04	-8.7	37.4	27.1	27.6	30.2	30.8	10.979	.8782-03
118.	600.	68.1	66.4	99.6	307.8	3.56	-9.1	37.6	26.4	27.6	29.4	30.8	12.885	.1424-02
119.	600.	66.8	64.6	100.3	304.9	4.96	-9.8	37.2	26.7	27.6	29.4	30.2	17.955	.3823-02
120.	600.	64.5	62.7	99.6	300.4	6.68	-11.0	36.3	26.3	27.2	30.0	30.2	24.801	.9691-02
161.	100.	11.0	11.5	14.2	61.3	.00	-2.0	31.4	25.7	25.7	25.6	23.8	.000	.0000
162.	100.	6.4	7.3	16.0	62.2	.08	-7.9	27.4	24.8	25.2	25.2	24.9	.517	.7433-07
163.	100.	6.5	7.6	16.2	61.4	.17	-8.2	27.7	25.4	25.6	25.2	24.4	1.033	.5979-06
164.	100.	6.9	7.7	16.5	62.6	.42	-5.8	27.3	25.4	25.6	25.3	24.3	2.519	.8577-05
165.	100.	6.6	7.2	15.6	63.4	.66	-6.6	26.9	25.2	25.4	25.2	24.4	3.907	.3172-04
166.	100.	7.8	10.5	10.8	64.7	1.07	-5.1	26.8	25.4	25.4	25.6	24.2	6.329	.1346-03
167.	100.	7.4	10.2	11.2	67.2	1.84	-2.2	26.7	25.0	25.6	25.3	24.3	10.979	.7000-03
168.	100.	7.1	9.5	11.0	67.6	2.15	-2.7	26.7	24.8	25.0	25.3	24.7	12.885	.1131-02
169.	100.	6.8	9.1	10.6	67.6	3.00	-2.9	26.3	25.2	25.0	25.2	24.4	17.955	.3037-02
170.	100.	6.2	8.6	9.9	65.9	4.12	-5.2	26.2	25.0	24.8	25.2	24.7	24.801	.7982-02
171.	200.	26.0	27.1	28.6	102.8	.00	-7.7	35.7	25.0	25.0	25.9	25.6	.000	.0000
172.	200.	20.7	22.1	33.5	108.8	.09	-7.4	29.7	23.7	24.4	25.0	25.3	.517	.7860-07
173.	200.	20.7	22.0	33.9	108.8	.18	-7.2	29.4	23.7	24.4	25.0	25.4	1.033	.6243-06
174.	200.	21.4	23.2	34.8	108.2	.44	-5.9	28.7	24.3	25.2	25.2	24.6	2.519	.8889-05
175.	200.	21.4	22.5	33.9	109.4	.69	-6.0	28.7	23.7	25.0	25.2	25.2	3.907	.3314-04
176.	200.	21.8	22.3	33.2	107.1	1.12	-7.2	28.1	23.9	24.8	25.3	24.8	6.329	.1387-03
177.	200.	22.2	22.3	33.2	111.2	1.94	-4.6	28.1	23.9	24.1	25.2	26.0	10.979	.7241-03
178.	200.	21.6	21.6	32.2	110.0	2.27	-6.1	27.9	23.9	24.6	25.2	25.7	12.885	.1165-02
179.	200.	21.2	20.5	30.9	109.2	3.17	-8.0	27.7	24.1	24.4	25.2	25.3	17.955	.3136-02
180.	200.	20.5	20.3	30.9	109.5	4.38	-7.2	27.5	23.9	24.4	25.1	25.3	24.801	.8232-02
181.	400.	46.7	49.0	55.0	215.7	.00	-8.4	43.0	26.3	26.7	26.0	25.9	.000	.0000
182.	400.	36.1	42.4	59.0	226.8	.01	-8.9	39.1	24.8	25.9	26.6	26.6	.065	.1652-09
183.	400.	34.4	39.8	57.9	230.6	.04	-9.3	35.8	24.8	25.9	26.7	26.8	.194	.4669-08
184.	400.	32.5	38.7	56.4	239.4	.11	-8.2	34.6	24.8	25.4	26.9	26.7	.517	.8687-07
185.	400.	33.9	37.6	57.2	249.9	.21	-5.3	33.2	24.8	25.6	26.9	26.1	1.033	.6734-06

186.	400.	35.2	38.7	57.5	240.7	.78	-6.8	32.2	24.6	25.9	27.0	26.1	3.907	.3569-04
187.	400.	34.4	37.9	57.5	236.8	1.30	-8.0	31.8	25.4	25.7	27.1	26.2	6.329	.1507-03
188.	400.	33.3	35.3	56.1	244.6	2.65	-7.0	31.0	25.0	25.6	27.0	25.0	12.885	.1252-02
189.	400.	31.9	33.9	53.8	228.2	3.70	-12.1	30.5	24.4	25.6	26.8	25.8	17.955	.3357-02
190.	400.	30.6	32.8	52.4	240.7	5.10	-9.6	30.2	24.6	25.6	26.9	25.3	24.801	.8794-02
191.	600.	82.0	84.5	83.3	293.1	.00	-9.5	54.7	28.1	29.8	28.6	28.0	.000	.0000
192.	600.	60.4	69.8	91.5	323.4	.02	-9.1	46.3	27.0	28.5	28.8	29.1	.065	.2099-09
193.	600.	58.3	68.1	95.3	315.2	.05	-10.5	44.4	26.5	27.6	28.9	30.8	.194	.5483-08
194.	600.	59.6	64.9	98.5	316.7	.13	-10.0	43.3	26.9	28.5	29.3	30.0	.517	.1021-06
195.	600.	62.9	66.5	102.8	311.2	.28	-9.4	42.2	27.0	27.8	29.7	31.8	1.033	.8018-06
196.	600.	62.8	67.7	107.1	295.8	1.08	-10.9	40.2	27.0	28.7	30.3	30.2	3.907	.4199-04
197.	600.	63.6	67.7	108.1	294.4	1.76	-10.7	39.4	27.0	28.3	30.4	32.1	6.329	.1758-03
198.	600.	64.0	66.5	106.0	297.1	3.67	-10.5	38.1	26.9	28.5	30.3	30.6	12.885	.1439-02
199.	600.	62.8	64.8	106.5	291.6	5.09	-11.5	37.3	27.0	28.3	30.6	30.8	17.955	.3836-02
200.	600.	61.6	61.1	104.9	290.2	6.89	-12.5	37.3	26.9	28.1	30.4	31.8	24.801	.1011-01
321.	100.	2.2	2.8	37.0	60.6	.00	2.5	32.4	27.6	28.1	27.9	25.2	.000	.0000
322.	100.	1.4	2.3	32.9	65.9	.01	2.5	30.4	27.0	27.6	27.8	25.8	.065	.1559-09
323.	100.	1.2	2.2	31.3	67.3	.03	2.0	29.9	26.7	27.4	27.6	25.6	.194	.4175-08
324.	100.	.9	1.7	28.9	70.2	.18	1.9	28.9	26.7	27.4	27.6	26.2	1.033	.6164-06
325.	100.	.9	1.4	26.3	73.7	1.11	3.3	28.3	26.9	27.0	26.9	26.3	6.329	.1395-03
326.	100.	.3	.9	23.2	72.3	3.13	-.2	27.7	26.5	26.7	26.3	26.3	17.955	.3140-02
327.	200.	12.3	20.0	56.7	107.6	.00	-1.7	36.2	25.9	26.9	27.2	24.4	.000	.0000
328.	200.	10.7	18.9	53.6	114.8	.01	-1.0	33.2	26.3	26.9	26.7	26.9	.065	.1642-09
329.	200.	10.1	18.6	52.3	114.7	.03	-2.1	32.2	25.7	26.9	26.7	27.7	.194	.4356-08
330.	200.	10.0	17.1	50.6	123.7	.18	.8	30.9	24.8	26.7	26.1	26.0	1.033	.6452-06
331.	200.	11.0	16.1	48.4	129.0	1.07	2.8	30.3	26.7	26.7	26.1	26.2	6.329	.1466-03
332.	200.	9.1	14.2	41.9	127.8	3.03	-1.9	28.8	25.4	26.1	25.6	25.7	17.955	.3229-02
333.	400.	24.8	39.3	97.6	226.2	.00	-3.1	44.7	28.0	28.9	29.4	26.9	.000	.0000
334.	400.	20.6	35.3	95.1	240.5	.01	-2.1	40.7	26.5	29.1	26.0	29.1	.065	.1911-09
335.	400.	18.7	35.1	92.0	245.7	.03	-2.1	38.8	27.2	29.1	27.8	28.9	.194	.4977-08
336.	400.	18.7	33.4	88.2	253.9	.17	-1.4	36.4	26.9	28.5	27.4	28.1	1.033	.7171-06
337.	400.	18.7	30.5	80.1	266.2	1.11	-.8	33.6	27.0	28.0	27.2	27.4	6.329	.1557-03
338.	400.	18.7	28.6	69.4	264.2	2.17	-4.2	32.2	25.4	28.0	26.7	28.2	12.885	.1281-02
339.	600.	44.5	70.6	164.4	345.0	.00	4.1	55.0	29.4	30.2	31.9	31.9	.000	.0000
340.	600.	35.5	61.6	127.0	360.7	.01	-2.5	45.7	28.7	31.3	30.2	31.2	.065	.2075-09
341.	600.	35.5	61.1	127.6	360.7	.04	-2.5	44.9	28.7	31.5	30.0	30.7	.194	.5529-08
342.	600.	36.3	59.3	125.7	364.6	.23	-2.5	42.7	27.2	31.3	29.7	33.0	1.033	.8090-06
343.	600.	40.8	57.1	127.0	359.8	1.52	-2.3	41.0	28.3	31.7	29.1	32.6	6.329	.1808-03
344.	600.	39.6	55.0	122.6	364.7	4.29	-2.3	39.3	28.7	31.3	29.1	32.9	17.955	.3999-02

Data for Porous Lower Boundary, Discrete Hole Side Boundaries, and Solid Upper Boundary with Upper Grid to Lower Plate Electrodes.

RUN NO.	POWER FRACTION SIDE	BOTTOM	TOP	NUSSELT NUMBER SIDE	BOTTOM	TOP	ASPECT RATIO	RAYLEIGH NO.	M	SUPERFICIAL GAS VELOCITY (CM/MIN)	(ReFr)
1.	.382	.120	.499	29.4	16.9	66.2	1.051	.8235+08	.1682+02	.000	.0000
2.	.187	.140	.673	49.0	82.0	283.6	1.051	.6869+08	.6953+02	.517	.7443-07
3.	.163	.135	.702	48.1	88.4	324.1	1.051	.5788+08	.7782+02	1.033	.5683-06
4.	.126	.135	.739	42.0	95.7	324.4	1.051	.6158+06	.8402+02	2.519	.8624-05
5.	.119	.143	.738	55.4	139.3	350.7	1.051	.7069+08	.1160+03	3.907	.3428-04
6.	.108	.126	.766	62.1	209.0	452.5	1.051	.6812+08	.1980+03	6.329	.1357-03
7.	.097	.117	.786	54.3	74.5	500.4	1.051	.6576+08	.7579+02	10.979	.7056-03
8.	.095	.117	.787	50.1	130.4	500.4	1.051	.6559+08	.1323+03	12.885	.1140-02
9.	.093	.114	.793	39.8	111.6	496.9	1.051	.6429+06	.1160+03	17.955	.3077-02
10.	.085	.112	.803	39.1	122.0	633.4	1.051	.6282+08	.1291+03	24.801	.8067-02
11.	.314	.115	.571	34.8	25.0	102.8	1.051	.1859+09	.2587+02	.000	.0000
12.	.205	.150	.645	52.2	65.0	273.1	1.051	.1607+09	.5156+02	.517	.7936-07
13.	.190	.132	.678	57.6	105.9	262.3	1.051	.1486+09	.9533+02	1.033	.6315-06
14.	.189	.132	.679	64.8	106.8	284.0	1.051	.1470+09	.9606+02	2.519	.9067-05
15.	.184	.128	.687	72.6	100.7	332.4	1.051	.1476+09	.9332+02	3.907	.3366-04
16.	.178	.126	.696	69.8	109.8	361.7	1.051	.1481+09	.1040+03	6.329	.1422-03
17.	.155	.122	.723	72.9	228.7	408.7	1.051	.1445+09	.2231+03	10.979	.7362-03
18.	.150	.120	.730	71.8	170.0	423.3	1.051	.1427+09	.1684+03	12.885	.1187-02
19.	.144	.118	.737	78.3	124.0	448.3	1.051	.1360+09	.1249+03	17.955	.3193-02
20.	.141	.116	.744	77.7	172.4	464.1	1.051	.1358+09	.1775+03	24.801	.8391-02
21.	.327	.094	.579	38.3	22.7	123.1	1.051	.4940+09	.2871+02	.000	.0000
22.	.215	.141	.644	63.4	105.2	339.5	1.051	.3410+09	.8860+02	.517	.8418-07
23.	.208	.137	.655	61.3	84.4	318.4	1.051	.3529+09	.7330+02	1.033	.6622-06
24.	.213	.143	.644	64.2	124.2	318.1	1.051	.3440+09	.1034+03	2.519	.9784-05
25.	.208	.141	.651	71.0	126.8	326.5	1.051	.3495+09	.1071+03	3.907	.3641-04
26.	.200	.137	.663	74.4	123.4	393.8	1.051	.3393+09	.1069+03	6.329	.1528-03
27.	.185	.131	.684	79.4	141.9	480.9	1.051	.3344+09	.1292+03	10.979	.7643-03
28.	.190	.134	.677	82.4	126.6	474.3	1.051	.3256+09	.1127+03	12.885	.1265-02
29.	.185	.135	.680	76.5	236.3	486.7	1.051	.3213+09	.2086+03	17.955	.3402-02
30.	.179	.133	.688	75.8	237.1	513.4	1.051	.3143+09	.2118+03	24.801	.8920-02
901.	.344	.105	.551	43.1	23.7	141.8	1.051	.9439+09	.2693+02	.000	.0000
902.	.280	.162	.557	56.7	72.8	330.3	1.051	.7079+09	.5334+02	.517	.9906-07
903.	.282	.174	.544	59.6	84.7	344.5	1.051	.6715+09	.5791+02	1.033	.7607-06
904.	.290	.175	.535	69.3	98.5	355.8	1.051	.6678+09	.6702+02	2.519	.1111-04
905.	.290	.174	.536	78.5	113.7	452.3	1.051	.6450+09	.7792+02	3.907	.4033-04
906.	.281	.174	.545	80.7	119.9	511.2	1.051	.6226+09	.8202+02	6.329	.1694-03
907.	.278	.173	.549	86.7	145.3	607.0	1.051	.6032+09	.9998+02	10.979	.8661-03
908.	.277	.172	.551	88.1	145.3	670.2	1.051	.6022+09	.1007+03	12.885	.1393-02
909.	.274	.180	.546	85.2	150.4	618.0	1.051	.5859+09	.9959+02	17.955	.3770-02
910.	.275	.180	.545	83.3	160.5	687.3	1.051	.5845+09	.1061+03	24.801	.9902-02
81.	.321	.139	.541	24.5	18.9	72.5	1.130	.6194+06	.1506+02	.000	.0000
82.	.171	.184	.645	41.4	81.9	259.7	1.130	.4936+08	.4913+02	.517	.7464-07
83.	.173	.192	.635	37.9	101.7	247.1	1.130	.4957+08	.5866+02	1.033	.5955-06
84.	.173	.187	.640	49.5	82.6	332.5	1.130	.4958+06	.4686+02	2.519	.8589-05
85.	.168	.185	.647	54.0	81.3	332.3	1.130	.4998+08	.4850+02	3.907	.3193-04
86.	.163	.182	.655	56.7	99.4	471.6	1.130	.4915+06	.6037+02	6.329	.1346-03
87.	.155	.179	.666	52.7	132.4	492.2	1.130	.4763+06	.8171+02	10.979	.6481-03
88.	.146	.172	.683	58.3	120.0	521.1	1.130	.4511+08	.7740+02	12.885	.1128-02
89.	.096	.183	.721	43.3	156.0	473.1	1.130	.4670+08	.9437+02	17.955	.3077-02

90.	.101	.182	.717	38.9	161.5	577.1	1.130	.4553+08	.9836+02	24.801	.8057-02
91.	.289	.111	.600	27.0	20.7	97.6	1.130	.1551+09	.2066+02	.000	.0000
92.	.190	.131	.680	44.7	87.5	304.0	1.130	.1221+09	.7419+02	.517	.7928-07
93.	.184	.126	.690	44.4	69.5	300.0	1.130	.1158+09	.6118+02	1.033	.6270-06
94.	.187	.134	.679	53.5	107.6	369.0	1.130	.1151+09	.8886+02	2.519	.9003-05
95.	.186	.130	.684	52.3	113.3	367.3	1.130	.1130+09	.9615+02	3.907	.3351-04
96.	.182	.127	.691	61.6	111.9	457.6	1.130	.1114+09	.9767+02	6.329	.1405-03
97.	.176	.124	.700	61.6	140.1	505.8	1.130	.1058+09	.1248+03	10.979	.7251-03
98.	.170	.119	.711	71.7	196.6	584.9	1.130	.1042+09	.1821+03	12.885	.1162-02
99.	.167	.118	.715	69.4	209.9	608.3	1.130	.1021+09	.1975+03	17.955	.3136-02
100.	.161	.118	.721	58.6	108.0	569.8	1.130	.9860+08	.1012+03	24.801	.8243-02
101.	.302	.114	.584	33.1	24.7	127.0	1.130	.3702+09	.2391+02	.000	.0000
102.	.214	.141	.645	43.6	63.0	308.8	1.130	.2670+09	.4950+02	.517	.8611-07
103.	.214	.152	.634	49.0	78.8	344.9	1.130	.2572+09	.5743+02	1.033	.6763-06
104.	.207	.161	.632	54.0	86.2	361.2	1.130	.2592+09	.5931+02	2.519	.9753-05
105.	.204	.158	.638	55.5	110.7	385.4	1.130	.2558+09	.7750+02	3.907	.3610-04
106.	.207	.161	.632	62.5	126.0	444.6	1.130	.2447+09	.8663+02	6.329	.1515-03
107.	.197	.157	.646	62.9	110.1	462.2	1.130	.2414+09	.7756+02	10.979	.7835-03
108.	.195	.155	.650	66.7	117.5	538.7	1.130	.2371+09	.8368+02	12.885	.1255-02
109.	.190	.154	.656	71.6	159.1	589.9	1.130	.2355+09	.1140+03	17.955	.3374-02
110.	.187	.156	.657	68.5	170.2	620.1	1.130	.2286+09	.1209+03	24.801	.8848-02
111.	.313	.112	.574	36.9	25.1	140.7	1.130	.6692+09	.2471+02	.000	.0000
112.	.238	.167	.595	45.4	80.3	303.3	1.130	.5304+09	.5321+02	.517	.9977-07
113.	.245	.179	.576	50.5	83.3	343.8	1.130	.5227+09	.5160+02	1.033	.7897-06
114.	.252	.185	.563	53.9	103.9	319.3	1.130	.5204+09	.6205+02	2.519	.1135-04
115.	.259	.187	.554	60.9	110.8	356.0	1.130	.4995+09	.6536+02	3.907	.4167-04
116.	.251	.186	.563	65.7	132.4	419.1	1.130	.4815+09	.7893+02	6.329	.1725-03
117.	.247	.183	.570	70.5	146.3	494.2	1.130	.4547+09	.8846+02	10.979	.8782-03
118.	.247	.183	.571	66.7	128.4	480.3	1.130	.4555+09	.7776+02	12.885	.1424-02
119.	.243	.185	.572	68.4	135.9	466.8	1.130	.4454+09	.8115+02	17.955	.3823-02
120.	.238	.187	.575	70.3	166.4	531.8	1.130	.4246+09	.9864+02	24.801	.9691-02
161.	.229	.145	.626	21.1	26.9	85.5	1.542	.1863+08	.1503+02	.000	.0000
162.	.149	.174	.676	30.5	77.5	261.7	1.542	.1451+08	.3608+02	.517	.7433-07
163.	.154	.176	.670	34.5	71.1	204.9	1.542	.1464+08	.3269+02	1.033	.5979-06
164.	.155	.175	.669	43.5	91.3	230.1	1.542	.1471+08	.4219+02	2.519	.8577-05
165.	.148	.166	.686	46.4	100.4	281.9	1.542	.1430+08	.4890+02	3.907	.3172-04
166.	.193	.114	.693	67.2	91.3	270.9	1.542	.1447+08	.6476+02	6.329	.1346-03
167.	.180	.114	.706	73.4	90.2	318.5	1.542	.1479+08	.6403+02	10.979	.7000-03
168.	.170	.113	.717	51.1	88.4	375.5	1.542	.1471+08	.6366+02	12.885	.1131-02
169.	.163	.109	.728	68.4	103.0	402.9	1.542	.1442+08	.7632+02	17.955	.3037-02
170.	.156	.105	.739	60.2	107.2	485.4	1.542	.1400+08	.8284+02	24.801	.7982-02
171.	.288	.155	.557	26.0	30.5	106.2	1.542	.4148+08	.1598+02	.000	.0000
172.	.231	.181	.588	41.1	76.6	267.9	1.542	.3277+08	.3432+02	.517	.7860-07
173.	.230	.183	.587	43.1	82.5	295.0	1.542	.3236+08	.3659+02	1.033	.6243-06
174.	.237	.185	.577	60.8	106.5	278.9	1.542	.3170+08	.4662+02	2.519	.8689-05
175.	.234	.180	.586	55.9	105.2	342.0	1.542	.3157+08	.4732+02	3.907	.3314-04
176.	.238	.179	.583	65.0	130.8	353.8	1.542	.3019+08	.5923+02	6.329	.1387-03
177.	.233	.174	.593	58.6	125.6	590.0	1.542	.3106+08	.5854+02	10.979	.7241-03
178.	.230	.172	.598	64.5	129.7	542.0	1.542	.3029+08	.6122+02	12.885	.1165-02
179.	.227	.168	.605	65.9	135.8	512.3	1.542	.2935+08	.6552+02	17.955	.3136-02
180.	.220	.167	.613	66.2	139.1	564.1	1.542	.2933+08	.6764+02	24.801	.8232-02
181.	.261	.150	.589	29.9	35.4	130.0	1.542	.1058+09	.1602+02	.000	.0000
182.	.215	.162	.623	30.0	49.1	189.0	1.542	.9360+08	.2461+02	.065	.1852-09
183.	.205	.160	.636	37.7	66.7	269.1	1.542	.8173+08	.3390+02	.194	.4669-08
184.	.194	.154	.652	38.6	74.7	308.7	1.542	.7977+08	.3944+02	.517	.8687-07
185.	.189	.151	.660	47.2	95.4	371.7	1.542	.7733+08	.5123+02	1.033	.6734-06
186.	.198	.154	.647	57.7	118.0	422.5	1.542	.7310+08	.6202+02	3.907	.3569-04

187.	.197	.156	.647	61.2	129.2	449.9	1.542	.7117+08	.6699+02	6.329	.1507-03
188.	.185	.151	.665	64.0	148.9	438.0	1.542	.6966+08	.8013+02	12.885	.1252-02
189.	.187	.153	.660	64.6	153.9	522.5	1.542	.6455+08	.8149+02	17.955	.3357-02
190.	.175	.145	.680	67.3	170.2	541.6	1.542	.6551+08	.9524+02	24.801	.8794-02
191.	.307	.153	.540	32.6	32.3	110.4	1.542	.2161+09	.1707+02	.000	.0000
192.	.239	.168	.593	36.0	53.3	192.2	1.542	.1733+09	.2576+02	.065	.2099-09
193.	.236	.177	.587	37.6	63.2	238.1	1.542	.1614+09	.2888+02	.194	.5483-08
194.	.231	.183	.587	41.4	72.9	246.0	1.542	.1571+09	.3236+02	.517	.1021-06
195.	.238	.189	.573	45.4	85.0	309.9	1.542	.1532+09	.3645+02	1.033	.8018-06
196.	.244	.200	.555	55.5	113.1	310.1	1.542	.1421+09	.4577+02	3.907	.4199-04
197.	.245	.202	.553	58.4	125.0	420.2	1.542	.1388+09	.5020+02	6.329	.1758-03
198.	.243	.197	.560	66.2	143.3	418.8	1.542	.1320+09	.5890+02	12.885	.1439-02
199.	.240	.201	.559	69.6	164.4	473.4	1.542	.1269+09	.6642+02	17.955	.3636-02
200.	.234	.200	.566	65.5	159.3	559.4	1.542	.1254+09	.6660+02	24.801	.1011-01
321.	.048	.361	.591	5.9	87.0	89.5	2.660	.2287+07	.1133+02	.000	.0000
322.	.036	.321	.643	6.6	134.2	152.1	2.660	.2115+07	.1964+02	.065	.1559-09
323.	.034	.306	.660	6.6	139.4	163.5	2.660	.2068+07	.2139+02	.194	.4175-08
324.	.026	.283	.690	8.5	231.6	282.0	2.660	.1955+07	.3639+02	1.033	.6164-06
325.	.022	.254	.724	9.4	202.5	412.1	2.660	.1921+07	.3746+02	6.329	.1395-03
326.	.012	.232	.756	5.8	178.9	582.6	2.660	.1861+07	.3622+02	17.955	.3140-02
327.	.165	.288	.547	17.6	66.5	96.3	2.660	.5077+07	.1084+02	.000	.0000
328.	.149	.271	.580	24.0	87.2	193.3	2.660	.4556+07	.1513+02	.065	.1642-09
329.	.147	.267	.586	26.6	99.8	266.9	2.660	.4342+07	.1755+02	.194	.4356-08
330.	.134	.251	.614	29.9	111.2	266.2	2.660	.4251+07	.2083+02	1.033	.6452-06
331.	.132	.236	.633	39.3	122.1	336.9	2.660	.4234+07	.2436+02	6.329	.1466-03
332.	.119	.214	.667	42.0	136.8	441.9	2.660	.3752+07	.3007+02	17.955	.3229-02
333.	.165	.252	.583	20.4	65.8	130.7	2.660	.1327+08	.1230+02	.000	.0000
334.	.143	.243	.614	23.4	77.9	216.0	2.660	.1193+08	.1507+02	.065	.1911-09
335.	.137	.235	.628	27.1	86.7	257.5	2.660	.1119+08	.1734+02	.194	.4977-08
336.	.132	.224	.644	32.5	103.4	321.8	2.660	.1027+08	.2172+02	1.033	.7171-06
337.	.124	.202	.674	44.0	133.5	461.9	2.660	.9263+07	.3108+02	6.329	.1557-03
338.	.123	.181	.695	50.0	132.4	705.4	2.660	.8495+07	.3433+02	12.885	.1281-02
339.	.184	.263	.552	23.1	71.6	150.2	2.660	.2827+06	.1276+02	.000	.0000
340.	.166	.217	.617	32.7	84.2	255.9	2.660	.2059+06	.1824+02	.065	.2075-09
341.	.165	.218	.617	34.7	88.0	260.4	2.660	.2014+06	.1896+02	.194	.5529-08
342.	.162	.215	.624	38.4	99.4	387.4	2.660	.1892+08	.2174+02	1.033	.8090-06
343.	.167	.217	.616	48.4	110.7	443.6	2.660	.1803+08	.2402+02	6.329	.1608-03
344.	.161	.209	.629	55.4	125.5	601.2	2.660	.1704+08	.2821+02	17.955	.3499-02

aFIN